The Social Determinants of Bank Runs

Robin Lenoir *

New York University

December 9, 2025

Abstract

Motivated by new evidence from the 2023 U.S. regional bank crisis, I develop a theory of how depositor social structure influences bank runs. Rumors about bank financial health spread via interpersonal communication, triggering withdrawals that may lead to collapse. I show that the occurrence, speed, and scale of runs depend on depositor connectedness—the likelihood that agents know and communicate with each other. Higher connectedness accelerates information spread, making runs faster and more severe. In contrast, dispersed depositor bases slow down runs, and can even prevent them entirely.

Latest version available here

*Email: lenoir.robin@gmail.com. I am deeply thankful to Dilip Abreu, Arjada Bardhi, Jess Benhabib, Jaroslav Borovička, Gian Luca Clementi, Erik Madsen, Thomas Philippon, Alexi Savov, Phillip Schnabl, Olivier Wang, and Basil Williams, as well as many participants in various NYU seminars, for comments on this project.

1 Introduction

The regional bank failures of March 2023 astonished observers with their extraordinary scale and speed. While previous large-scale runs on Continental Illinois and Washington Mutual lasted an estimated ten and sixteen days (Rose 2023), the run on Silicon Valley Bank led to its collapse in less than one. Why was this time different? In an essay placing the collapse in historical perspective, Federal Reserve historian Jonathan Rose (2023) writes: *"The most significant departure from historical comparisons is that depositors were unusually connected or similar to each other. As a result, they withdrew in a coordinated or similar way."*

Coordination has been central to bank-run theory since Diamond and Dybvig (1983), whose model features multiple equilibria driven by self-fulfilling beliefs. Rose's use of the word *coordinated*, however, suggests something different. He employs it adverbially—qualifying *how* agents withdrew—implying that coordination is not merely a binary switch between good and bad equilibria but a *process*. In his reading, what made 2023 unusual was not simply that depositors ran; it was the way the run diffused through the depositor base.

The idea that withdrawal behavior spreads through interpersonal channels is well documented empirically. Kelly and O Grada (2000) show that during the 1854 and 1857 New York bank runs, Irish immigrants' social networks played a central role in shaping the runs: withdrawal decisions traveled along diasporic ties. Iyer and Puri (2012) similarly find that during a regional bank run in India, an individual's withdrawal probability rises when neighbors withdraw, even after controlling for depositor characteristics.

If withdrawal behavior propagates through social connections at the individual level, then the structure of those connections ought to matter for bank-level fragility. This is the broader implication of Rose's interpretation, and it is consistent with what the 2023 crisis appeared to reveal: institutions whose deposits were concentrated among a few highly interconnected clients—such as SVB—experienced sharper and more sudden withdrawals than peers with more diffuse depositor bases. As I show in the empirical motivation in Section 2, these differences persist even after controlling for balance-sheet fundamentals. Taken together, the evidence suggests that depositor social structure may be an independent force shaping run dynamics.

But how exactly does the aggregation from individual social ties to bank-level run risk operate? Would rational depositors take the social structure of their peers into account when deciding whether to run? The SVB episode, and Rose's perspective of it, suggest that tighter depositor ties could intensify panics. But does the converse hold—does a more dispersed or weakly connected depositor base meaningfully slow withdrawals? Can it prevent runs altogether? These questions cannot be settled with empirics alone and require a model.

Most theories of runs, however, do not model the process through which depositors coordinate, making it difficult to evaluate how social structure shapes run dynamics. My paper develops a model in which information diffuses through interpersonal communication. Agents learn about potential runs from others and decide when to withdraw based on their beliefs about both bank fragility and how many others they expect to have learned. The interplay between information diffusion and belief updating generates testable bank-level dynamics: a more dispersed depositor base can slow runs and even prevent them.

The model I develop builds on Abreu and Brunnermeier (2003) and He and Manela

(2016)'s frameworks of sequential awareness in bubbles and runs. It features a continuum of depositors and a single bank. Depositors derive utility from deposits in the form of convenience flows (interest-bearing deposits are introduced as an extension) but face the risk of losing their funds in a bank collapse.[1] The bank is subject to solvency shocks that arrive at a Poisson rate. These shocks can leave the bank in one of two states: fragile or healthy. A fragile bank can sustain only a fraction κ of withdrawals before collapsing; a healthy bank can withstand any level of withdrawals—the shock was a false alarm.

Crucially, agents do not learn about the shock simultaneously. Instead, information spreads gradually through social contacts. I model this diffusion process explicitly using a tool from mathematical epidemiology: the Susceptible–Infected (SI) process, widely used to model disease transmission. Agents meet each other at rate β; when an uninformed agent meets an "informed" one, they learn about the shock. This generates logistic diffusion dynamics: information initially accelerates as more agents become aware, then decelerates as the informed population saturates. Agents receiving information learn that a shock has occurred but cannot observe whether the bank is fragile or healthy. Cases in which the shock leaves the bank healthy can thus be interpreted as false rumors—information spreads about a solvency shock that poses no actual threat.

The meeting rate β is the key structural parameter governing coordination frictions—that is, how readily information spreads among depositors. It captures the intensity of interpersonal communication and can arise from various sources: geographical deposit concentration (the measure I use for the motivational evidence in Section 2), social media exposure (Cookson et al. 2023), or any channel affecting the speed of information diffusion. A higher β implies faster information transmission and thus lower coordination frictions, which I show makes banks more vulnerable to runs in equilibrium.

Coordination frictions matter not only because they determine how quickly information spreads, but also because they discipline how rational depositors update their beliefs and time their actions. When agents learn about a potential solvency shock, they must decide *when* to withdraw—or when to return if they come to believe the rumor was false. Their decision depends on beliefs about both the bank's true state and the anticipated withdrawal behavior of others. Solving this problem in full generality is intractable, so I focus on a natural subset of equilibria—*stationary equilibria*—in which agents' strategies depend only on the time elapsed since learning, not on calendar time. Each moment after becoming informed, a depositor faces a dynamic trade-off: holding deposits for longer provides utility, but continued exposure increases the risk to be caught in a crash. The key statistic governing this decision is the perceived instantaneous crash probability, or *hazard rate*.

The hazard rate can be decomposed into two components: the conditional probability that a fragile bank collapses, which rises with withdrawal pressure, and the posterior belief that the bank is indeed fragile. These two components evolve in opposite directions, creating rich dynamics. On the one hand, an agent anticipating the collapse understands that more depositors will learn about the shock and withdraw, raising the conditional crash probability. On the other hand, the bank's continued survival provides Bayesian evidence that the shock was likely a false rumor. Beliefs about fragility therefore decline over time. In

[1] As discussed in Section 4, one can interpret deposit utility directly as a risk-tolerance threshold below which agents are willing to remain in the bank.

the period immediately following agents' learning, the first force dominates: anticipation of rising withdrawal pressure overwhelms any improvement in beliefs, so the combined hazard rate increases, prompting agents to withdraw if the risk exceeds the utility benefits. But as survival evidence accumulates and the logistic learning curve saturates—decelerating information flow—the second force takes over. Agents who withdrew earlier now rationally reenter, confident the rumor was false. This decomposition generates hump-shaped aggregate withdrawal dynamics—withdrawals rise as panic spreads, then fall as confidence rebuilds, pushing reentry.

The recovery mechanism distinguishes my model from prior dynamic run theories. He and Manela (2016) also feature false rumors, but their assumption of exponential learning implies monotonically increasing hazard rates—panic can only accelerate, never abate. (Abreu and Brunnermeier (2003) similarly generate only monotonic hazard rates.) My logistic learning assumption, by contrast, generates natural saturation: as most agents become informed, information spread decelerates, allowing survival evidence to dominate and triggering recovery. This prediction aligns with evidence from the 2023 crisis: Cipriani et al. (2024) document, using Federal Reserve regulatory data, that most banks surviving the initial run saw deposit levels return to near pre-crisis levels by summer 2023.

The model's central result is an existence threshold for runs. Because withdrawn agents eventually reenter as crash fears subside, aggregate withdrawals necessarily peak and then decline if the bank survives. The height of this peak depends critically on depositor connectedness β and on deposit utility. When depositors are dispersed, information spreads slowly and withdrawals are staggered over time, lowering the peak of simultaneous withdrawals. Conversely, rapid diffusion compresses withdrawals in time, raising the peak. There exists a critical threshold: when connectedness is sufficiently low, peak withdrawals remain within the bank's solvency capacity. In that case, runs become impossible— even at the height of panic, withdrawals never breach solvency, eliminating any incentive to run. Conversely, concentrated depositor bases—like SVB's—imply low coordination frictions that make runs not just faster but more severe.

Deposit utility shapes recovery dynamics in a similar way. When deposits are attractive, agents reenter quickly to enjoy their benefits despite remaining crash risk, reducing the number of agents withdrawn at any given moment and lowering the peak. Normatively, this suggests that enhancing deposit attractiveness can serve as a viable run-prevention policy. However, as I show in Section 5, the effectiveness of such measures depends on the underlying social structure of depositors, β.

The model's tractability enables structural estimation. As a methodological exercise, I illustrate this by fitting the model's closed-form withdrawal path to intraday stock returns during the March 2023 crisis. This allows me to recover bank-specific estimates of depositor connectedness β and other model parameters directly from observed price movements. The approach complements the balance-sheet and network-based proxies used in Section 2 to motivate the model. Rather than measuring these parameters independently, the structural estimates reveal them as implicit forces shaping market outcomes during the crisis. I then test whether the original proxies correlate with the structural parameters and find that they do, suggesting that the model provides a useful organizing framework for understanding cross-sectional differences—though I emphasize this as an illustrative exercise demonstrating tractability rather than a definitive empirical test.

Three extensions enrich the baseline framework. First, I allow for heterogeneous learning speeds across different groups of depositors. Well-connected agents can time withdrawals strategically, while poorly connected ones must exit immediately, creating inequality in run exposure and generating asymmetric recovery dynamics. Second, I extend the model to incorporate interest-bearing deposits. Higher deposit rates encourage earlier reentry and lower peak withdrawals, making rate increases an effective run-prevention tool—Cipriani et al. (2024) document that many banks raised rates to moderate outflows during the 2023 crisis—though effectiveness still depends on coordination frictions. Third, I replace the "word-of-mouth" information diffusion assumption with a social-learning environment in which agents observe others withdrawals. Numerical exercises confirm that all three extensions preserve the model's core features.

Literature review. Understanding how depositors coordinate on bank runs has been a central question in banking theory since Diamond and Dybvig (1983). My paper is part of an established branch of this literature that focuses on the *dynamics* of coordination. Dynamic aspects were first brought into the Diamond-Dybvig model through sequential service constraints (Green and Lin (2003), Peck and Shell (2003), Gu (2011)). More recent efforts model run dynamics in tractable frameworks using alternative models: He and Xiong (2012) introduced a dynamic debt run model based on firm debt rollover, while Tran (2019) proposed a behavioral model wherein agents possess imperfect signals on aggregate withdrawals, delineating the frequency, speed, and abruptness of runs as a function of signal quality.

Within that strand, I am particularly indebted to He and Manela (2016), which itself builds on Abreu and Brunnermeier (2003). The latter introduced "sequential awareness" in the context of rational bubbles: agents become aware of the bubble sequentially but are uncertain about their position in the sequence, gambling that they are early enough to delay exit and thereby preventing standard backward induction.[2] He and Manela (2016) adapted this framework to bank runs, introducing uncertainty about whether the bank is fragile or healthy and allowing agents to acquire additional noisy information. My paper retains the fragile-versus-healthy uncertainty but replaces information acquisition with explicit modeling of information diffusion using Susceptible-Infected (SI) epidemiological dynamics. This modeling choice incidentally shift focus to recovery: after observing no crash for sufficient time, agents rationally infer the bank is likely healthy and reenter. These recovery dynamics feed back into the run phase itself—if coordination frictions or deposit utility push agents to reenter early enough, runs can be eliminated entirely even at fragile banks.

Empirical evidence supports the importance of social structure in coordinating depositor behavior. Already mentioned are the studies of Kelly and O Grada (2000) and Iyer and Puri (2012) on depositor networks in specific bank run episodes. Kiss et al. (2014) provide experimental evidence of similar mechanisms. Schmidt et al. (2016) discuss the informational advantage of institutional investors during the 2008 runs on Money Market Funds, and Liu et al. (2023) highlights the role of online exposure during the Terra Luna run. Finally Cookson et al. (2023) and Benmelech et al. (2024) provide similar evidence during the 2023 run[3]. My paper complements this empirical work by developing a theoretical framework that shows

[2]This type of game is sometimes referred to as a "clock game" (Brunnermeier and Morgan (2010)).

[3]See Section 2 for a detailed discussion on the empirical literature on the 2023 regional banking crisis.

how micro-level social interactions aggregate to determine bank-level run dynamics.

Methodologically, my paper contributes to the literature on network diffusion in economics. This literature includes models of learning and opinion formation (Golub and Jackson (2010)) and network games (Calvó-Armengol et al. (2015), Galeotti et al. (2020)). Most directly, I build on Jackson and Lopez-Pintado (2011), López-Pintado (2006), López-Pintado (2008), and López-Pintado (2012), who applied mean-field epidemiological approximations developed by Pastor-Satorras and Vespignani (2001) to model product adoption as disease transmission. The critical distinction is that in those papers agents are mostly concerned with a coordination problem: they face strategic complementarities in adoption decisions. The problem in my paper is more complex mixing coordination and competition incentives (agents want to withdraw before others).

Stepping back, my focus on information diffusion through social networks connects to a broader theoretical literature on how information structure shapes coordination in financial crises. The global games tradition, pioneered by Morris and Shin (2001) for currency attacks and adapted by Peck and Shell (2003) to bank runs, demonstrates that coordination outcomes depend critically on the precision of public versus private information. Angeletos and Pavan (2004) show that greater transparency in public information can either facilitate or hinder coordination depending on the degree of strategic complementarity. Morris and Shin (2002) establish that enhanced public information dissemination can reduce welfare when agents have socially valuable private information. More recently, Parlatore (2024) demonstrates that more precise information increases an economy's vulnerability to bank runs: as information quality improves, depositors can better distinguish fragile from healthy states, strengthening their incentives to withdraw and making run-proof contracts costlier. My contribution to this literature lies in the dynamics: showing how information *diffusion dynamics* determine runs.

The paper proceeds as follows. Section 2 presents empirical evidence on the complementarity between fundamental and coordination risk. Section 3 develops the theoretical framework. Section 4 characterizes stationary equilibria and derives the hazard rate decomposition. Section 5 analyzes how coordination frictions and deposit attractiveness determine run dynamics, establishing the main result. Section 6 explores how the model can be used for structural estimation using crisis-period stock returns. Section 7 explores extensions with heterogeneity, interest rates, and social learning.

2 Empirical Evidence: The Role of Depositor Concentration

I present motivating empirical evidence on the role of depositor concentration during the 2023 U.S. regional bank crisis. Following the litterature, I proxy run severity by drops in banks stock returns. Substantial drops occurred predominantly among banks with both high fundamental risk and concentrated deposit bases. Banks with weak fundamentals but dispersed depositor bases experienced milder stress. This pattern suggests that fundamental fragility alone is necessary but not sufficient for runs; "coordination risk" plays a complementary role, motivating the theoretical framework developed in subsequent sections.

2.1 Perspectives on the 2023 Regional Bank Crisis.

The regional banking crisis of March 2023 emerged following Federal Reserve interest rate hikes during 2022–2023 that eroded the value of fixed-rate securities held by many regional banks. Silicon Valley Bank (SVB) announced a $1.8 billion loss on securities sales on March 8, 2023, triggering a rapid deposit run; two days later, SVB failed after $42 billion in deposit outflows. Signature Bank followed on March 12, and First Republic collapsed on May 1, while several other regional banks faced severe stress but survived. Regulatory interventions were announced on March 12, including the Federal Reserve's Bank Term Funding Program and FDIC guarantees of uninsured deposits, sought to prevent contagion. The crisis prompted commentary attributing failures to structural balance sheets, digital banking technologies, and social media—with one puzzle: why did some banks with similar fundamentals survive while others failed? In empirical finance, two complementary strands of literature have emerged to answer this question.[4]

The first emphasizes fundamental risk stemming from re-composition of bank value. A series of papers[5] document that monetary tightening had strong adverse effects on bank balance sheets. Banks like SVB that invested heavily in short-term assets experienced significant mark-to-market depreciation after the rate hikes. Loss of asset value, however, does not suffice to explain the sudden, *coordinated*, nature of depositor withdrawals. Drechsler et al. (2025) highlights a complementary effect of monetary tightening: while asset values declined, deposit franchise values actually increased because higher market rates allowed banks to capture larger spreads on deposits. Increased reliance on deposit franchises subjected banks to solvency runs, particularly when most depositors are uninsured (as was the case for SVB). Indeed those franchises are fragile: if depositors run, the franchise is destroyed, destroying the bank's value overall and thereby justifying the run in the first place.

The second strand focuses on depositor characteristics. Some papers emphasize the *individual* behavior of depositors, documenting that certain clienteles—such as uninsured depositors or those from sectors under pressure (crypto, venture capital)—were particularly sensitive to fragility concerns.[6] Other papers, motivated by the historical speed of the

[4] I refer to Kelly and Rose 2025 and Cipriani et al. 2024 for a very rich account of the crisis and the subsequent literature.

[5] See notably Jiang et al. (2024), Choi et al. (2023) and Koont et al. (2024).

[6] Chang et al. (2023) emphasize the fundamental role of uninsured depositors in propagating the crisis,

run, emphasize the *collective* behavior of depositors, examining how relationships among depositors facilitated coordination. Cookson et al. (2023) demonstrate that banks with high pre-existing Twitter exposure lost 4.3 percentage points more stock value during the SVB run, showing that social media relationships acted as a catalyst for coordinating depositor withdrawals. Benmelech et al. (2024) find that bank branch density—a proxy for physical coordination frictions—significantly affected run vulnerability.

2.2 Measure of fundamental risk and coordination frictions

The distinct perspectives on fundamental versus coordination-driven vulnerabilities raise the question of how these forces interact to generate runs. To explore this interaction and motivate the theoretical framework I develop in Section 3, I construct measures that capture both dimensions. For fundamental risk, I follow Drechsler et al. (2025)'s deposit franchise approach. For coordination frictions—structural impediments to information diffusion—I use a simple measure of geographic concentration of deposits. Together, these measures reveal a stark complementarity: severe runs occurred predominantly at banks where weak fundamentals coincided with low coordination frictions (high concentration).

Fundamental risk My measure of fundamental risk is directly from the work of Drechsler et al. (2025). They show that a bank's total economic value can be decomposed as the sum of, on the one hand, the marked-to-market value of assets net of the book value of total deposits, on the other hand, the franchise value of deposits. The authors provide a quantitative framework to estimate each component from the Call Reports. A bank becomes insolvent when its total value falls below a critical threshold $\underline{v}$.[7] From the bank value decomposition, I define the solvency measure κ as the critical fraction of the total deposit franchise that must be lost for the bank to reach this threshold:

$$\underbrace{A - D}_{\text{MTM Equity Value}} + (1 - \kappa) \times \underbrace{DF}_{\text{Deposit Franchise Value}} = \underline{v}$$

Banks with $\kappa < 1$ face genuine fundamental risk: a sufficiently large run can render them insolvent. Banks with $\kappa > 1$ remain solvent even after losing their entire deposit franchise, making runs unlikely in the first place. Appendix B.2 discusses the construction of this measure in detail.

Coordination frictions. To measure coordination frictions, I use a simple, transparent proxy: the geographic concentration of deposits across bank branches. I measure concentration using the Herfindahl-Hirschman Index (HHI) of branch-level deposits. Formally, the

documenting that uninsured depositors represent valuable clients whose loan demand creates core lending relationships, rather than merely unstable funding sources. Kelly and Rose (2025) show that banks with business models oriented toward sectors under pressure (crypto, venture capital) faced greater stress, independent of their fundamental balance sheet exposures.

[7] Following Drechsler et al. 2025, I set $\underline{v}$ to 3% of assets in my empirical analysis. 3% corresponds to the Basel III recommendation for banks in good standing.

HHI is defined as:

$$\text{HHI} = \sum_{i \in \text{Branches}} \left(\frac{\text{Deposits in } i}{\sum_i \text{Deposits in } i} \right)^2.$$

HHI has a natural interpretation as the probability that two randomly selected deposit dollars originate from the same branch. The key insight is straightforward: when deposits are geographically concentrated, depositors are more likely to share local networks and encounter each other, allowing information about bank health to spread more rapidly. This faster information transmission reduces coordination frictions—depositors can better assess how many others have learned about potential problems and are likely withdrawing, making their own withdrawal decisions clearer.

While other measures could be proposed, HHI offers a parsimonious measure of the network structure relevant for information transmission. It is computed from publicly available regulatory data (FDIC's Summary of Deposits) and can be readily constructed for other crisis episodes. Appendix B provides additional discussion of HHI's distribution across banks, its time-series evolution, and its correlation with other bank characteristics.

2.3 Empirical Strategy and Results

To test whether fundamental and coordination risk jointly determine bank vulnerability during the crisis, I examine cumulative stock returns during the week of March 6–13, 2023—around SVB's collapse.[8] Absent high-frequency data on deposit outflows, stock returns provide the best available proxy for run severity during this period and have been standard in the 2023 banking crisis literature.[9]

Figure 1 presents the relationship between stock returns during the crisis week, fundamental risk (κ), and coordination risk (HHI), with color intensity indicating return magnitude. The figure reveals that banks experiencing large stock price declines cluster in the bottom-right region: low κ (high fundamental risk) combined with high HHI (high depositor concentration). SVB, First Republic, Signature Bank, Western Alliance, and PacWest all are in that category.[10] In contrast, banks with $\kappa \geq 1$ generally show small price drops, consistent with the interpretation that such banks remain solvent even after complete deposit franchise destruction (which prevents any incentive to run in the first place). Wells Fargo, JPMorgan Chase, and Citigroup fall in this category.[11] Among fragile banks ($\kappa < 1$), those with low HHI experienced substantially smaller stock price declines despite their fundamental weakness—US Bank and Bank of America exemplify this pattern. The theoretical model I develop in subsequent sections focuses particularly on explaining this protective effect: why dispersed depositor bases can prevent runs even at fundamentally fragile institutions.

[8] Stock returns are sourced from CRSP; see Appendix B.2 for construction details.

[9] Cookson et al. (2023) and Benmelech et al. (2024), for example, directly use stock returns as the testable outcome of their bank vulnerability measures. Importantly, Cipriani et al. (2024) validate this approach using confidential Federal Reserve data, showing that stock returns exhibit a strong correlation with actual deposit outflows during the run phase.

[10] Some banks in this high-risk region experienced only mild stock price declines; investigation suggests these are predominantly small regional banks outside of California.

[11] Interestingly, Citigroup exhibits relatively high depositor concentration and strong fundamentals.

To formalize these patterns, I estimate two baseline specifications assessing the interplay between coordination and fundamental risk. The first specification tests whether both HHI and κ predict crisis outcomes after controlling for each other:

$$\text{Stock Return}_i = \beta_1 \text{HHI}_i + \beta_2 \kappa_i + \epsilon_i. \tag{8}$$

The second specification introduces an interaction term to test whether the effect of depositor concentration depends on fundamental fragility:

$$\text{Stock Return}_i = \beta_1 \text{HHI}_i + \beta_2 \mathbb{1}_{\kappa_i<1} + \beta_3 \text{HHI}_i \times \mathbb{1}_{\kappa_i<1} + \epsilon_i. \tag{9}$$

The indicator $\mathbb{1}_{\kappa_i<1}$ identifies banks with genuine fundamental vulnerability—those that would become insolvent if their deposit franchise were sufficiently eroded. The interaction coefficient β_3 captures whether coordination risk (HHI) has a differential effect for fundamentally weak versus strong banks, testing the core complementarity between fundamental and coordination risk.

Table 1 presents the results. Column (1) shows that κ leads to higher returns (smaller price drops), suggesting that safer banks—those requiring more destruction of their deposit franchise to become insolvent—were more protected against runs. Column (2) shows that depositor concentration (HHI) is strongly associated with worse stock performance. Column (3) includes both measures simultaneously: the coefficients remain nearly unchanged, suggesting these two sources of risk are largely orthogonal. The R^2 increases from 0.052 (Column 1) to 0.159 (Column 3) when adding in HHI to risk on bank value, suggesting an important role of depositor concentration. Column (5) presents the key complementarity test: among safe banks ($\kappa > 1$), the HHI effect is small and barely significant. Among fragile banks ($\kappa < 1$), the total HHI effect is substantially larger and highly significant. Notably, the effect of being fragile when HHI equals zero is effectively null, suggesting that both fundamental fragility and depositor concentration are necessary to identify banks that experienced severe runs. Additional robustness checks and alternative specifications, including controls for size, uninsured shares and wholesale funding, are provided in Appendix B.3.2.

3 Model: A Fragile Bank and a Rumor Spreading

Motivated by the empirical evidence of how depositor concentration and fundamental risk interact to determine run outcomes, I now develop a theoretical framework that captures these mechanisms. The model extends the frameworks of Abreu and Brunnermeier (2003) and He and Manela (2016) to explicitly incorporate the role of communication speed among depositors. In this section, I formalize the object of communication and model its diffusion using epidemiological tools. The next section analyzes the equilibrium implications.

3.1 Many Agents, One Bank

Time is continuous and extends forever. There is a continuum of agents of measure one (with no atoms) who, at any time, can choose how much of their wealth to hold in deposits versus cash. All agents are endowed with one unit of wealth. Deposits yield a utility flow of u per

Dependent Variable:	**Cumulative Stock Return (Mar 6-13, 2023)**				
	(1)	(2)	(3)	(4)	(5)
Solvency κ	0.072***		0.069***	0.034	
	(0.023)		(0.022)	(0.034)	
Depositor HHI		-0.284***	-0.278***	-0.453***	-0.131*
		(0.061)	(0.059)	(0.142)	(0.076)
Depositor HHI $\times\kappa$				0.170	
				(0.126)	
Indicator ($\kappa < 1$)					-0.000
					(0.019)
$\kappa < 1\times$ Depositor HHI					-0.354***
					(0.120)
Constant	-0.255***	-0.154***	-0.225***	-0.190***	-0.152***
	(0.025)	(0.010)	(0.025)	(0.036)	(0.012)
Observations	176	176	176	176	176
R^2	0.052	0.112	0.159	0.168	0.179

*Note: *** p<0.01, ** p<0.05, * p<0.1.*

Table 1: Deposit concentration, franchise value and bank returns.

Reading note: OLS regressions of cumulative stock returns on HHI (depositor concentration) and κ (solvency measure). Standard errors in parentheses.

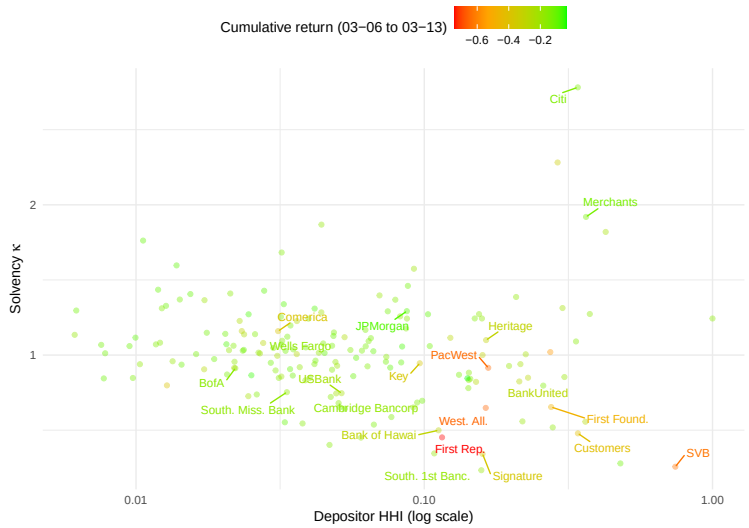

Figure 1: Stock returns, fundamental risk, and coordination risk.

Reading note: Scatterplot of individual BHCs by HHI (x-axis) and solvency κ (y-axis). Color represent cumulative returns on stocks between March 6 and March 13 2023. Banks who experienced the largest price declines, including SVB and First Republic, all displayed high HHI and low κ (lower right).

unit,[12] while cash yields no utility flow. Cash represents the best outside option, so u captures the excess utility from holding deposits. Agents directly maximize their expected utility flow

[12]Deposits do not accrue interest. Section 7.2 extends the model to interest-bearing deposits, which doesn't change the core mechanics.

without explicit consumption modeling. I remain agnostic on specific interpretations for u, treating it as a reduced-form representation of non-pecuniary benefits such as convenience.[13]

The risk facing depositors takes the form of a run-triggered crash. At some random time $t_0 \sim \mathcal{E}(\lambda)$ (exponentially distributed[14] with rate λ), the bank faces a shock on its value. For all $t \geq t_0$, the bank is potentially[15] *fragile*. A fragile bank can only cover the withdrawal of κ of its depositors. If a mass of agents exceeding the threshold κ attempts to withdraw, the bank crashes, and all deposits are lost (including those in the process of being withdrawn). In such an event the game ends and agents' payoffs are equal to how much wealth they store in cash[16]. The solvency threshold κ maps directly to the empirical measure defined in Section 2, where it captured the critical fraction of the deposit franchise that must be lost for a bank to become insolvent. Banks with $\kappa < 1$ face genuine fragility risk because the destruction of the deposit franchise from a run would render the bank insolvent. The deposit franchise interpretation is not necessary, κ could for example represent liquidity reserve. κ captures a general idea with simple tool: a fragile bank will crash if too many agents (more than κ) try to withdraw simultaneously.

3.2 Solvency Shocks and the Spread of Panic

While the previous subsection established the bank's vulnerability to mass withdrawals, the critical question is how depositors learn about and react to potential fragility. At the heart of my model lies an information friction: knowledge of the shock faced by the bank diffuses gradually among agents through social interactions.

A simple backward induction argument shows that if the shock were perfectly observed by all agents, it would lead to an immediate run in equilibrium. In contrast, I assume a form of sequential awareness as in Abreu and Brunnermeier (2003): agents learn about the shock gradually. I microfound sequential awareness explicitly as information diffusion through interpersonal communication, building on the susceptible-infected (SI) epidemiological framework.

At each time $t \geq t_0$, the mass of agents who have learned about the shock, denoted $G(t)$, evolves according to the ordinary differential equation:

$$dG(t) = (1 - G(t))G(t)\beta dt.$$

A mass $1 - G(t)$ of uninformed agents meets other agents at rate β, and each meeting has probability $G(t)$ of being with an informed agent who passes along information about the shock. Agents are informed that "a shock happened" but not of *when* it did.

The function $G(t)$ represents the measure of agents who have learned about the shock by time t. The differential $dG(t)$ captures both the fraction of the population learning in

[13]The next section emphasizes an alternative interpretation for u: it represents the crash-risk threshold agents are willing to accept when they hold deposits.

[14]The assumption of an exponential distribution is at heart an assumption on agents' *priors* for the shocks rather than the actual physical probability which doesn't play a role in my model.

[15]Section 3.3 explains why *potentially*.

[16]Effectively this is saying that agents value wealth directly and are risk-neutral. Before crash the value of a dollar in more than its nominal value because of the potential utility flow from deposit. After a crash the bank disappear and agents value their wealth at nominal value.

the interval $[t, t+dt]$ and—by the law of large numbers—an individual agent's probability of learning in that interval.

The meeting rate β is a key parameter capturing coordination frictions: higher β implies faster information transmission, which I will show increases "coordination risk" from the bank point of view. In the empirical analysis of Section 2, I proxy coordination frictions using deposit concentration (HHI)—when deposits are geographically concentrated (high HHI), information spread faster because depositors are more likely to interact. More broadly, β can be interpreted as reflecting exposure to social media, shared investment networks, or any channel determining how rapidly information spreads between depositors.

The solution to this differential equation is the well-known logistic function:

$$G(t-t_0) = \frac{e^{\beta(t-t_0)}}{C + e^{\beta(t-t_0)}},$$

where C is determined by the initial condition $G(0)$, assumed exogeneous. Figure 2 displays the population dynamics of informed agents for three scenarios where the learning rate β takes values 0.5, 1, and 2. The learning curve is S-shaped: it starts slowly because only a small portion of agents are informed, then accelerates as more agents become informed and pass the rumor on, and finally slows down as most agents are informed and the rumor has less room to spread. Note that the distribution of learning times with lower β first-order stochastically dominates that with higher β: when communication is faster, agents learn earlier.

Following He and Manela (2016), I further assume the learning process is bounded by an "awareness window". Once a sufficient portion of agents have learned, i.e. $G(t) > 1-\epsilon$ for some $\epsilon > 0$, I assume the shock is publicly revealed. This is primarily a technical assumption to ensure stationarity in the model—it keeps agents' belief supports bounded and, crucially, ensures the support size is independent of calendar time.[17] Without it, agents learning later would have progressively wider supports for their beliefs about when the shock happened, complicating the analysis substantially. It will be convenient to parametrize the awareness window directly as $\eta := G^{-1}(1-\epsilon)$, the time it takes to reach $1-\epsilon$ informed agents. Just as He and Manela (2016), I focus on realizations where $t_0 \geq \eta$, ensuring the belief support remains time-invariant.

Section 7 discusses an alternative learning structure where agents learn by observing others' withdrawal behavior rather than through word-of-mouth communication. This "social learning" mechanism introduces additional complexity that requires numerical methods. The core insights of the model remain unchanged under this alternative specification.

Finally, notice that agents only learn once: they ignore any information they get from subsequent meetings. Analyzing what happens if one relaxes that assumption gets intractable quickly, as it requires to understand how beliefs updates conditional on a rich state-space (the timing of each meetings). It is nonetheless a fascinating question, that I leave for future research.

[17] One could directly make the behavioral assumption that agents put 0 probability on the event that shocks happened much earlier that their learning time.

Figure 2: Dynamics of informed agents

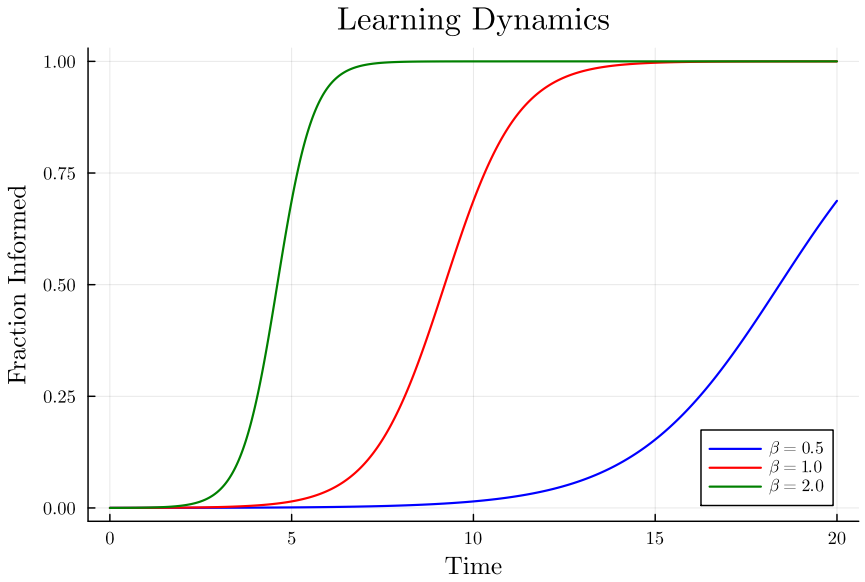

Reading note: Logistic curves showing the fraction of informed agents $G(t)$ over time for different communication speeds $\beta \in \{0.5, 1, 2\}$. S-shaped dynamics: slow initial spread, rapid middle phase, saturation. Higher β implies faster information diffusion and earlier learning.

3.3 False Rumors and Recovery Dynamics

I make the crucial additional assumption that the piece of information spreading in the process described above may be *false*. Formally, when a "shock" happens, two events may realize. With probability p the bank truly becomes fragile with reduced withdrawal capacity $\kappa < 1$. With probability $(1 - p)$, the bank remains healthy, able to withstand any level of withdrawals ($\kappa = 1$)[18]. Throughout the analysis, I maintain $p < 1$. One can interpret the information spread following the shock as a *rumor*, which may be true with probability p or false with probability $(1 - p)$.

Agents cannot distinguish between true and false rumors—they only observe that a shock event has occurred. They must infer the bank's actual state from observing whether a crash materializes over time. If many periods pass without a crash despite widespread (estimated) withdrawals, agents rationally update their beliefs toward the shock being false. This Bayesian updating drives recovery dynamics: agents who initially withdrew out of caution gradually return to holding deposits as confidence rebuilds. These complex dynamics are analyzed in detail in the next section.

The existence of false rumors is essential to the model's mechanism. Without them, any shock would guarantee bank fragility, and rational agents would never return to deposits after withdrawing, making runs always successful. A central result of the paper is that even banks that are *truly fragile* may escape runs if coordination frictions are strong enough; it is only possible because agents put some probability on the event that the bank is safe.

[18] Alternatively, one may think of the bank as being ex-ante of a type robust to shock, with probability $1 - p$.

Remark 1 (Comparison with Exponential Learning Models)**.** *He and Manela (2016) also incorporate false rumors in their model of bank runs. However, their assumption of exponential learning—where the mass of informed agents grows at rate $\beta(1 - G(t))$ rather than the logistic rate $\beta G(t)(1 - G(t))$ used here—fundamentally changes the equilibrium dynamics. Under exponential learning, the hazard rate for crash increases monotonically over time, preventing the kind of recovery dynamics studied in Section 5.*

I focus throughout on the dynamics generated by a single rumor—even if false, the bank faces no additional shocks during the analysis period. This allows me to clearly characterize how a single informational event propagates through the depositor network and potentially resolves through either collapse or recovery. Finally, for simplicity, I assume agents hold all wealth in deposits until learning about the shock[19], although we could do without the assumption and focus on a parameter space where agents don't want to leave ex-ante.

4 Analysis: The Structure of Run Equilibria

I now characterize the equilibrium withdrawal strategies of informed depositors—those who have learned about potential bank fragility through social interactions. By focusing on stationary equilibria, where behavior depends only on time since learning rather than calendar time, the strategic problem becomes tractable. A key tool to build intuition is a hazard rate decomposition: the perceived instantaneous crash probability splits into two components that evolve in opposite directions—rising withdrawal pressure from expanding information diffusion and declining beliefs from Bayesian updating on survival. These two opposing forces create a characteristic hump-shaped pattern: withdrawals rise as the first force dominates, peak when forces balance, and then decline as survival evidence accumulates and the second force takes over. This decomposition explains both the panic phase (acceleration) and the recovery phase (deceleration), distinguishing the model from prior theories with monotonic dynamics.

4.1 The Agent Problem

Once informed about a potential solvency shock, depositors face a fundamental tension. They wish to enjoy the utility benefits of holding deposits, yet fear losing everything if mass withdrawals trigger collapse.

The agent's decision can be formalized through dynamic programming. Let $V(t)$ denote the expected value of \$1 in wealth at time t. Since deposits do not accrue interest, wealth remains constant absent a crash. The value function satisfies the Hamilton-Jacobi-Bellman equation:

$$0 = \dot{V}(t) + \max_{\alpha} \{u(1 - \alpha) + h(t)[\alpha - V(t)]\},$$

where $h(t)$ is the hazard rate—the instantaneous probability of a crash conditional on survival—and $\alpha \in [0, 1]$ is the fraction of wealth held in cash. The first term captures

[19]This focuses the analysis on run dynamics following information revelation. Modeling pre-shock deposit choice is interesting in itself but not the focus of this paper.

utility flow from deposits; the second captures expected value from a crash, equal to the probability $h(t)$ times the net gain $\alpha - V(t)$ (the agent retrieves the cash portion α but loses the continuation value $V(t)$).

Rearranging, the HJB becomes $0 = \dot{V} + u - h(t)V(t) + \max_\alpha\{(h(t) - u)\alpha\}$. Linearity in α implies bang-bang solutions: if $h(t) > u$, the agent withdraws everything ($\alpha^* = 1$); if $h(t) < u$, the agent holds everything in deposits ($\alpha^* = 0$). The intuition is simple: at the margin, moving one unit of wealth to cash costs u in utility flow but provides expected crash protection $h(t)$. The following lemma formalizes this result. Because these probabilities depend on the agent's learning time t_i, I henceforth write $h(t; t_i)$.

Lemma 1. *The optimal holding $\alpha^*(t; t_i)$ of an agent who learned at t_i at time t is given by:*

$$\begin{cases} \alpha^*(t;t_i) = 1 & \text{if } h(t;t_i) > u \\ \alpha^*(t;t_i) = 0 & \text{if } h(t;t_i) < u \\ \alpha^*(t;t_i) \in [0,1] & \text{if } h(t;t_i) = u \end{cases}$$

The result suggests a more reduced form interpretation for u. It represents a risk-tolerance threshold. Agents maintain deposits when crash risk falls below this threshold and withdraw when it exceeds it. This behavioral rule could be taken as primitive rather than derived from utility flows.

4.2 Stationary Equilibrium

The hazard rate $h(t; t_i)$ is the central equilibrium object. Agents' beliefs about others' withdrawal strategies determine the hazard rate, which in turn shapes their own optimal strategies. We can make this fixed-point problem tractable by focusing on stationary equilibria, where equilibrium behavior depends only on time since learning, not calendar time.

Definition 1. *A **stationary equilibrium** is an Perfect Bayesian Equilibrium satisfying:*

1. *The bank crashes at a fixed interval after the shock: $t_0 + \xi$.*
2. *Agents' holdings depend solely on elapsed time since learning the rumor: $\alpha(t; t_i) := \alpha(\tau)$, with $\tau = t - t_i$.*

Conditions (1) and (2) are two alternative way to define equilibria, they are logically equivalent. To understand why condition (2) implies condition (1), define the aggregate withdrawals at time t, given a shock at t_0, as:

$$AW(t; t_0) = \int_{t_0}^{t} \alpha(t; t_i)\, dG(t_i - t_0).$$

This expression integrates the withdrawal decisions $\alpha(t; t_i)$ of all agents, weighted by the density of agents who learned at each time $t_i \in [t_0, t]$. The collapse happens if and when $AW(t; t_0)$ reaches the threshold κ.

Suppose agents' optimal holdings depend only on $\tau = t - t_i$ (condition 2). Substituting into the expression for aggregate withdrawals and letting $\xi = t - t_0$ denote time since the shock, we obtain:

$$AW(\xi) = \int_0^{\xi} \alpha(\xi - s)\, dG(s).$$

The crash time is therefore characterized by $\xi^* = \inf\{\xi : AW(\xi) = \kappa\}$, which guarantees that the crash happens after a fixed amount of time, completing the proof that condition (2) implies condition (1).

The reverse implication is discussed in the next subsection.

4.3 Understanding the Hazard Rate

Lemma 2 below is one of central technical piece allowing tractability in the model. It shows that hazard rates depend only on the time since learning when crash is a the form $t_0 + \xi$, ensuring consistency in the definition of stationary equilibrium. Further, this form of stationarity in hazard rate allows a tractable description of their evolution, which will allow to establish sharp characterization of agent withdrawal behavior.

Lemma 2. *Suppose the crash happens a fixed amount of time after t_0, at $t_0 + \xi^*$. Consider $h(t_i + \tau; t_i)$, the hazard rate of collapse for an agent who learned at time t_i and evaluates it at τ periods after learning. The following properties hold:*

- *$h(t_i + \tau; t_i)$ is a function of τ only, i.e., it suffices to write $h(\tau) := h(t_i + \tau; t_i)$.*
- *$h(\tau) = \pi(\tau) h_f(\tau)$ where:*
  - *$\pi(\tau)$ is the posterior belief that the bank is fragile, and is decreasing in τ.*
  - *$h_f(\tau)$ is the posterior hazard rate of collapse of a fragile bank (which collapses with probability 1 if κ is reached), and is increasing in τ.*
  - *We have:*

$$\begin{cases} d\pi(\tau) = -(1 - \pi(\tau))\pi(\tau) h_f(\tau) d\tau, \\ dh_f(\tau) = \left(h_f(\tau) - \left(\frac{G''(\xi^* - \tau)}{G'(\xi^* - \tau)} + \lambda \right) \right) h_f(\tau) d\tau. \end{cases}$$

  .

- *$h(\tau)$ is unimodal.*

Proof. See Appendix A. □

Intuitively, if the crash occurs at $t_0 + \xi^*$, agents need only estimate t_0. Consider two agents who learn at different calendar times. The memoryless property of the exponential distribution ensures they update their estimate of t_0 identically. An agent's learning time reveals nothing about their position in the sequential awareness process. Consequently, all informed agents share the same initial hazard rate, regardless of when they learn. As time

passes, the only new information—that no crash has yet occurred—is common knowledge among informed agents, causing them to update beliefs identically and maintain synchronized hazard rates over time.

Figure 3 illustrates the dynamics captured by Lemma 2.[20] The total hazard rate $h(\tau)$ (purple curve) exhibits a characteristic hump shape: initially increasing as agents grow more worried about collapse, then decreasing as survival evidence accumulates and agents infer the rumor was likely false.

The decomposition $h(\tau) = \pi(\tau)h_f(\tau)$ reveals two opposing forces driving this pattern. The posterior belief that the bank is fragile ($\pi(\tau)$, blue curve) decreases monotonically as agents update based on survival. Each period without a crash provides evidence against fragility, with the strength of this evidence proportional to how likely a crash would have been had the bank been fragile (captured by h_f). The differential equation $d\pi = -(1-\pi)\pi h_f d\tau$ has logistic structure, making updates fastest when uncertainty is highest (π near 1/2) and slowest when beliefs approach certainty.

The dynamics of the conditional hazard h_f are best interpreted viewed backwards from the moment of collapse ξ (marked by the golden bar). In a reversed time scale, the process follows a logistic curve strictly *above capacity*. It begins at infinity—reflecting that the crash is imminent—and decays toward the time-varying capacity line $\lambda + G''/G'$ as we recede from the deadline. To build intuition, consider the simplified case where $G''/G' \approx 0$, corresponding to a constant speed of information diffusion (eg, uniform learning). Here, the capacity reduces to λ, the fundamental arrival rate of shocks; absent acceleration in learning, the hazard rate would simply settle toward the background risk of a shock (in backward time, as we get away form collapse time). The term G''/G' acts as a dynamic correction to this baseline, capturing the *curvature* of the rumor's spread. When information diffusion accelerates ($G''/G' > 0$), the effective risk floor rises above λ; when it decelerates, the floor drops, modulating the urgency of the run.

The interaction of these forces produces the unimodal total hazard rate. Early on, rapid increases in h_f dominate gradual declines in π, causing h to rise. Later, as survival evidence mounts and learning saturates, declining π dominates, causing h to fall. Since the hazard rate crosses the threshold u at most twice—once rising, once falling—agents optimally exit and reenter deposits once, as formalized in the following corollary.

Corollary 1. *In a stationary equilibrium with crash at $t_0 + \xi$, agents optimally exit at time τ_O and optimally reenter at time τ_I, with $\tau_O, \tau_I \in [0, \xi]$. We have $\tau_O < \tau_I$ and*

$$\tau_O = \inf\{\tau : h(\tau) > u\},$$
$$\tau_I = \sup\{\tau : h(\tau) > u\}.$$

If $h(\tau) < u$ for all $\tau \in [0, \xi]$, the agents never get out, and we write by convention $\tau_O = \tau_I = \xi$.

[20] All figures (excluding figures on empirical results Section 2 and Section 6) correspond to equilibrium quantities computed numerically. See Appendix C for details on the computational implementation. Baseline parameter values and figure-specific parameters are documented in Tables 6 and 7.

4.4 Characterization of Stationary Equilibria

The simplicity introduced by stationary equilibrium allows a clear characterization of equilibrium through a concise three-equation system, formalized in Proposition 1.

Proposition 1. *A stationary equilibrium comprises a learning distribution G, optimal exit time τ_O^*, reentry time τ_I^*, and crash time ξ^* satisfying:*

- *Learning dynamics:*
$$dG = (1 - G)G\beta dt$$
- *Exit and reentry conditions:*
$$\tau_O^* = \inf_{[0,\xi]}\{\tau : h(\tau) > u\}, \quad \tau_I^* = \sup_{[0,\xi]}\{\tau : h(\tau) > u\}$$
- *Crash condition:*
$$\xi^* = \inf\{\xi : G(\xi - \tau_O^*) - G(\xi - \tau_I^*) = \kappa\}$$

The exit and reentry conditions follow from Corollary 1. The crash condition exploits the single-exit, single-reentry structure: aggregate withdrawals equal the mass of agents who have exited but not yet reentered, which is simply $G(\xi - \tau_O^*) - G(\xi - \tau_I^*)$: the difference between the curves for exit and reentry, evaluated at crash time ξ^*.

The characterization exhibits a structure common to macroeconomic and mean-field game frameworks with three components: (1) individual optimality conditions—the exit and reentry rules from Lemma 1; (2) forward dynamics governing aggregate state variables—the

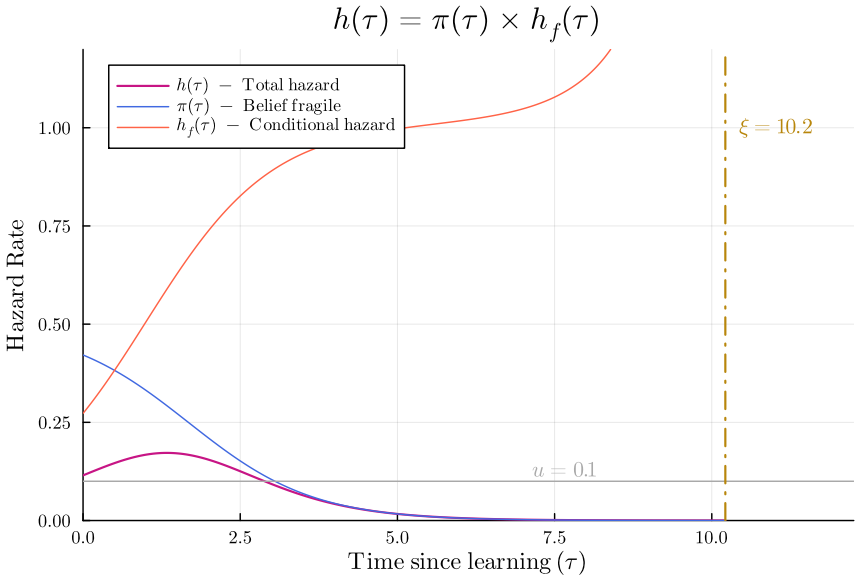

Figure 3: Hazard rate decomposition

Reading note: Decomposition of total hazard rate $h(\tau)$ (purple) into posterior fragility belief $\pi(\tau)$ (blue, declining) and conditional hazard under fragility $h_f(\tau)$ (orange, rising). Product $h = \pi \cdot h_f$ creates hump shape: initially rising as h_f increase dominates, later falling as π decline dominates.

logistic learning process that determines how information spreads through the depositor network; and (3) an aggregate consistency requirement—the crash condition ensuring that aggregate withdrawals $G(\xi^* - \tau_O^*) - G(\xi^* - \tau_I^*)$ equal the bank's withdrawal capacity κ precisely when the crash occurs. This system of equations can be solved numerically to compute equilibrium quantities (see Appendix C).

The system admits two types of equilibria. A "no-run" equilibrium occurs when $\xi^* = \infty$: the hazard rate never exceeds u, so agents never withdraw, and the bank survives (justifying the flat hazard-rate at 0). Such an equilibrium always exists (agents can always ignore the rumor). Conversely, a "run" equilibrium occurs when $\xi^* < \infty$: agents do withdraw, and the bank crashes at $t_0 + \xi^*$ if genuinely fragile. The existence of run equilibria depends on whether deposit utility (u) is sufficiently low and communication speed (β) sufficiently high to make collective withdrawals self-fulfilling despite agents' uncertainty about bank health. I characterize these existence conditions precisely in Section 5.

An important technical observation concerns the timing of withdrawals. Since the learning dynamics determine G, Proposition 1 effectively solves for three unknowns (τ_O^*, τ_I^*, ξ^*) using three conditions. However, the crash condition and the hazard rates[21] depends only on time differences ($\xi^* - \tau_O^*$ and $\xi^* - \tau_I^*$), making the system underdetermined. For generic parameter values, this forces a corner solution. The following corollary establishes that $\tau_O^* = 0$: agents withdraw immediately upon learning.

Corollary 2. *For generic parameter sets, any existing run equilibrium involves immediate withdrawal upon learning ($\tau_O^* = 0$).*

The intuition is the following. Suppose, as a candidate equilibrium, all agents withdraw immediately upon learning, leading to a crash at time $t_0 + \xi$. Consider an individual agent who takes this crash time as given. If $h(0) < u$, this agent would prefer to wait some $\tau > 0$ periods before withdrawing. However, since all agents are symmetric, they would form similar best-responses, which would push the crash from time ξ to $\xi + \tau$. Appendix A shows that shifting the crash by τ periods shifts the entire hazard schedule by τ periods.[22] Thus agents facing a crash at $\xi + \tau$ would find it optimal to wait 2τ, which further delays the crash, inducing still longer waiting, etc. This feedback continues without bound: waiting breeds more waiting, preventing any interior fixed point from existing. The system unravels to a no-run equilibrium with $\xi^* = \infty$. Only $\tau_O^* = 0$ can survive as an equilibrium—immediate withdrawal upon learning. Whenever parameters force $h(0) < u$ the equilibrium will therefore be a no-run equilibrium similar to a bubble[23]: agents keep their deposits even if they believe the bank is fragile because they believe other agents will similarly "speculate" and keep their deposits.

5 Flattening the Curve

Having characterized stationary run equilibria, this section turn to their dynamic properties. Runs exhibit a characteristic hump-shaped pattern of withdrawals—first rising, then

[21] See Appendix A.

[22] This is because agents care about how far away they estimate being from the crash.

[23] This is the kind of dynamics studied in Abreu and Brunnermeier (2003).

peaking, and finally falling if the bank survives. This "curve" of withdrawals is central to understanding run dynamics: the height determines whether the bank crashes. As in epidemic control, slowing the rate of contagion and reducing exposure duration can "flatten" this curve of withdrawals, reducing peak stress and potentially preventing crashes altogether.

5.1 The Anatomy of a Run

Figure 4 display the typical run dynamics. Aggregate withdrawals rise, peak when the gap between exits and reentries is largest, then decline as confidence returns. The peak's height determines whether the bank crashes.

To understand better the dynamics consider $G(t)$, the cumulative mass of informed agents, represented in red with a dotted line. Since agents withdraw immediately upon learning (Corollary 2), this curve also tracks the mass of agents who have withdrawn. The blue curve is $G(t-\tau_I)$ the mass of agents who have returned to holding deposits after initially withdrawing. Visually, it is simply $G(t)$ shifted by τ_I. The vertical distance between these curves equals aggregate withdrawals $AW(t) = G(t) - G(t-\tau_I)$ at each instant, in solid red (for $t \leq \tau_I$, no agents have yet reentered, so $AW(t) = G(t)$). Crash happens whenever AW crosses the horizontal line marking κ. For a fragile bank, the trajectory stops at crash time ξ^*; the continuation beyond this point shows the recovery dynamics that would occur for a safe bank that survives the peak.

The hump arises from the interplay between exits and reentries. Early on, rumors spread fast and many agents exit simultaneously. Since most just learned, they don't reenter yet, causing AW to rise. Over time, however, more agents who exited early accumulated enough evidence from the absence of crash to believe the rumor was false begin reentering, causing the rate of withdrawal growth to slow. For healthy banks that survive collapse reentries eventually outpace new exits, and AW begins to decline—the recovery phase begins.

Visually it is clear that the peak depends on two factors: how steep are the exit and reentry curves and how close they are to each others. The first depends on β, the second on agents optimal actions and notably on u. Figure 5a and Figure 5b show how run dynamics vary with communication speed and deposit utility. Fast communication (high β) produces a sharper, taller peak that arrives sooner, reflecting rapid information diffusion. Low deposit utility (low u) also produces a higher peak because agents stay withdrawn longer: when deposits are less attractive, the hazard rate must fall further before agents are willing to reenter, increasing τ_I. With agents withdrawn for longer periods, more agents are simultaneously withdrawn at any given time, increasing the gap between exits and reentries. Understanding these forces is essential for designing policies to mitigate runs, a topic I turn to next.

5.2 Reentry Time

The peak of aggregate withdrawals—denoted $\bar{AW} = \max_t AW(t)$—is the critical quantity determining whether a run leads to collapse. As discussed in the previous subsection, the peak arises from the interplay between the learning curve's steepness (governed by β) and the gap between exit and reentry (τ_I, since $\tau_O = 0$). Borrowing insight from epidemiology, we can identify two main drivers of peak height: the "contact rate" (communication speed β) and the "sickness period" (withdrawal duration τ_I). Just as epidemic peaks depend on

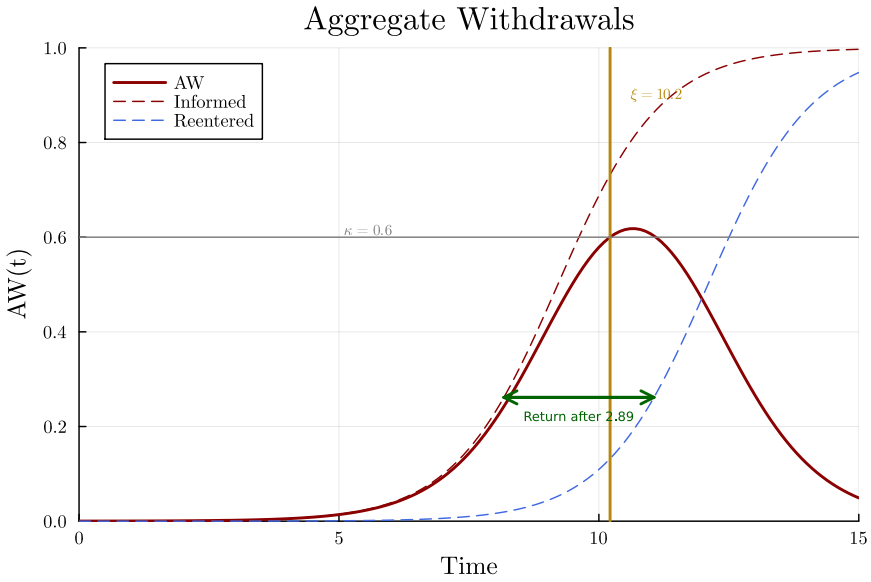

Figure 4: Dynamics of a run equilibrium

Reading note: Dotted red curve shows cumulative mass of informed/withdrawn agents $G(t)$. Dotted blue curve shows mass who reentered $G(t - \tau_I)$. Horizontal distance correspond to reentry time. Vertical distance equals aggregate withdrawals $AW(t)$, in solid red. Horizontal line at κ marks collapse threshold. Hump-shaped AW peaks then declines as reentries accelerate.

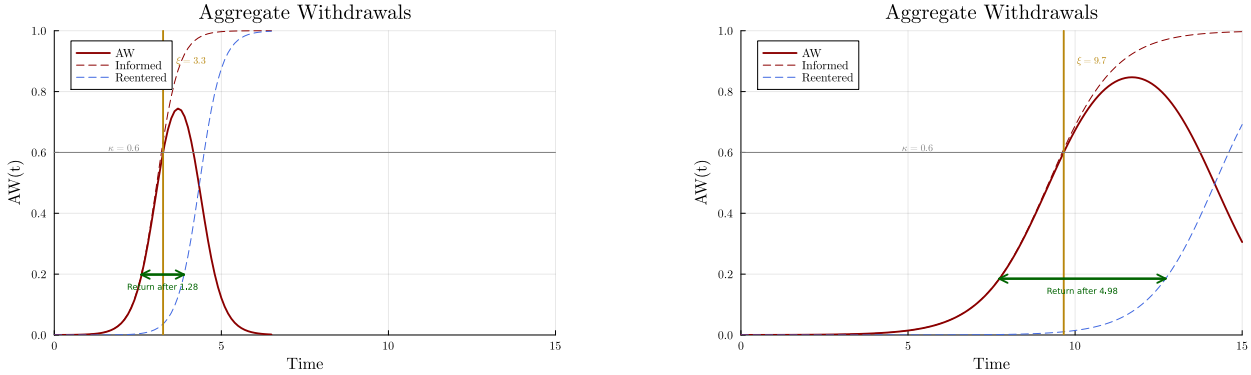

(a) Fast communication

(b) Low deposit utility

Figure 5: Dynamics under alternative contexts.

Reading note: Panel (a): Fast communication produces steeper curves and higher, earlier peak. Panel (b): Low deposit utility increases reentry time τ_I, widening gap between exit/reentry curves and raising peak withdrawals.

how fast a disease spreads and how long individuals remain sick, run peaks depend on how fast rumors spread and how long agents remain withdrawn.[24]

[24]Longer withdrawal durations increase stress on banks balance sheets like extended patient stays exercise stress on hospital capacity. Standard epidemiology is typically also concerns about how long agents are *contagious*. In my model agents are contagious forever, because informed agents always pass on the information, even after reentry. However, in the social learning extension (Section 7.3) agents are contagious only when

A key difference from standard epidemiological models is that the withdrawal duration is endogenous in my model—agents choose when to reenter based on their assessment of immediate crash risk. The reentry time τ_I is determined by when the hazard rate $h(\tau)$ falls below the utility threshold u. Higher deposit utility leads to earlier reentry because agents are willing to accept higher risk to enjoy deposit benefits. The following lemma formalizes how parameter changes affect reentry timing.

Lemma 3 (Reentry Time Comparative Statics)**.** *Consider a stationary run equilibrium characterized by (ξ^*, τ_I^*), where $\xi^* < \infty$ is the crash time and τ_I^* is the reentry time. Assume such run equilibria continue to exist in a neighborhood of the parameters. Then, τ_I^* is locally:*

- *non-increasing with respect to increases in u, and η.*
- *non-decreasing with respect to increases in p.*

Furthermore, if $\tau_I^* < \xi^*$ then the above relationships hold strictly: τ_I^* is strictly decreasing in u, η and strictly increasing in p.

Proof. See Appendix A. The Appendix also discuss parameter restrictions ensuring $\tau_I^* < \xi^*$. □

The lemma confirms that making deposits more attractive (higher u) induces agents to reenter sooner, reducing τ_I. This in turn reduces the peak of withdrawals by decreasing the time interval during which agents are simultaneously withdrawn. Similarly, stronger bank fundamentals (lower p, meaning higher probability the bank is healthy) accelerate reentry because agents become reassured more quickly that the rumor was false.[25]

5.3 How to Kill Runs

Can we reduce the peak sufficiently to prevent runs altogether? The answer is yes—there exists a threshold level of deposit utility above which run equilibria cease to exist.

The intuition is straightforward. As u increases, agents reenter sooner, lowering the peak of withdrawals. At some critical value $\bar{u}$, the peak falls below the fragility threshold κ, meaning that even if the bank is fragile, withdrawals never reach the critical mass needed to trigger collapse. But if withdrawals never reach κ, a fragile bank never crashes, which eliminates the very risk that would justify withdrawing in the first place. Agents anticipating that the peak stays below κ have no reason to run, and the run equilibrium unravels. The result is formalized in Proposition 3.

---

they are withdrawn themselves, creating interesting dynamics.

[25] When interpreting the empirical evidence from Section 2, it is important to clarify how the model's solvency parameter κ relates to the empirical measure of bank safety. In the model, κ represents the mechanical withdrawal capacity—the fraction of the deposit franchise that can be lost before insolvency. However, the empirical κ (constructed from balance sheet data) better captures overall bank safety, which operates primarily through the prior probability p that the shock is real. One can formalize this by interpreting the empirical measure as an expected value: $\bar{\kappa} = p\kappa_{\text{low}} + (1-p)\kappa_{\text{high}}$, where $\kappa_{\text{low}} < 1$ and $\kappa_{\text{high}} > 1$ are fixed across banks, and variation in $\bar{\kappa}$ reflects changes in perceived safety p rather than mechanical capacity. Under this interpretation, higher empirical κ (safer banks) corresponds to lower p, which accelerates learning and induces earlier reentry—as shown in the lemma above. The empirical findings in Section 2 and their interpretation in Section 6 reflect this "safety belief channel" rather than the direct mechanical effect of withdrawal capacity.

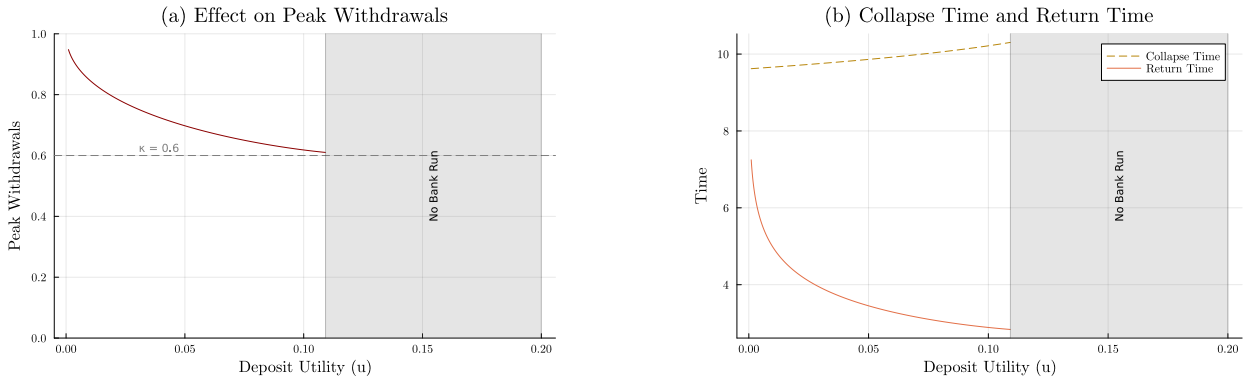

Figure 6: Effect of deposit utility on withdrawals and collapse

Reading note: Panel (a): Peak aggregate withdrawals $A\bar{W}$ versus deposit utility u. Higher u reduces peak, approaching threshold κ (dashed line). At $\bar{u}$, peak vanishes (no run). Panel (b): Crash time ξ^* and reentry time τ_I^* versus u. Higher u delays crash, principally because agents reenter sooner, making peaks lower.

Proposition 2. *Given parameters (β, κ, p, η), there exists a threshold $\bar{u}$[26] such that:*

- *No run equilibrium exists if $u \geq \bar{u}$.*
- *A unique run equilibrium exists if $u < \bar{u}$.*

Additionally, the peak withdrawal level $A\bar{W} = \max_t AW(t)$ is decreasing in u for $u < \bar{u}$.

Proof. See Appendix A. □

Figure 6 illustrates these dynamics. Panel (a) shows that peak withdrawals decrease monotonically in u, approaching κ from above and vanishing at threshold $\bar{u}$.[27] Panel (b) shows that crash time ξ^* increases with u as agents reenter sooner, slowing withdrawal accumulation.

From a normative perspective, Proposition 3 suggests that increasing deposit attractiveness—through higher interest rates[28] or improving deposit convenience—can prevent runs altogether. The next subsection examines how the effectiveness of such policies depends critically on communication speed.

5.4 The Role of Depositor Connectedness

Depositor connectedness β affects run dynamics first through a direct channel—faster communication steepens the learning curve G, concentrating withdrawals in a shorter time window. However, equilibrium effects are more subtle: faster communication also alters the

[26] Under the natural assumption $G(\eta) \geq \kappa + G(0)$ we have $\bar{u} > 0$. It is a natural assumption guaranteeing the awareness window is large enough so that at least κ agents have learned by the time learning stops. $G(0)$ is the initial condition, typically close to 0.

[27] It is possible in some cases that runs stop existing before reaching κ. Such cases arise when $h(0)$ drops below u and agents start waiting before withdrawals, prompting unraveling of the collapse described at the end of Section 4.

[28] Section 7.2 extends the model to interest-bearing deposits ($r > 0$). The interest rate r plays a similar role to the utility flow u: higher r induces earlier reentry and reduces peak withdrawals.

hazard rate h that agents form, potentially changing their reentry decisions. Fortunately, the model exhibits a useful scaling property that allows studying the effect of β analytically.

The key observation is that β rescales time in the model. To see this, note that all time derivatives in the equilibrium system are proportional to β. If we transform time by $t \to t/\beta$, then the differential equations remain unchanged except that $\beta \to 1$, $u \to u/\beta$, and $\lambda \to \lambda/\beta$. Since $\eta := G^{-1}(1-\epsilon)$ represents the time to reach awareness saturation, it scales inversely with β. Specifically, in the non-scaled system there exists a $\bar{\eta}$ such that $\eta = \bar{\eta}/\beta$. Under the time transformation, $\eta \to \bar{\eta}$, which is independent of β, ensuring the model structure remains intact.

Recalling the interpretation of learning dynamics as random matching, β represents the (Poisson) meeting rate between agents (which can be informed or non-informed). Accordingly, $1/\beta$ is the expected time between two meetings. The relevant statistic for determining run dynamics are u/β—the expected utility flow accumulated between meetings—and λ/β—the relative speed of shocks versus information diffusion. Increasing β is equivalent to jointly reducing deposit utility and the prior distribution for t_0. While it is complex to tease out both effects in full generality, I can show that under a mild restriction of parameters, the first effect will dominate.

Corollary 3. *Assume parameters $(u, \lambda, \kappa, p, \eta)$ satisfy $\eta \leq 1/\lambda$. There exists a threshold*[29] *$\bar{\beta} \geq 0$ such that:*

- *No run equilibrium exists if $\beta < \bar{\beta}$.*
- *A unique run equilibrium exists if $\beta > \bar{\beta}$.*

Additionally:

- *The peak withdrawal $A\bar{W} = \max_t AW(t)$ is increasing in β for $\beta > \bar{\beta}$.*

Proof. See Appendix A. □

The condition $\eta \leq 1/\lambda$ is sufficient but not necessary.[30] It has a natual interpretation for the banking context: the time scale of learning should be shorter than the one of solvency shocks. More precisely, the time it takes for a shock to spread to almost the full population (i.e. reach $G(1-\epsilon)$) should be shorter than the expected time before another shock occurs, that is $(\frac{1}{\lambda})$.[31]

Corollary 3 establishes that lower coordination frictions amplify runs: higher β increases peak withdrawals. The result aligns with the empirical observations made in Section 2: banks with high HHI (low coordination frictions, high coordination risk) experienced substantially larger stock price declines during the 2023 crisis. More importantly it establish the reverse direction: disperse base can make run less severe, to a point where the peak drops below solvency requirement, precluding runs altogether.

[29] If $\kappa + G(\eta) > 1$, then $\bar{\beta} > 0$. Since $G(\eta) = 1 - \epsilon$ for small ϵ, this condition typically holds.

[30] Numerical investigation actually suggests the corollary holds without restriction.

[31] In the model I assume only on shock realization, but the interpretation remains.

In addition, the fact that deposit utility becomes u/β under rescaling has an interesting normative implication: the effectiveness of deposit-enhancing policies depends critically on coordination frictions. The threshold $\bar{u}$ required to prevent runs scales roughly linearly with β[32]: when coordination frictions are two times lower (higher β, faster communication), deposits must be made twice as attractive to achieve the same run-prevention effect.

Figure 7 illustrates this interaction through a heatmap showing how peak withdrawals vary jointly with u and $1/\beta$ (the average time between meetings). The figure reveals two key patterns. First, the threshold relationship is approximately linear—the frontier where runs disappear traces out an inverse relationship between u and $1/\beta$, consistent with the scaling property. Second, the marginal effect of increasing u is larger when communication is slow (high $1/\beta$): the heatmap's color gradient is steeper in regions of slow communication.

This interaction has important implications for bank risk management. When choosing deposit yields (which have a similar effect as u, see Section 7.2), banks trade off stability against profitability: higher yields prevent runs by inducing earlier reentry and reducing peak withdrawals, but erode profit margins. The severity of this tradeoff depends critically on depositor concentration. Banks with concentrated, well-connected depositor bases must offer substantially higher yields to achieve run-prevention, which may severely erode profitability. In contrast, banks with geographically dispersed depositors can achieve run-stability with more modest yield enhancements. This suggests that depositor base composition—a feature typically considered in the context of funding stability—also matters for run prevention through its effect on communication speed.

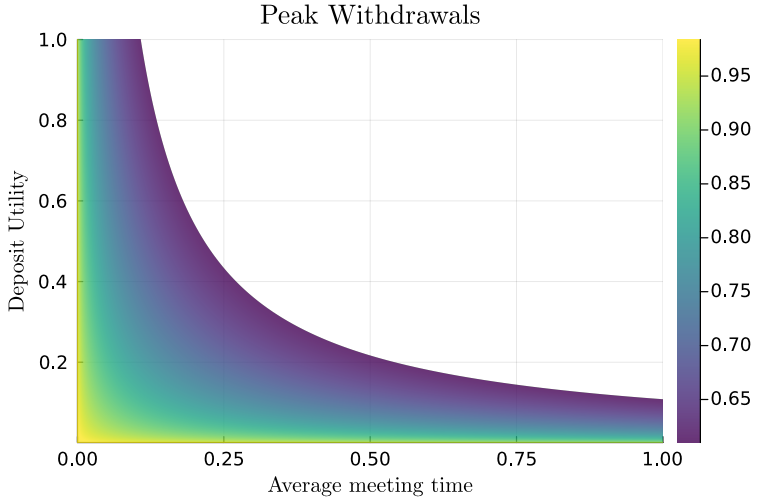

Figure 7: Interaction of u and $1/\beta$ on the peak of withdrawals

Reading note: Heatmap shows peak withdrawals $A\bar{W}$ as function of deposit utility u (x-axis) and average meeting time $1/\beta$ (y-axis). Dark blue indicates low peaks while yellow indicate high peaks. Run-prevention threshold shows the inverse relationship between u and $1/\beta$. Steeper gradient at high $1/\beta$ shows stronger marginal effect of u when communication is slow.

[32]It scales linearly if we ignore effects from λ/β in the re-scaling, which are typically small.

6 Fitting the Model to Crisis Dynamics

I now demonstrate the model's tractability by fitting the closed-form expression for aggregate withdrawals to intraday stock returns during the crisis period, treating stock prices as a proxy for deposit dynamics. The exercise serves two purposes. First, and most importantly, it demonstrates the model's tractability: the closed-form solution makes it feasible to recover structural parameters from observational data. Second, it allows to interpret the crisis thorough the lenses of my model—in particular, whether observed heterogeneity reflects differences in depositor communication networks or differences in perceived bank fragility.

6.1 Methodology

I fit the model to intraday stock returns for banks in my sample during an extended crisis period, including the beginning of recovery (March 6–21, 2023).[33] Specifically, I estimate the following reduced form equation for aggregate withdrawals from my model:

$$AW(t) = G(t) - G(t - \tau_I) = \frac{1}{1 + e^{-\beta(t - t_{\text{mid}})}} - \frac{1}{1 + e^{-\beta(t - \tau_I - t_{\text{mid}})}},$$

where G is the logistic learning curve and t_{mid} denotes the midpoint of the logistic curve (determined by the initial condition). I fit this functional form to observed stock returns separately for each bank in my sample using nonlinear least squares, estimating three parameters: communication speed β, reentry time τ_I, and the timing parameter t_{mid}. The model is estimated on 10-minute high-frequency return data, smoothed with a 1h rolling window to reduce noise.

Remark 2 (Interpretation of Estimated Parameters)**.** *The communication speed β is an exogenous structural parameter, determined by the depositor network's infrastructure (geographical clustering in Section 2 but alternatively social media penetration, shared VC networks, etc.). In contrast, the reentry time τ_I is an endogenous equilibrium outcome—a model-implied parameter that depends on both exogenous primitives (β, κ) and equilibrium actions. My estimation strategy treats both as parameters in the reduced-form equation, then examines how they vary with observable bank characteristics.*

6.2 Fit

Figure 8 presents model fits for six representative banks spanning different crisis experiences. These banks were selected to represent diverse cases: banks that faced severe difficulties

[33] Two methodological caveats merit acknowledgment. First, Cipriani et al. (2024) document that while stock returns correlate strongly with deposit outflows during the run phase of the 2023 crisis, this correlation weakens during recovery periods—suggesting stock prices may not fully capture reentry dynamics. Second, my model require that agents cannot observe aggregate withdrawal curves in real time, as this would allow them to time runs precisely. Stock prices, however, are publicly observable. I reconcile this tension by viewing stock returns as reflecting information available to market participants distinct from depositors. These limitations however are real and the exercise is best interpreted as illustrating the model's quantitative tractability—showing that the closed-form solution can be meaningfully estimated—rather than providing a definitive empirical test. An ideal setting would perform that exercise on actual deposit outflows.

during the crisis (SVB, Signature, PacWest), large retail banks (US Bank, Citi), and a local regional bank (Bank of Hawaii). SVB and Signature exhibit rapid price declines, while Citi and US Bank show more gradual dynamics despite similar initial conditions. The model captures these patterns reasonably well, achieving a median $R^2 = 0.812$ across all banks.[34] The heterogeneity arises naturally from variation in the estimated parameters: banks experiencing severe crises have higher estimated β (faster information spread) and higher τ_I (longer withdrawal periods).

6.3 Analysis of Estimated Parameters

Using the estimated model parameters, I examine whether these model-implied measures correlate with the exogenous proxies for fundamental risk and coordination frictions introduced in Section 2. Specifically, I test whether estimated communication speed $\hat{\beta}$ correlates with depositor HHI (my proxy for coordination frictions), and whether estimated reentry time $\hat{\tau}_I$ correlates with the κ solvency threshold measured from deposit franchise values.

I first examine whether depositor concentration proxies for communication speed. If the HHI measure captures information diffusion rates as the model suggests, one should observe a positive correlation between HHI and estimated $\hat{\beta}$. Table 2 reports the results. Columns (2) to (4) shows that HHI is indeed strongly positively correlated with $\hat{\beta}$, supporting the interpretation that depositor concentration facilitates information transmission.

Interestingly, κ also seems to play a role. Safer banks (higher κ) exhibit slower estimated $\hat{\beta}$. This is somewhat puzzling from the model's perspective, since κ is a measure of fundamental fragility rather than network structure, and should not directly affect communication speed. The correlation may reflect omitted factors—for instance, banks with riskier business models (low κ) might also attract depositors who are better connected through industry networks. Alternatively, it could indicate that information spread depends on depositors' behavior such as through social learning mechanisms discussed in Section 7.

The reentry time τ_I presents a different pattern. Table 3 regresses estimated τ_I on both HHI and κ. The solvency measure κ is strongly negatively correlated with $\hat{\tau}_I$: safer banks exhibit shorter withdrawal durations. Interpreting this through the model requires nuance. Strictly speaking, increasing the withdrawal capacity κ in the model mechanically extend run duration, and through it extend τ_I. This is because when κ is high, runs take time to coalesce, making agents wait longer. It is a mechanical effect, unrelated to the riskiness of a bank. The empirical result is better interpreted through the view that high-solvency banks are perceived as having lower ex ante probability of fragility (lower p in the model). As established in Lemma 3, lower p accelerates belief updating and induces significantly earlier reentry. The data suggest this "safety belief channel" dominates the "capacity channel": strong fundamentals shorten runs by reassuring depositors, not by lengthening the time to collapse. The HHI coefficient is statistically insignificant. As discussed in Appendix A (Remark 3), the theoretical effect of connectedness on physical reentry time is actually ambiguous: while higher β increases reentry time in scaled units, translating to physical time shrinks it back. The insignificant HHI coefficient is therefore consistent with the model's predictions.

[34] Figure 22 in Appendix B presents the full distribution of R^2 values and additional fit examples.

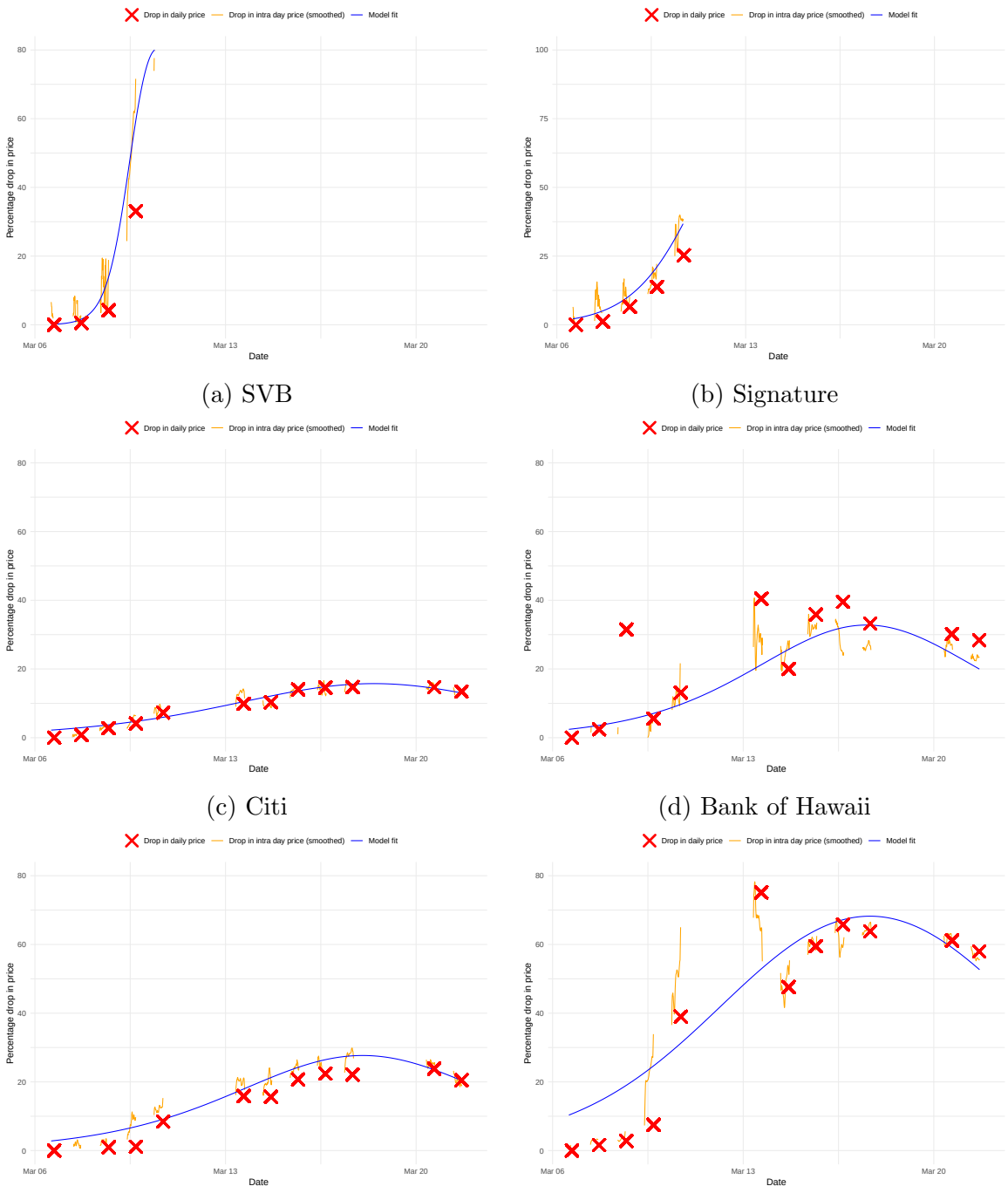

(a) SVB (b) Signature

(c) Citi (d) Bank of Hawaii

(e) US Bank (f) PacWest

Figure 8: Stock prices and model fit for selected banks.

Reading note: In orange, high frequency price change (TAQ) from March 6th baseline price. In red end-of-day cumulative returns (CRSP) from same date. In blue, fitted logistic curve. Panels illustrate heterogeneous dynamics: sharp decline with no recovery (SVB, Signature), strong decline followed by partial slow recovery (PacWest), or moderate declines (Citi, Bank of Hawaii, US Bank). Overall

Taken together, these results illustrate that the model developed in Sections 3–5 can be brought to data in a meaningful way. The closed-form expression for aggregate withdrawals allows estimation of structural parameters using standard methods, and the recovered parameters vary sensibly with observable bank characteristics. While this exercise does not constitute a definitive test of the model's microfoundations—the data limitations and proxy measures discussed above preclude strong causal claims—it demonstrates that the theoretical mechanisms provide a useful lens for interpreting heterogeneous crisis dynamics.

Dependent Variable:	**Estimated β**			
	(1)	(2)	(3)	(4)
Solvency κ	-0.131***		-0.129***	
	(0.034)		(0.031)	
Depositor HHI		0.469***	0.465***	0.060
		(0.089)	(0.085)	(0.098)
Indicator ($\kappa < 1$)				-0.062**
				(0.024)
$\kappa < 1\times$ Depositor HHI				1.062***
				(0.155)
Uninsured Share	0.433***	0.332***	0.293***	0.237***
	(0.093)	(0.094)	(0.090)	(0.084)
Dom. Deposits (log)	0.006	0.004	0.013	0.007
	(0.010)	(0.009)	(0.009)	(0.008)
Wholesale sh. of dep.	-0.273	-0.463*	-0.367	-0.525**
	(0.248)	(0.240)	(0.230)	(0.211)
Constant	0.143	0.041	0.042	0.052
	(0.143)	(0.140)	(0.134)	(0.127)
Observations	173	173	173	173
R^2	0.227	0.276	0.344	0.449

*Note: *** p<0.01, ** p<0.05, * p<0.1.*

Table 2: Relationship of estimated β with bank characteristics.

Reading note: Regressions of estimated communication speed $\hat{\beta}$ on bank characteristics. Column (2) shows HHI is strongly positively correlated with $\hat{\beta}$ ($R^2 = 0.276$), supporting the hypothesis that depositor concentration facilitates information transmission. Solvency measure κ is negatively correlated, suggesting safer banks experience slower rumor diffusion.

Dependent Variable:	**Estimated τ**			
	(1)	(2)	(3)	(4)
Solvency κ	-1.730***		-1.726***	
	(0.490)		(0.491)	
Depositor HHI		1.028	0.979	0.712
		(1.386)	(1.342)	(1.715)
Indicator ($\kappa < 1$)				0.699
				(0.430)
$\kappa < 1\times$ Depositor HHI				0.428
				(2.713)
Uninsured Share	5.025***	5.245***	4.730***	4.868***
	(1.356)	(1.456)	(1.417)	(1.465)
Dom. Deposits (log)	0.410***	0.308**	0.425***	0.366**
	(0.143)	(0.145)	(0.145)	(0.147)
Wholesale sh. of dep.	3.691	2.203	3.494	2.708
	(3.605)	(3.722)	(3.621)	(3.707)
Constant	-3.993*	-4.220*	-4.207**	-5.341**
	(2.079)	(2.172)	(2.102)	(2.226)
Observations	173	173	173	173
R^2	0.244	0.190	0.246	0.213

*Note: *** p<0.01, ** p<0.05, * p<0.1.*

Table 3: Relationship of estimated τ_I with bank characteristics.

Reading note: Regressions of estimated reentry time $\hat{\tau}_I$ on bank characteristics. Solvency measure κ is strongly negatively correlated with $\hat{\tau}_I$: safer banks exhibit shorter withdrawal durations. This reflects the "safety belief channel" (lower perceived fragility p induces earlier reentry) dominating the mechanical capacity effect. HHI coefficient is statistically insignificant, consistent with the ambiguous theoretical prediction discussed in the appendix.

7 Extensions

This section extends the baseline model in three directions. First, heterogeneity in learning speeds allows some depositors to be better connected than others. Second, deposits may accrue interest at rate $r > 0$. Third, agents may learn by observing others' withdrawal behavior rather than through word-of-mouth communication.

While some analytical results may be possible, they are generally complex and the results obtained in this section are numerical. I refer to Appendix C for a discussion on the numerical implementaion.

7.1 Heterogeneity in Learning Speed

The baseline model assumes all agents learn at the same rate β. In practice, depositors vary in how connected they are to information networks. Some depositors—such as large institutional investors or those active on social media—learn quickly about rumors, while others learn more slowly. The effects of such heterogeneity are not obvious as it affects both individual withdrawal strategies and aggregate run dynamics.

I extend the model by dividing agents into K types indexed by k, each learning at rate β_k. Type k comprises a fraction p_k of the population. The learning dynamics for each type are:

$$dG_k(t) = (1 - G_k(t)) \times \omega(t) \times \beta_k \, dt,$$

where $\omega(t) = \sum_{k'} p_{k'} G_{k'}(t)$ is the overall fraction of informed agents. An uninformed agent of type k meets others at rate β_k, with probability $\omega(t)$ of meeting an informed agent. The system of equations can be explicitly interpreted as a mean-field approximation of rumor spreading on an actual network. As discussed in Newman (2018), the approximation holds when the expected degree of a randomly selected neighbor is independent of one's own degree.[35]

Faster learners become informed earlier, which accelerates information spread to slower learners, coupling the dynamics across types. Equilibria can still be characterized as before: each type has its own exit time $\tau_{O,k}$ and reentry time $\tau_{I,k}$. As in the homogeneous case, a counting argument shows that not all exit times can be interior.

However, faster types need not exit immediately. Because they learn earlier and have better information about the timing of the run, they can afford to speculate by delaying their exit. Well-connected agents therefore face less run risk. They can wait until the last moment to withdraw, maximizing their time holding deposits while still avoiding the crash. Network position thus creates inequality: better-connected agents gain both earlier information and the ability to exploit it.

Figure 9 illustrates equilibrium dynamics in a two-type model with mostly slow agents (90%) and a small fraction of very fast agents (10%, learning 100 times faster). Aggregate withdrawals primarily track the gradual buildup from slow agents who withdraw immediately upon learning. Fast agents, despite being few, create a sharp concentrated spike that triggers the crash as they coordinate their exit. Visually we observe an intense run pressure in a narrow window before collapse. Figure 9 also shows interesting recovery dynamics. After

[35] Alternatively we can keep the interpretation of random matching but with heterogeneous rates.

the crash, the withdrawal curve exhibits a slight relapse as fast agents reenters. Slow agents however continue exiting and reach their peak withdrawal rate only later, causing aggregate withdrawals to briefly increase again before the long recovery begins. The asymmetric run and recovery is consistent with empirical evidence on protracted recoveries.

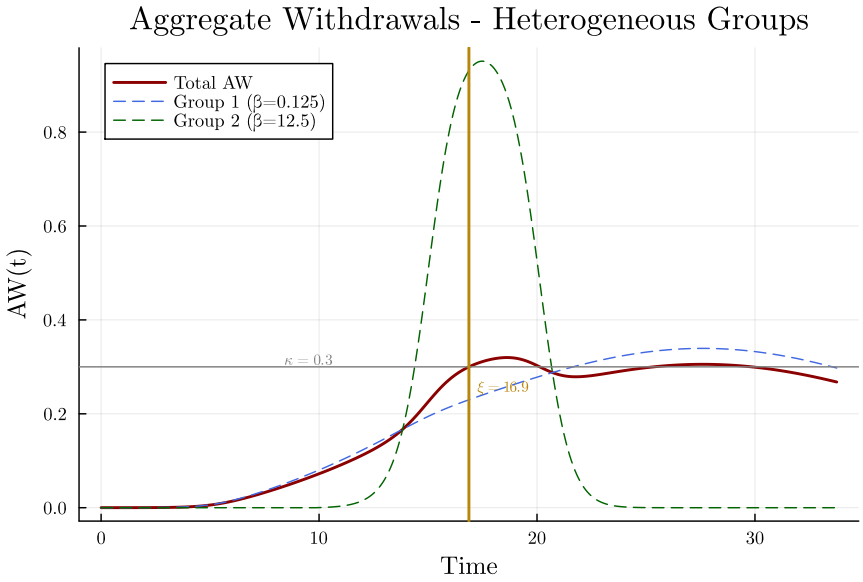

Figure 9: Equilibrium dynamics under heterogeneous learning speeds

Reading note: Aggregate withdrawals with two depositor types: slow agents (90%) who withdraw immediately upon learning, and fast agents (10%, learning 100× faster) who delay withdrawal to speculate. The curve primarily tracks gradual buildup from slow agents, with a sharp concentrated spike just before crash from fast agents' coordinated exit. After the crash, a slight relapse occurs as slow agents reach their peak withdrawal rate, before entering a prolonged recovery.

7.2 Interest Bearing Deposits

Throughout the main analysis, I assumed deposits do not accrue interest, making agents' holding decisions essentially static. I now relax this assumption and show how to solve the problem when deposits earn interest at rate $r > 0$. While this complicates the analysis, numerical exercises confirm that all main results continue to hold.

When $r > 0$, the agent's problem becomes a dynamic programming problem. With wealth growing at rate r, the agent's continuation value depends on both wealth level W and time since learning τ: $V(W, \tau)$. However, utility's homothetic structure—linear in wealth—implies multiplicative separability of the value function: $V(W, \tau) = W \times V(\tau)$, where $V(\tau)$ is the value of \$1 of wealth. The optimal value $V(\tau)$ solves the Hamilton-Jacobi-Bellman equation:

$$\begin{aligned} 0 &= \dot{V} + \max_{\alpha(\tau)} \{(u + rV(\tau))(1 - \alpha(\tau)) + h(\tau)(\alpha(\tau) - V(\tau))\} \\ \iff 0 &= \dot{V} + h(\tau)(1 - V(\tau)) + \max\{u + rV(\tau) - h(\tau), 0\}. \end{aligned}$$

The HJB captures the agent's tradeoff when deciding how much wealth to stash in cash. The marginal cost is $(u+rV(\tau))$, which now includes both utility flow u and deposit returns $rV(\tau)$. The benefit mirrors Section 4.1: retrieving the dollar stashed in cash if the bank crashes immediately, which occurs with probability $h(\tau)$. Crucially, agents retrieve the nominal dollar value, not the continuation value $V(\tau)$.

As in the main case, linearity in α implies bang-bang solutions: the agent either holds everything in deposits or withdraws everything to cash. Unlike with no interest, however, $V(\tau)$ now depends on future actions and must be solved as part of the equilibrium. The optimal strategy is:

$$\alpha^*(\tau) = \begin{cases} 1 & \text{if } u + rV(\tau) < h(\tau) \\ 0 & \text{if } u + rV(\tau) > h(\tau) \end{cases}$$

To prevent V from growing unboundedly when crash risk vanishes, I introduce an exogenous maturity process:[36] deposits mature at rate $\delta > r$, yielding \$1 upon maturity (e.g., the bank closes after repaying all deposits). The modified HJB becomes:

$$0 = \dot{V} + (h(\tau) + \delta)(1 - V(\tau)) + \max\{u + rV(\tau) - h(\tau), 0\},$$

with terminal condition $V(0) = (u+\delta)/(r+\delta)$, representing the present value of holding \$1 in a safe deposit: convenience yield u, interest r, and maturity payoff 1 at rate δ.

The value function $V(\tau)$ inherits properties from $h(\tau)$: it is non-monotonic, reflecting the interplay between capital gains, crash risk, and maturity. Figure 10 shows the hazard rate decomposition in this extended model. The dynamics remain qualitatively similar to the baseline, with $h(\tau)$ unimodal and unique exit and reentry times.

Intuitively, the effect of r parallels that of u: higher interest rates make deposits more attractive, inducing earlier reentry and reducing peak withdrawals. Numerical exercises confirm that the comparative statics from Section 5 continue to hold. In particular, there exists a threshold $\bar{r}$ (analogous to $\bar{u}$) above which runs cannot occur, and this threshold scales linearly with communication speed β.

7.3 Social Learning

The baseline model assumes agents learn about solvency shocks through word-of-mouth: informed agents directly communicate the rumor to those they meet. A more realistic mechanism that I study now is social learning: agents observe others' withdrawal behavior and infer the presence of a rumor from these actions. While this mechanism offers additional realism and aids interpretation of empirical patterns, the resulting equilibria remain qualitatively analogous to the baseline case, with equilibrium objects differing only modestly in quantitative terms.

Under social learning, agents meet others at rate β as before, but now observe only whether the person they meet is currently withdrawn from the bank. If they observe a

[36]The constraint $\delta > r$ ensures that the value of deposits remains bounded. Economically, it requires that deposits mature faster than they appreciate and the continuation value would diverge. Alternatively we can think of δ as the rate of an idiosyncratic liquidity shock forcing agents to consume their wealth.

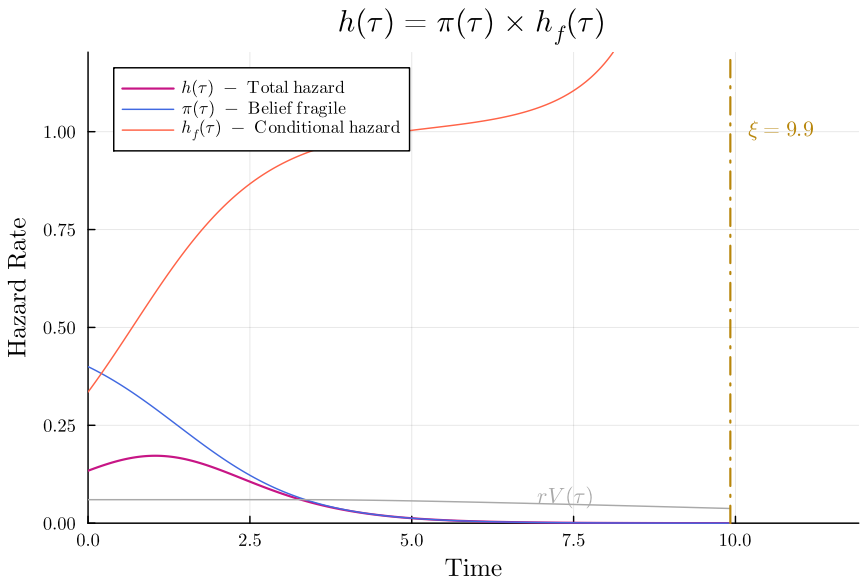

Figure 10: Hazard rate decomposition with interest rates

Reading note: The hazard rate $h(\tau)$ (purple) remains unimodal, equaling subjective crash probability $\pi(\tau)$ (blue, declining) times conditional crash rate $h_f(\tau)$ (red, rising). In gray the instantaneous reward for deposit: utility and wealth appreciation.

withdrawal, they infer a rumor may be circulating. The learning dynamics now depend on aggregate withdrawals rather than the fraction of informed agents:

$$dG(t) = (1 - G(t))AW(t)\beta\, dt.$$

Uninformed agents still meet others at rate β. However, the probability that this meeting is with a withdrawn agent equals $AW(t)$, the aggregate withdrawal level. This couples learning directly to withdrawal behavior.

The equilibrium definition must be modified to account for this coupling. A stationary equilibrium now requires that learning and withdrawal dynamics jointly satisfy:

$$\begin{aligned} dG(t) &= (1 - G(t))AW(t)\beta\, dt \\ AW(t) &= G(t) - G(t - \tau_I), \end{aligned}$$

where the second equation uses the fact that agents still withdraw immediately upon learning and reenter at τ_I. The equilibrium is characterized by solving these coupled equations simultaneously.

One key difference from the baseline is that withdrawn agents act as "infectious" only while withdrawn. In the baseline, agents remain informed forever, continuing to spread the rumor even after reentering. Under social learning, agents who reenter no longer contribute to information diffusion because they no longer exhibit withdrawal behavior. Figure 11 illustrates this mechanism: social learning produces slower, more gradual runs because the "infectious period" is now endogenous, equaling the withdrawal duration τ_I. This creates an amplification effect: increasing u not only induces earlier reentry (reducing the peak directly) but also shortens the infectious period (reducing information spread). The curve-flattening

effect of higher deposit yields therefore operates through an additional channel under social learning.

The social learning mechanism offers a potential explanation for the negative correlation between fundamental fragility (κ) and estimated communication speed ($\hat{\beta}$) documented in Section 6. Under social learning, fundamentally stronger banks induce earlier reentry, shortening the period during which withdrawn agents remain "infectious". This slows information diffusion. The estimated β would thus appear lower for safer banks, even though the underlying network structure (proxied by HHI) remains unchanged.

Under social learning, the initial condition of the learning process is a"seed" of withdrawals must occur before uninformed agents can observe and react. It could potential be an interesting parameter to study. Initial withdrawals could arise from various sources: agents who receive direct news about the shock (e.g., through media reports), liquidity-driven outflows following interest rate changes, or idiosyncratic withdrawals unrelated to coordination. The size of this initial condition generates potentially interesting comparative statics that I have not fully explored. A priori, the effect of initial withdrawal size is ambiguous: a larger seed accelerates learning, potentially amplifying runs, yet sophisticated agents might also interpret large initial withdrawals as evidence of fundamental stress—a true solvency problem rather than coordination-driven panic—which could dampen their own withdrawal incentives. Characterizing these competing effects represents a promising direction for future research.

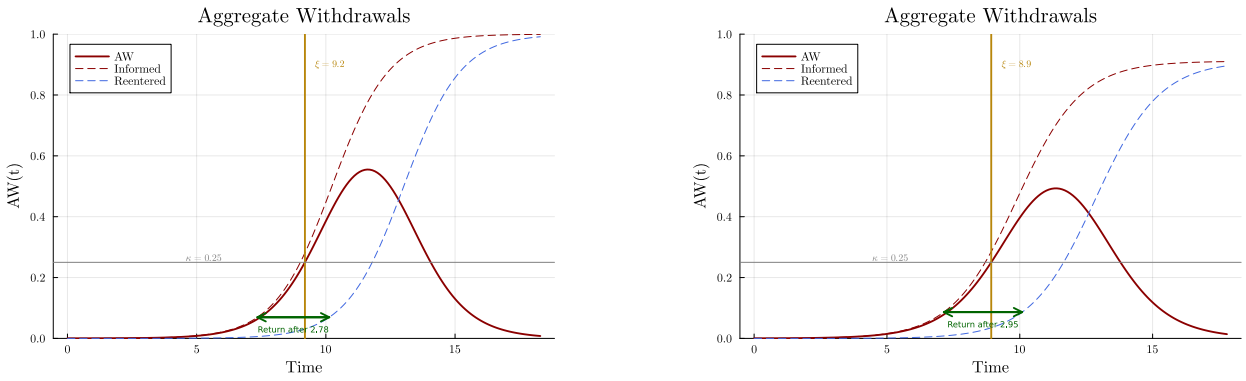

(a) Word-of-mouth learning

(b) Learning from others' actions

Figure 11: Comparison of run dynamics under different learning mechanisms

Reading note: Panel (a): baseline word-of-mouth learning where informed agents spread rumors indefinitely. Panel (b": social learning where agents infer rumors by observing withdrawal behavior. Social learning produces slower, more gradual runs because agents who reenter stop being "infectious," dampening information spread.

8 Conclusion

I develop a dynamic model of bank runs where information about potential insolvency spreads gradually through depositor networks following epidemiological diffusion processes. The model shows that coordination frictions—captured through the speed of information transmission—do not merely slow runs but can prevent them entirely: sufficiently high coordination frictions imply peak withdrawals never exceed the bank's solvency capacity, even when fundamentals are genuinely fragile. Beyond the immediate context of banking, this framework applies broadly to many coordination problems in finance (and beyond), where the structure of the asset holder base determines the feasibility of collective attacks (bubbles, currency attacks, sovereign debt crises, etc.). We do observe such phenomena empirically, suggesting a fertile area for future research: Internet-based assets like cryptocurrencies or meme stocks, characterized by concentrated and highly connected holder bases, face rapid coordinated runs and high volatility. Conversely, globally dispersed safe assets like U.S. Treasury debt may source some of their stability form a dispersed base of heterogeneous international investors where information circulates slowly. This general principle suggests that what makes an asset "safe" or "fragile" depends not only on its intrinsic value but also on the social structure of its investors.

References

Dilip Abreu and Markus K. Brunnermeier, (2003), Bubbles and Crashes, *Econometrica* 71, pp. 173–204.

George-Marios Angeletos and Alessandro Pavan, (2004), Transparency of Information and Coordination in Economies with Investment Complementarities, *American Economic Review* 94, pp. 91–98.

Efraim Benmelech, Jun Yang, and Michal Zator (2024). *Bank Branch Density and Bank Runs*. Working Paper. NBER.

Markus K. Brunnermeier and John Morgan, (2010), Clock Games: Theory and Experiments, *Games and Economic Behavior* 68, pp. 532–550.

Antoni Calvó-Armengol, Joan de Martí, and Andrea Prat, (2015), Communication and Influence, *Theoretical Economics* 10, pp. 649–690.

Briana Chang, Ing-Haw Cheng, and Harrison G. Hong (2023). *The Fundamental Role of Uninsured Depositors in the Regional Banking Crisis*. Working Paper.

Dong Beom Choi, Paul Goldsmith-Pinkham, and Tanju Yorulmazer (Oct. 2023). *Contagion Effects of the Silicon Valley Bank Run*. Working Paper. NBER.

Marco Cipriani, Thomas M. Eisenbach, and Anna Kovner (May 2024). *Tracing Bank Runs in Real Time*. Staff Reports. Federal Reserve Bank of New York.

J. Anthony Cookson, Corbin Fox, Javier Gil-Bazo, Juan Felipe Imbet, and Christoph Schiller (2023). *Social Media as a Bank Run Catalyst*. Working Paper.

Douglas W. Diamond and Philip H. Dybvig, (1983), Bank Runs, Deposit Insurance, and Liquidity, *Journal of Political Economy* 91, pp. 401–419.

Itamar Drechsler, Alexi Savov, Philipp Schnabl, and Olivier Wang (2025). *Deposit Franchise Runs*. Working Paper.

Andrea Galeotti, Benjamin Golub, and Sanjeev Goyal, (2020), Targeting Interventions in Networks, *Econometrica* 88, pp. 2445–2471.

Benjamin Golub and Matthew O. Jackson, (2010), Naïve Learning in Social Networks and the Wisdom of Crowds, *American Economic Journal: Microeconomics* 2, pp. 112–149.

Edward J Green and Ping Lin, (2003), Implementing Efficient Allocations in a Model of Financial Intermediation, *Journal of Economic Theory* 109, pp. 1–23.

Chao Gu, (2011), Herding and Bank Runs, *Journal of Economic Theory* 146, pp. 163–188.

Zhiguo He and Asaf Manela, (2016), Information Acquisition in Rumor-Based Bank Runs, *The Journal of Finance* 71, pp. 1113–1158.

Zhiguo He and Wei Xiong, (2012), Dynamic Debt Runs, *The Review of Financial Studies* 25, pp. 1799–1843.

Rajkamal Iyer and Manju Puri, (2012), Understanding Bank Runs: The Importance of Depositor-Bank Relationships and Networks, *American Economic Review* 102, pp. 1414–1445.

Matthew O. Jackson and Dunia Lopez-Pintado (Nov. 2011). *Diffusion and Contagion in Networks with Heterogeneous Agents and Homophily*. Working Paper.

Erica Xuewei Jiang, Gregor Matvos, Tomasz Piskorski, and Amit Seru, (2024), Monetary Tightening and U.S. Bank Fragility in 2023: Mark-to-market Losses and Uninsured Depositor Runs? *Journal of Financial Economics* 159,

Morgan Kelly and Cormac O Grada, (2000), Market Contagion: Evidence from the Panics of 1854 and 1857, *American Economic Review* 90, pp. 1110–1124.

Steven Kelly and Jonathan Rose (2025). *Rushing to Judgment and the Banking Crisis of 2023*. Working Paper.

Hubert Janos Kiss, Ismael Rodriguez-Lara, and Alfonso Rosa-García, (2014), Do Social Networks Prevent or Promote Bank Runs? *Journal of Economic Behavior & Organization* 101, pp. 87–99.

Naz Koont, Tano Santos, and Luigi Zingales (2024). *Destabilizing Digital 'Bank Walks'*. Working Paper 4443273.

Shohini Kundu, Seongjin Park, and Nishant Vats (2025). *The Geography of Bank Deposits and the Origins of Aggregate Fluctuations*. Working Paper.

Jiageng Liu, Igor Makarov, and Antoinette Schoar (Apr. 2023). *Anatomy of a Run: The Terra Luna Crash*. Working Paper. NBER.

Dunia López-Pintado, (2006), Contagion and Coordination in Random Networks, *International Journal of Game Theory* 34, pp. 371–381.

Dunia López-Pintado, (2008), Diffusion in Complex Social Networks, *Games and Economic Behavior* 62, pp. 573–590.

Dunia López-Pintado, (2012), Influence Networks, *Games and Economic Behavior* 75, pp. 776–787.

Stephen Morris and Hyun Song Shin (Aug. 2001). *Global Games: Theory and Applications*. Working Paper 284813.

Stephen Morris and Hyun Song Shin, (2002), Social Value of Public Information, *The American Economic Review* 92, pp. 1521–1534.

Mark Newman (Sept. 2018). *Networks*. Second Edition. Oxford University Press.

Cecilia Parlatore, (2024), Transparency and Bank Runs, *Journal of Financial Intermediation* 60,

Romualdo Pastor-Satorras and Alessandro Vespignani, (2001), Epidemic Spreading in Scale-Free Networks, *Physical Review Letters* 86, pp. 3200–3203.

James Peck and Karl Shell, (2003), Equilibrium Bank Runs, *Journal of Political Economy* 111, pp. 103–123.

Jonathan Rose, (2023), Understanding the Speed and Size of Bank Runs in Historical Comparison, *Economic Synopses* 2023,

Lawrence Schmidt, Allan Timmermann, and Russ Wermers, (2016), Runs on Money Market Mutual Funds, *American Economic Review* 106, pp. 2625–2657.

Dan H. Tran (2019). *Bank Runs, Fast and Slow: From Behaviors to Dynamics*. Working Paper.

A Proofs

I prove results under a general continuous, differentiable and increasing information diffusion process $G(\cdot)$, imposing additional structure only when needed. This clarifies which conclusions depend on the logistic specification versus more general learning dynamics. I maintain the assumption that learning completes within time η.

One assumption I will make repeatidly is that the likelihood intensity function $g(t) = \frac{dG(t)}{dt}$ is log-concave. It is straightforward to check that for the logistic model $dG = G(1-G)\beta dt$, that assumption holds.

A.1 Proof of Lemma 2 (hazard rate).

In this subsection, I present an extended version of Lemma 2 detailing key properties of the hazard rate. Hazard rates are analyzed using reversed time, $\bar{\tau} = \xi^* - \tau$, where τ is time since learning and ξ^* is the duration until collapse for a fragile bank relative to the initial event t_0. This shifts the focus to the time remaining before the potential collapse. It will be useful to introduce the following notation.

- $T_0 \sim \text{Exp}(\lambda)$: time of solvency shock, with realization t_0
- T_i: calendar learning time for agent i, with realization t_i
- $\mathcal{L}_i = T_i - T_0 \in [0, \eta]$: lag before agent i learns about the shock, the time between t_0 and when the agent learns. Note that G is the CDF of $\mathcal{L}_i$.
- T the random variable for the time of collapse ($T = \infty$ if no collapse).
- $\mathbb{1}_f$ be the indicator for the bank being fragile with $P(\mathbb{1}_f = 1) = p$.
- When focusing on stationary equilibirum, let $h_T(t; \xi^* | t_i)$ be instantaneous hazard rate of collapse at time t for an agent who learned at t_i, which depends on the crash delay after t_0: ξ^*.

Using the notation defined above, in a stationary equilibrium, we have $T = T_0 + \xi^*$ if $\mathbb{1}_f = 1$ and $T = \infty$ if $\mathbb{1}_f = 0$. The lemma below is an extended version of Lemma 2 that formally characterized $\bar{h}$, the hazard rate in reversed time $\bar{\tau}$. The rest of the proofs will always work directly with that object.

Lemma 2 (extended). *Suppose that for any realization of the shock t_0, the collapse occurs at time $t_0 + \xi^*$, where ξ^* is a fixed positive constant. The following properties hold:*

1. *The hazard rate depends only on the time elapsed since learning, $\tau = t - t_i$, crash delay ξ^* and parameters p, λ, η, g. It does not depend explicitly on the specific learning time t_i. We can therefore write $h(\tau; \xi^*) = h_T(t_i + \tau | t_i)$, and specifically:*

$$h(\tau; \xi^*) = \frac{p e^{\lambda(\xi^* - \tau)} g(\xi^* - \tau)}{p \int_0^{\xi^* - \tau} e^{\lambda s} g(s)\, ds + (1-p) \int_0^{\eta} e^{\lambda s} g(s) ds}, \quad \text{for } \xi^* \geq \tau \tag{1}$$
$$h(\tau, \xi^*) = 0 \quad \text{otherwise.}$$

2. *For $\tau \in [0, \xi^*]$, define reversed time $\bar{\tau} = \xi^* - \tau \in [0, \xi^*]$. The hazard rate in reversed time, $\bar{h}(\bar{\tau}) := h(\tau, \xi^*)$, depends only on $\bar{\tau}$.*

3. *The (reversed time) hazard rate can be decomposed as $\bar{h}(\bar{\tau}) = \pi(\bar{\tau})\bar{h}_f(\bar{\tau})$ where:*

   - *$\pi(\bar{\tau})$ is the posterior belief that the bank is fragile given information at reversed time $\bar{\tau}$, and is non-decreasing in $\bar{\tau}$.*
   - *$\bar{h}_f(\bar{\tau})$ is the posterior hazard rate of collapse conditional on the bank being fragile ($\mathbb{1}_f = 1$).*
   - *The evolution of these components in reversed time for $\bar{\tau} \in (0, \eta)$ is governed by:*

$$\begin{cases} d\pi(\bar{\tau}) = \pi(\bar{\tau})(1 - \pi(\bar{\tau}))\bar{h}_f(\bar{\tau})\, d\bar{\tau}, \\ d\bar{h}_f(\bar{\tau}) = -\Big(\bar{h}_f(\bar{\tau}) - \Big(\frac{G''(\bar{\tau})}{G'(\bar{\tau})} + \lambda\Big)\Big)\bar{h}_f(\bar{\tau})\, d\bar{\tau}. \end{cases}$$

Suppose furthermore that $g \in C^2[0, \eta]$ is strictly log-concave with $g(0) > 0$ and $g'(0)$ finite. Then the following also hold for $\bar{\tau} \in (0, \eta]$:

4. *$\bar{h}_f(\bar{\tau})$ is non-increasing in $\bar{\tau}$.*

5. *$\bar{h}(\bar{\tau})$ is unimodal in $\bar{\tau}$.*

A.1.1 Proof of point 1.

Step 1: crash time hazard-rate. The hazard rate for collapse at time t, conditional on learning at t_i and crash happening at $T_0 + \xi^*$ is

$$h_T(t; \xi^* | T_i = t_i) = f_T(t|t_i)/S_T(t|t_i),$$

where $f_T(t|t_i)$ is the overall posterior density and $S_T(t|t_i)$ is the posterior survival function. The subscript T highlights that we take these quantity with respect to the *crash time* random variable. They implicitly depend on the equilibrium object ξ^*.

Using the law of total probability, the fact that fragility is independent of learning time, and the fact that $P(T \leq t; t_i, \mathbb{1}_f = 0) = 0$ for finite t, we can express:

$$h_T(t; \xi^* | T_i = t_i) = \frac{p\, f_T(t|t_i, \mathbb{1}_f = 1)}{1 - pP(T \leq t|t_i, \mathbb{1}_f = 1)}. \tag{2}$$

Step 2: shifting to the T_0 random variable. Letting $t_0 = t - \xi^*$, we can relate the required conditional density and CDF of T to those of T_0. Given the independence of the $(T_0, \mathcal{L}_i)$ process from $\mathbb{1}_f$, conditioning on $\mathbb{1}_f = 1$ does not alter the posterior distribution of T_0 given $T_i = t_i$. Therefore:

- $f_T(t_0 + \xi^*|t_i, \mathbb{1}_f = 1) = f_{T_0}(t_0|t_i, \mathbb{1}_f = 1) = f_{T_0}(t_0|t_i)$
- $P(T \leq t_0 + \xi^*|t_i, \mathbb{1}_f = 1) = P(T_0 \leq t_0|t_i, \mathbb{1}_f = 1) = P(T_0 \leq t_0|t_i)$

where $f_{T_0}(\cdot|t_i)$ and $P(T_0 \leq \cdot|t_i)$ are the posterior density and CDF of T_0 given $T_i = t_i$. Noting that the event $T = t = t_0 + \xi^*$ is the same as $T_0 = t - \xi^*$, it suffices to study the following quantity[37]:

$$h_{T_0}(t_0|T_i = t_i) := \frac{p\, f_{T_0}(t_0|t_i)}{1 - pP(T_0 \leq t_0|t_i)}.$$

Step 3: computing posteriors.

The posterior density $f_{T_0}(t_0|t_i)$ can be computed using Bayes' theorem:

$$f_{T_0}(t_0|T_i = t_i) \propto f_{T_0}(t_0) \times \text{Likelihood}(T_i = t_i|T_0 = t_0).$$

Note that the event $\{T_i = t_i \text{ given } T_0 = t_0\}$ is equivalent to the event $\{T_0 + \mathcal{L}_i = t_i \text{ given } T_0 = t_0\}$, which simplifies to $\{\mathcal{L}_i = t_i - t_0\}$ (given the independence of $\mathcal{L}_i$ and T_0). Recall that $g(s)$ characterizes the likelihood intensity associated with the underlying learning process completing at lag s. The above expression can thus be rewritten as:

$$f_{T_0}(t_0|T_i = t_i) \propto f_{T_0}(t_0)g(t_i - t_0) = \lambda e^{-\lambda t_0} g(t_i - t_0).$$

Since we focus on realizations $t_0 \geq \eta$ the support for t_0 (given t_i) is $[t_i - \eta, t_i]$. The normalization constant $C(t_i)$ is found by integrating the expression $\lambda e^{-\lambda t_0'} g(t_i - t_0')$ over this support:

$$\begin{aligned} C(t_i) &= \int_{t_i - \eta}^{t_i} \lambda e^{-\lambda t_0'} g(t_i - t_0') dt_0' \\ &= \lambda e^{-\lambda t_i} \int_0^{\eta} e^{\lambda s} g(s) ds, \quad \text{using substitution } s = t_i - t_0'. \end{aligned}$$

Let $I_\eta := \int_0^\eta e^{\lambda s} g(s) ds$ (note that constant is independent of t_i). The posterior density of T_0 conditional on $T_i = t_i$ is[38]:

$$f_{T_0}(t_0|T_i = t_i) = \frac{\lambda e^{-\lambda t_0} g(t_i - t_0)}{C(t_i)} = \frac{\lambda e^{-\lambda t_0} g(t_i - t_0)}{\lambda e^{-\lambda t_i} I_\eta} = \frac{e^{\lambda(t_i - t_0)} g(t_i - t_0)}{I_\eta}. \tag{3}$$

This expression holds for $t_0 \in [t_i - \eta, t_i]$. For $t_0 < t_i - \eta$, the posterior density is 0. For $t_0 > t_i$, the posterior density is also 0, as it would imply a negative learning lag.

The posterior cumulative distribution function $P(T_0 \leq t_0|T_i = t_i)$ is obtained by integrating the posterior density (3) over the relevant range. After change of variable we obtain:

$$P(T_0 \leq t_0|T_i = t_i) = \frac{1}{I_\eta} \int_{t_i - t_0}^{\eta} e^{\lambda s} g(s) ds,$$

[37]The notation has an hazard rate for T_0 is a slight abuse: the event T_0 doesn't depend on bank fragility and the real hazard rate for T_0 should be written with 1 instead of p.

[38]Seemingly innocuous, the final equality below, where $e^{-\lambda t_i}$ is brought to the numerator, is the crucial stepping stone that will allow focusing on stationary equilibrium (as already noted in Abreu and Brunnermeier (2003)). It follows from the memoryless property of the exponential distribution and tells us that we can focus only on the time between t_0 and t_i rather than their calendar values.

Step 4: Final formula for hazard rate. Substituting the derived $f_{T_0}(t_0|t_i)$ and $P(T_0 \leq t_0|t_i)$ into the hazard rate formula (2), evaluated at $t = t_0 + \xi^*$, we get:

$$h_{T_0}(t_0|T_i = t_i) = \frac{p\, e^{\lambda(t_i - t_0)} g(t_i - t_0)}{I_\eta - p \int_{t_i - t_0}^{\eta} e^{\lambda s} g(s) ds},$$

which can be re-expressed as:

$$\frac{p\, e^{\lambda(t_i - t_0)} g(t_i - t_0)}{p \int_0^{t_i - t_0} e^{\lambda s} g(s) ds + (1-p) \int_0^{\eta} e^{\lambda s} g(s) ds}. \tag{4}$$

Step 5: Time since learning.

Let $\tau = t - t_i$ be time since learning. We evaluate the hazard at $t = t_i + \tau$, which corresponds to $t_0 = t - \xi^* = t_i + \tau - \xi^*$.

$$h_T(t_i + \tau, \xi^*|t_i) = h_{T_0}(t_i + \tau - \xi^*|T_i = t_i) = \frac{p\, e^{\lambda(\xi^* - \tau)} g(\xi^* - \tau)}{p \int_0^{\xi^* - \tau} e^{\lambda s} g(s) ds + (1-p) \int_0^{\eta} e^{\lambda s} g(s) ds}. \tag{5}$$

A.1.2 Proof of point 2.

Immediate from closed form.

A.1.3 Proof of point 3.

Point 5 decomposes the hazard rate into belief and conditional hazard components, and derives their evolution in reversed time. I first establish this decomposition generally, then specialize to our model.

Lemma 4. *Let T be a random variable representing the time of failure of a system, with positive support. Suppose the system can be of two types: fragile (with prior probability p) or fail-safe (with prior probability $1-p$). Assume the failure time is $T = \infty$ if the system is fail-safe. Let $\mathbb{1}_f$ be the indicator variable for the fragile state. Define:*

- $h(t) = \lim_{\Delta t \to 0} \frac{P(t \leq T < t + \Delta t | T \geq t)}{\Delta t}$ *is the overall hazard rate.*
- $\pi(t) = P(\mathbb{1}_f = 1 \mid T \geq t)$ *is the posterior probability of being fragile given survival up to t.*
- $h_f(t) = \lim_{\Delta t \to 0} \frac{P(t \leq T < t + \Delta t | T \geq t, \mathbb{1}_f = 1)}{\Delta t}$ *is the hazard rate conditional on being fragile.*

The following properties hold:

1. $h(t) = \pi(t) h_f(t)$.
2. *Furthermore, if the failure time distribution for the fragile type admits a density then:*

$$\frac{d\pi(t)}{dt} = -\pi(t)(1 - \pi(t)) h_f(t).$$

Proof. Proof of Claim 1: By the law of total probability, conditioning on the type $\mathbb{1}_f$:

$$\begin{aligned}P(t \leq T < t + \Delta t \mid T \geq t) =& P(t \leq T < t + \Delta t \mid T \geq t, \mathbb{1}_f = 1) P(\mathbb{1}_f = 1 \mid T \geq t) \\ &+ P(t \leq T < t + \Delta t \mid T \geq t, \mathbb{1}_f = 0) P(\mathbb{1}_f = 0 \mid T \geq t).\end{aligned}$$

Since $T = \infty$ if $\mathbb{1}_f = 0$, the second term is zero. Substituting the definitions of $\pi(t)$ and $h_f(t)$:

$$\begin{aligned}h(t) &= \pi(t) \lim_{\Delta t \to 0} \frac{P(t \leq T < t + \Delta t \mid T \geq t, \mathbb{1}_f = 1)}{\Delta t} \\ &= \pi(t) h_f(t).\end{aligned}$$

Proof of Claim 2: We first express $\pi(t)$ using Bayes' theorem. Denoting $S_f(t)$ the survival function conditional on being fragile, we have:

$$\begin{aligned}\pi(t) = P(\mathbb{1}_f = 1 \mid T \geq t) &= \frac{P(T \geq t \mid \mathbb{1}_f = 1) P(\mathbb{1}_f = 1)}{P(T \geq t)} \\ &= \frac{p S_f(t)}{p S_f(t) + 1 \times (1 - p)},\end{aligned}$$

Assuming $S_f(t)$ is differentiable with density $f(t) = -S_f'(t)$, we differentiate $\pi(t)$ with respect to t to obtain:

$$\frac{d\pi(t)}{dt} = -h_f(t)\pi(t)(1 - \pi(t)).$$

□

I now turn the proof of the point 3. Applying the lemma to the hazard rate obtained in the proof of point 1, we have:

$$h(t|t_i) = \pi(t|t_i) h_f(t|t_i) \tag{6}$$

and

$$\frac{d\pi(t|t_i)}{dt} = -\pi(t|t_i)(1 - \pi(t|t_i)) h_f(t|t_i). \tag{7}$$

We need to show how that the decomposition holds in the single-variable reversed time formulation, i.e. using $\bar{h}(\bar{\tau})$.

Step 1: independence of learning time. Note that the conditional hazard rate $h_f(t|t_i)$ corresponds to the scenario where fragility is certain ($p = 1$). Setting $p = 1$ in the derivation for $h(t_i + \tau|t_i)$ (specifically, applying it to the structure derived in (5)), we see that the resulting expression for $h_f(t_i + \tau|t_i)$ depends only on τ. We can write $h_f(\tau) = h_f(t_i + \tau|t_i)$. From (6), since $h(\tau)$ and $h_f(\tau)$ depend only on τ, it follows that $\pi(t_i + \tau|t_i) = h(\tau)/h_f(\tau)$ must also depend only on τ. We write $\pi(\tau) = \pi(t_i + \tau|t_i)$.

Define $\bar{\tau} = \xi^* - \tau$ and $\bar{h}(\bar{\tau}) = h(\tau)$, $\bar{\pi}(\bar{\tau}) = \pi(\tau)$, and $\bar{h}_f(\bar{\tau}) = h_f(\tau)$. The decomposition (6) holds in reversed time:

$$\bar{h}(\bar{\tau}) = \bar{\pi}(\bar{\tau}) \bar{h}_f(\bar{\tau}).$$

This establishes the first part of point 5.

Step 2: Dynamics of π. Note that $\frac{d}{dt} = \frac{d\tau}{dt}\frac{d}{d\tau} = \frac{d}{d\tau}$ and $\frac{d}{d\tau} = \frac{d\bar{\tau}}{d\tau}\frac{d}{d\bar{\tau}} = (-1)\frac{d}{d\bar{\tau}}$. Substituting into (7):

$$-\frac{d\pi(\bar{\tau})}{d\bar{\tau}} = -\pi(\bar{\tau})(1-\pi(\bar{\tau}))h_f(\tau) = -\pi(\bar{\tau})(1-\pi(\bar{\tau}))\bar{h}_f(\bar{\tau}).$$

Dynamics in reversed time are therefore:

$$\frac{d\pi(\bar{\tau})}{d\bar{\tau}} = \pi(\bar{\tau})(1-\pi(\bar{\tau}))\bar{h}_f(\bar{\tau}).$$

Since $\pi \in (0,1)$ and $\bar{h}_f \geq 0$ (as it's a hazard rate), we have $d\pi/d\bar{\tau} \geq 0$, confirming that $\pi(\bar{\tau})$ is non-decreasing (and increasing if $\bar{h}_f > 0$).

Step 4: Dynamics of h_f
Set $p = 1$ in the final expression for $\bar{h}(\bar{\tau})$ given in (1):

$$\begin{aligned}\bar{h}_f(\bar{\tau}) &= \left.\frac{p\, e^{\lambda\bar{\tau}} g(\bar{\tau})}{p\int_0^{\bar{\tau}} e^{\lambda s} g(s)ds + (1-p)\int_0^{\eta} e^{\lambda s} g(s)ds}\right|_{p=1} \\ &= \frac{e^{\lambda\bar{\tau}} g(\bar{\tau})}{\int_0^{\bar{\tau}} e^{\lambda s} g(s)ds}.\end{aligned}$$

This provides the closed form for the conditional hazard rate $\bar{h}_f(\bar{\tau})$ that we can differentiate. Let $N(\bar{\tau}) = e^{\lambda\bar{\tau}} g(\bar{\tau})$ and $D(\bar{\tau}) = \int_0^{\bar{\tau}} e^{\lambda s} g(s)ds$. Then $\bar{h}_f = N/D$. We have:

$$\begin{aligned}N'(\bar{\tau}) &= \frac{d}{d\bar{\tau}}(e^{\lambda\bar{\tau}} g(\bar{\tau})) = \lambda e^{\lambda\bar{\tau}} g(\bar{\tau}) + e^{\lambda\bar{\tau}} g'(\bar{\tau}) = N(\bar{\tau})\left(\lambda + \frac{g'(\bar{\tau})}{g(\bar{\tau})}\right), \\ D'(\bar{\tau}) &= \frac{d}{d\bar{\tau}}\left(\int_0^{\bar{\tau}} e^{\lambda s} g(s)ds\right) = e^{\lambda\bar{\tau}} g(\bar{\tau}) = N(\bar{\tau}).\end{aligned}$$

Then,

$$\begin{aligned}\frac{d\bar{h}_f}{d\bar{\tau}} &= \frac{N'D - ND'}{D^2} = \frac{N(\lambda + g'/g)D - N(N)}{D^2} \\ &= \frac{N}{D}\left(\lambda + \frac{g'(\bar{\tau})}{g(\bar{\tau})}\right) - \left(\frac{N}{D}\right)^2 \\ &= \bar{h}_f(\bar{\tau})\left(\lambda + \frac{g'(\bar{\tau})}{g(\bar{\tau})}\right) - [\bar{h}_f(\bar{\tau})]^2 \\ &= -\left[\bar{h}_f(\bar{\tau}) - \left(\lambda + \frac{G''(\bar{\tau})}{G'(\bar{\tau})}\right)\right]\bar{h}_f(\bar{\tau}),\end{aligned}$$

where we use $g'/g = (G')'/G' = G''/G'$ (recalling that $g = dG/dt$).

A.1.4 Proof of point 4.

We want to show that $\bar{h}_f(\bar{\tau})$ is non-increasing in $\bar{\tau}$ for $\bar{\tau} \in [0, \eta]$, under the assumption that the function $g(s)$ is strictly log-concave (and satisfies the associated regularity conditions

stated in the Lemma, including $g \in C^2$, $g(0)$ positive and finite, $g'(0)$ finite). From Step 4 (dynamics of h_f) in the proof of point 3, we have the ODE:

$$\frac{d\bar{h}_f}{d\bar{\tau}} = -\left[\bar{h}_f(\bar{\tau}) - k(\bar{\tau})\right] \bar{h}_f(\bar{\tau}),$$

where $k(\bar{\tau}) = \lambda + \frac{G''(\bar{\tau})}{G'(\bar{\tau})}$. Since $\bar{h}_f(\bar{\tau}) \geq 0$, the sign of the derivative is determined by the sign of $-[\bar{h}_f(\bar{\tau}) - k(\bar{\tau})]$. Thus, $\bar{h}_f$ is non-increasing if and only if $\delta(\bar{\tau}) := \bar{h}_f(\bar{\tau}) - k(\bar{\tau}) \geq 0$.

Let's analyze the behavior of $\delta(\bar{\tau})$ near $\bar{\tau} = 0$. Under the stated regularity conditions for g at $\bar{\tau} = 0$:

$$\lim_{\bar{\tau}\to 0^+} \bar{h}_f(\bar{\tau}) = \lim_{\bar{\tau}\to 0^+} \frac{e^{\lambda\bar{\tau}} g(\bar{\tau})}{\int_0^{\bar{\tau}} e^{\lambda s} g(s) ds} = +\infty$$

$$\lim_{\bar{\tau}\to 0^+} k(\bar{\tau}) = \lambda + \frac{g'(0)}{g(0)}, \quad \text{which is finite.}$$

Therefore, $\lim_{\bar{\tau}\to 0^+} \delta(\bar{\tau}) = +\infty > 0$.

Suppose, for the sake of contradiction, that $\delta(\bar{\tau})$ becomes negative for some $\bar{\tau}$ in $(0, \eta]$. Since $\delta(\bar{\tau})$ starts positive and is continuous, there must exist a first point $\bar{\tau}_c \in (0, \eta]$ where $\delta(\bar{\tau}_c) = 0$ and $\delta'(\bar{\tau}_c) \leq 0$. We have at that point:

$$\delta'(\bar{\tau}_c) = -\delta(\bar{\tau}_c)\bar{h}_f(\bar{\tau}_c) - k'(\bar{\tau}_c) = -(0) \times \bar{h}_f(\bar{\tau}_c) - k'(\bar{\tau}_c) = -k'(\bar{\tau}_c).$$

The assumption that g is strictly log-concave means $(\log g)''(\bar{\tau}) = k'(\bar{\tau}) < 0$ for $\bar{\tau} \in (0, \eta]$. Therefore, we must have $\delta'(\bar{\tau}_c) = -k'(\bar{\tau}_c) > 0$, a contradiction.

We can conclude that:

$$\frac{d\bar{h}_f}{d\bar{\tau}} = -\underbrace{\delta(\bar{\tau})}_{>0}\underbrace{\bar{h}_f(\bar{\tau})}_{\geq 0} \leq 0.$$

A.1.5 Proof of point 5.

We want to show that $\bar{h}(\bar{\tau})$ is unimodal in $\bar{\tau}$ under the assumption that the function $g(s)$ is log-concave.

Suppose $\bar{h}(\bar{\tau})$ has an interior critical point $\bar{\tau}^* \in (0, \eta)$, where $\frac{d\bar{h}}{d\bar{\tau}}|_{\bar{\tau}^*} = 0$ (if not it is monotonic, hence unimodal). We will show that this must be a local maximum by examining the second derivative of $\log \bar{h}(\bar{\tau})$. Indeed $\left.\frac{d^2 \log \bar{h}}{d\bar{\tau}^2}\right|_{\bar{\tau}^*} < 0$ is a sufficient condition for $\bar{\tau}^*$ to be a local maximum. If all interior critical points are local maxima, the function cannot have any interior local minima and must therefore be unimodal ($\bar{h}$ being continuous).

Consider the logarithm of $\bar{h}(\bar{\tau})$:

$$\log \bar{h}(\bar{\tau}) = \log \pi(\bar{\tau}) + \log \bar{h}_f(\bar{\tau})$$

Differentiating with respect to $\bar{\tau}$:

$$\begin{aligned}\frac{d\log\bar{h}(\bar{\tau})}{d\bar{\tau}} &= \frac{1}{\pi(\bar{\tau})}\frac{d\pi(\bar{\tau})}{d\bar{\tau}} + \frac{1}{\bar{h}_f(\bar{\tau})}\frac{d\bar{h}_f(\bar{\tau})}{d\bar{\tau}} \\ &= (1-\pi(\bar{\tau}))\bar{h}_f(\bar{\tau}) - \left[\bar{h}_f(\bar{\tau}) - \left(\lambda + \frac{g'(\bar{\tau})}{g(\bar{\tau})}\right)\right] \\ &= -\pi(\bar{\tau})\bar{h}_f(\bar{\tau}) + \lambda + \frac{g'(\bar{\tau})}{g(\bar{\tau})} \\ &= -\bar{h}(\bar{\tau}) + \lambda + \frac{g'(\bar{\tau})}{g(\bar{\tau})}.\end{aligned}$$

Once more:

$$\begin{aligned}\frac{d^2\log\bar{h}(\bar{\tau})}{d\bar{\tau}^2} &= \frac{d}{d\bar{\tau}}\left(-\bar{h}(\bar{\tau}) + \lambda + \frac{g'(\bar{\tau})}{g(\bar{\tau})}\right) \\ &= -\frac{d\bar{h}(\bar{\tau})}{d\bar{\tau}} + \frac{d}{d\bar{\tau}}\left(\frac{g'(\bar{\tau})}{g(\bar{\tau})}\right).\end{aligned}$$

Evaluating at the critical point $\bar{\tau}^*$, where $\frac{d\bar{h}}{d\bar{\tau}}|_{\bar{\tau}^*} = 0$:

$$\left.\frac{d^2\log\bar{h}(\bar{\tau})}{d\bar{\tau}^2}\right|_{\bar{\tau}^*} = \left.\frac{d}{d\bar{\tau}}\left(\frac{g'(\bar{\tau})}{g(\bar{\tau})}\right)\right|_{\bar{\tau}^*}.$$

We assumed that g is (strictly) log-concave, which implies $\frac{d}{d\bar{\tau}}\left(\frac{g'(\bar{\tau})}{g(\bar{\tau})}\right) < 0$.

Therefore, at any interior critical point $\bar{\tau}^*$:

$$\left.\frac{d^2\log\bar{h}(\bar{\tau})}{d\bar{\tau}^2}\right|_{\bar{\tau}^*} < 0.$$

This shows that $\log\bar{h}(\bar{\tau})$ is strictly concave at $\bar{\tau}^*$, meaning $\bar{\tau}^*$ must correspond to a local maximum for $\bar{h}(\bar{\tau})$. This completes the proof of point 5.

A.2 Proof of Lemma 3

A.2.1 Preliminary Result

I start by a series of useful preliminary lemmas.

Lemma 5 (Unimodality of $AW(\cdot)$)**.** *Let $g(t)$ be strictly log-concave and positive. For any fixed $\tau > 0$, the function $AW(t)$ is single-peaked (unimodal).*

Proof. Step 0. Case $t < \tau$. Suppose $t < \tau$, then $AW(t) = G(t)$ is strictly increasing. Hence it does not achieve a maximum in this region. The rest of the proof assumes $t \geq \tau$.

Step 1. Re-expressing the condition. We analyze the derivative $AW'(t) = g(t) - g(t-\tau)$. A function is unimodal if its derivative crosses zero at most once, from positive to negative. Letting $R(t) = \frac{g(t)}{g(t-\tau)}$, we can write:

$$AW'(t) = g(t-\tau)\left[R(t) - 1\right].$$

Since $g(t-\tau) > 0$, the sign of $AW'(t)$ is determined by the sign of $R(t) - 1$.

Step 2. $R(t)$ is decreasing. Consider the ratio $R(t) = \frac{g(t)}{g(t-\tau)}$ for $t \geq \tau$. Letting $\phi(t) = \log(g(t))$, the derivative of the logarithm of the ratio is:

$$\frac{d}{dt}\log R(t) = \frac{d}{dt}[\phi(t) - \phi(t-\tau)] = \phi'(t) - \phi'(t-\tau).$$

Since $\phi(t)$ is strictly concave, its derivative $\phi'(t)$ is strictly decreasing and we get $\phi'(t) < \phi'(t-\tau)$. Therefore, $\frac{d}{dt}\log R(t) < 0$, $R(t)$ is strictly decreasing in t.

Step 3. Consequence for unimodality. Because $R(t)$ is strictly decreasing, the equation $R(t) = 1$ has at most one solution. Let t^* be such a solution if it exists.

- If t^* exists: For $t < t^*$, $R(t) > 1 \implies AW'(t) > 0$. For $t > t^*$, $R(t) < 1 \implies AW'(t) < 0$.
- If $R(t) > 1$ for all t, then $AW'(t) > 0$ always.
- If $R(t) < 1$ for all t, then $AW'(t) < 0$ always.

In all cases, $AW'(t)$ changes sign at most once, from positive to non-positive. □

Lemma 6 (Relationship between τ_I^* and $\bar{\tau}_I^*$)**.** *Maintain g is log-concave. Suppose an equilibrium (τ_I^*, ξ^*) exist. Consider $\bar{\tau}_I^* = \xi^* - \tau_I^*$, we have:*

$$\frac{d\tau_I^*}{d\bar{\tau}_I^*} \leq 0.$$

Furthermore, if $\kappa < max_{t\in[0,\eta]}AW(t)$, then the inequality is strict:

$$\frac{d\tau_I^*}{d\bar{\tau}_I^*} < 0.$$

Proof. Step 1. Weak inequality. Implicitly differentiating the equilibrium condition $G(\xi^*) - G(\bar{\tau}_I^*) = \kappa$ with respect to $\bar{\tau}_I^*$ yields:

$$G'(\xi^*)\frac{d\xi^*}{d\bar{\tau}_I^*} - G'(\bar{\tau}_I^*) \times 1 = 0.$$

Since $G'(\xi^*) > 0$, we have:

$$\frac{d\xi^*}{d\bar{\tau}_I^*} = \frac{G'(\bar{\tau}_I^*)}{G'(\xi^*)}.$$

Finally, differentiating the identity $\tau_I^* = \xi^* - \bar{\tau}_I^*$ gives:

$$\frac{d\tau_I^*}{d\bar{\tau}_I^*} = \frac{d\xi^*}{d\bar{\tau}_I^*} - 1 = \frac{G'(\bar{\tau}_I^*)}{G'(\xi^*)} - 1.$$

The crash time is $\xi^* = \inf\{t : AW(t) = \kappa\}$. Since AW is unimodal (Lemma 5), this infimum corresponds to the first crossing of the threshold κ, which must occur on the increasing branch of AW. Therefore, $AW'(\xi^*) \geq 0$, which gives $G'(\xi^*) - G'(\bar{\tau}_I^*) = AW'(\xi^*) \geq 0$. Hence:

$$\frac{d\tau_I^*}{d\bar{\tau}_I^*} = \frac{G'(\bar{\tau}_I^*)}{G'(\xi^*)} - 1 \leq 0.$$

Step 2. Strict inequality. Equality $\frac{d\tau_I^*}{d\bar{\tau}_I^*} = 0$ holds if and only if $AW'(\xi^*) = G'(\xi^*) - G'(\bar{\tau}_I^*) = 0$. By Lemma 5, $AW(t)$ is unimodal and achieves its maximum at a unique time t^* where $AW'(t^*) = 0$. Thus, equality holds if and only if the crash occurs exactly at the peak of the aggregate withdrawal function, i.e., $\xi^* = t^*$ and $\kappa = AW(t^*)$. Under the assumption $\kappa < AW(t^*)$ stated in the lemma, the crash occurs strictly before the peak ($\xi^* < t^*$). Since AW is strictly increasing on $[\bar{\tau}_I^*, t^*]$, we have $AW'(\xi^*) > 0$, giving $G'(\xi^*) > G'(\bar{\tau}_I^*)$. Hence,

$$\frac{d\tau_I^*}{d\bar{\tau}_I^*} < 0.$$

□

A.2.2 Proof of Comparative Statics for u, p, η

We analyze the local effects of u, p, η on the equilibrium reentry time τ_I^*. By Lemma 6, $\frac{d\tau_I^*}{d\bar{\tau}_I^*} \leq 0$, so it is enough to analyze the effect on $\bar{\tau}_I^*$.

Step 1. Case $\tau_I = \xi^*$. Note that $\tau_I = \xi^* \iff \bar{\tau}_I^* = 0 \iff u < \bar{h}(0)$ (otherwise $\tau_I < \xi^*$). In that case $\bar{\tau}_I$ is constant in u, p and η. Since ξ^* only depends on $\bar{\tau}_I$ and G, it is also constant in those parameters.

Step 2. Case $\tau_I < \xi^*$. In that case $\bar{\tau}_I$ must be interior and $\bar{h}(\bar{\tau}_I^*) = u$. By point 5 of lemma A.1, the equilibrium occurs on the increasing branch of the unimodal $\bar{h}$, ensuring $\partial\bar{h}/\partial\bar{\tau}_I^* > 0$. Applying the Implicit Function Theorem to $\bar{h}(\bar{\tau}_I^*; p, \eta) - u = 0$ gives:

$$\frac{d\bar{\tau}_I^*}{du} = \frac{1}{\partial\bar{h}/\partial\bar{\tau}_I^*} > 0,$$

$$\frac{d\bar{\tau}_I^*}{dp} = -\frac{\partial\bar{h}/\partial p}{\partial\bar{h}/\partial\bar{\tau}_I^*} < 0, \qquad \text{since } \frac{\partial\bar{h}}{\partial p} > 0 \text{ (from Lemma A.1 closed-form),}$$

$$\frac{d\bar{\tau}_I^*}{d\eta} = -\frac{\partial\bar{h}/\partial\eta}{\partial\bar{h}/\partial\bar{\tau}_I^*} > 0, \qquad \text{since } \frac{\partial\bar{h}}{\partial\eta} < 0 \text{ (from Lemma A.1 closed form).}$$

If $\kappa < \max_t AW(t)$ we must have $\frac{d\tau_I^*}{d\bar{\tau}_I^*} < 0$ (by Lemma 6) and the strictness in comparative statics case 2 is passed on to τ_I.

A.3 Proof of Proposition 2

Proposition 3 (Existence and Uniqueness of Run Equilibria)**.** *Given parameters (β, κ, p, η) and log-concavity of the learning intensity g, there exists a threshold $\bar{u} \geq 0$ such that:*

1. *A unique run equilibrium exists if and only if $u < \bar{u}$*
2. *No run equilibrium exists if $u \geq \bar{u}$*

Moreover,

- *If $G(\eta) > \kappa + G(0)$, then $\bar{u} > 0$.*

- *The peak withdrawal level* $\bar{AW} = \max_t AW(t)$ *is non-increasing for* $u < \bar{u}$ *and strictly decreasing in* u *for* $u \in (\bar{h}(0), \bar{u})$.

Proof. **Part 1: Existence and Uniqueness of Run Equilibrium**

The substance of the proof is to show that the set of u that admits an equilibrium is in the form of an interval $[0, \bar{u}]$ (as opposed to a collection of interval, etc.).

I prove this result constructively by building a threshold $\bar{u}$ as the minimum of three cut-offs, each arising from a necessary condition for equilibrium (together they are sufficient). For any u, we attempt to construct a candidate equilibrium pair $(\xi^*(u), \bar{\tau}_I(u))$ satisfying: (i) crash condition $G(\xi^*) - G(\bar{\tau}_I) = \kappa$; (ii) reentry optimality $\bar{\tau}_I = \inf\{s \in [0, \eta] : \bar{h}(s) \geq u$; and (iii) immediate exit $\bar{h}(\xi^*) > u$. I then establish uniqueness and defer the proof that $\bar{u} > 0$ to the end.

Step 1: Candidate Construction. Fix $u \geq 0$.

Reentry time. From Lemma 2, the reversed hazard rate $\bar{h}(t)$ is continuous and unimodal on $[0, \eta]$ with peak value $\bar{u}_1 = \max_{t \in [0,\eta]} \bar{h}(t)$ achieved at some $t_{peak} \in [0, \eta]$. Define $\bar{\tau}_I(u) = \inf\{s \in [0, \eta] : \bar{h}(s) \geq u\}$ for all $u \geq 0$. For $u \leq \bar{h}(0)$, we have $\bar{\tau}_I(u) = 0$ (corner solution). For $u \in (\bar{h}(0), \bar{u}_1]$, the function $\bar{\tau}_I(u) \in (0, t_{peak}]$ is the unique solution to $\bar{h}(t) = u$ on the increasing branch and is continuous and strictly increasing by the Implicit Function Theorem. For $u > \bar{u}_1$, no solution exists, delimiting the first cutoff $\bar{u}_1$.

Crash time. Given $\bar{\tau}_I(u)$, the crash condition $G(\xi^*) - G(\bar{\tau}_I) = \kappa$ uniquely determines $\xi^*(u) = G^{-1}(\kappa + G(\bar{\tau}_I(u)))$, provided $\kappa + G(\bar{\tau}_I(u)) < 1$. Since $\bar{\tau}_I(u)$ is non-decreasing and G is strictly increasing, this constraint becomes binding as u increases. Define $\bar{u}_2 = \sup\{u \in (0, \bar{u}_1) : \kappa + G(\bar{\tau}_I(u)) < 1\}$ (set $\bar{u}_2 = \bar{u}_1$ if the constraint never binds), delimiting the second cutoff. For $u < \min(\bar{u}_1, \bar{u}_2)$, the candidate pair $(\xi^*(u), \bar{\tau}_I(u))$ is well-defined, with both components continuous and $\xi^*(u)$ strictly increasing in u. For $u \geq \min(\bar{u}_1, \bar{u}_2)$ no run equilibrium exists.

Step 2: Equilibrium Verification. Suppose $u < \min(\bar{u}_1, \bar{u}_2)$ so that $\xi^*(u)$ and $\bar{\tau}_I(u)$ are well defined. The candidate equilibrium need to satisfy the immediate exit condition: $\bar{h}(\xi^*(u)) > u$. We analyze two cases based on whether $\bar{h}$ is globally monotone or unimodal.

Case (i): $\bar{h}(t)$ *is strictly increasing on* $[0, \eta]$. Since $\bar{h}$ is monotone and $\xi^*(u) > \bar{\tau}_I(u)$ (from $G(\xi^*) = \kappa + G(\bar{\tau}_I)$ and G strictly increasing), we immediately have $\bar{h}(\xi^*(u)) > \bar{h}(\bar{\tau}_I(u)) = u$.

Case (ii): $\bar{h}(t)$ *is unimodal (increasing on* $[0, t_{peak}]$*, decreasing on* $[t_{peak}, \eta]$*) or decreasing (*$t_{peak} = 0$*).* Define $\bar{\tau}_O(u) = \sup\{s \in [0, \eta] : \bar{h}(s) \geq u\}$ for all $u \geq 0$. Form the unimodality of $\bar{h}$, the condition $\bar{h}(\xi^*(u)) > u$ is equivalent to $\xi^*(u) < \bar{\tau}_O(u)$.

Consider the gap function $\Delta(u) = \bar{\tau}_O(u) - \xi^*(u)$. If at u, $\bar{\tau}_O(u)$ is given by a corner solution $\bar{\tau}_O(u) = \eta$ (when $\bar{h}(\eta) > u$), $\bar{\tau}_O(u)$ is constant at that point. If not, then by the Implicit Function Theorem, $\bar{\tau}_O(u)$ is strictly decreasing in u (using $\bar{h}'(\bar{\tau}_O(u)) < 0$). In both cases $\xi^*(u)$ is strictly increasing. Thus $\Delta(u)$ is strictly decreasing in u. If $\Delta(u) < 0$ for all $u \in [0, \min(\bar{u}_1, \bar{u}_2)]$, then the immediate exit condition can never be satisfied, set $\bar{u} = 0$. Otherwise, since $\Delta(u)$ is strictly decreasing, either $\Delta(u) > 0$ throughout, in which case set $\bar{u} = \min(\bar{u}_1, \bar{u}_2)$, or there exists a unique threshold $u^* \in (0, \min(\bar{u}_1, \bar{u}_2))$ where $\Delta(u^*) = 0$, set $\bar{u} = u^*$. In any case, equilibrium exists if and only if $u < \bar{u}$.

Step 3: Uniqueness. For $u \leq \bar{h}(0)$, the reentry time is $\bar{\tau}_I(u) = 0$ (corner solution), then $G(\xi^*) = \kappa$, since G is strictly increasing, both $\bar{\tau}_I^*$ and ξ^* are unique. For $u \in (\bar{h}(0), \bar{u})$,

the function $\bar{\tau}_I(u)$ is the unique solution to $\bar{h}(t) = u$ on the (stricly) increasing branch of the unimodal $\bar{h}$ (by construction in Step 1). Given $\bar{\tau}_I(u)$, the crash time $\xi^*(u) = G^{-1}(\kappa + G(\bar{\tau}_I(u)))$ is uniquely determined by the strict monotonicity of G. Thus, the equilibrium pair $(\xi^*(u), \bar{\tau}_I(u))$ is unique for all $u < \bar{u}$.

Step 4: Case $\bar{u} > 0$. To see when $\bar{u} > 0$, note that as $u \to 0$, we have $\xi^*(u) \to G^{-1}(\kappa + G(0))$ (since $\bar{\tau}_I(u) \to 0$ by the corner solution in Step 1, and the crash condition gives $G(\xi^*(u)) = G(\bar{\tau}_I(u)) + \kappa$). Furthermore $\bar{\tau}_O(u) \to \eta$ as $u \to 0$ by the same argument. The condition $\eta > G^{-1}(\kappa + G(0))$ therefore ensures $\Delta(u) > 0$ for u near 0, implying $\bar{u} > 0$.

Part 2: Comparative Statics of $A\bar{W}$ with respect to u

For $u \leq \bar{h}(0)$, we have the corner solution $\bar{\tau}_I(u) = 0$. Then $\tau_I = \xi^*$, which is independent of u, and $AW(t) = G(t) - G(t - \xi^*)$ which is also independent of u. So the the peak withdrawal $A\bar{W}$ is constant in u.

Suppose now $u > \bar{h}(0)$. Then, $AW(t; \tau_I) = G(t) - G(t - \tau_I)$ and $\tau_I^*(u)$ is the equilibrium reentry time duration, which is interior. Let $t^*(u)$ denote the time that maximizes $AW(t; \tau_I^*(u))$. Then $A\bar{W}(u) = AW(t^*(u), \tau_I^*(u))$. By the Envelope Theorem, the derivative of the maximized value with respect to u is:

$$\frac{dA\bar{W}}{du} = \left.\frac{\partial AW(t, \tau_I)}{\partial \tau_I}\right|_{t=t^*(u), \tau_I = \tau_I^*(u)} \times \frac{d\tau_I^*}{du}.$$

The partial derivative of AW with respect to τ_I is:

$$\frac{\partial AW(t, \tau_I)}{\partial \tau_I} = \frac{\partial}{\partial \tau_I}[G(t) - G(t - \tau_I)] = G'(t - \tau_I).$$

Substituting this into the Envelope Theorem expression:

$$\frac{dA\bar{W}}{du} = G'(t^*(u) - \tau_I^*(u)) \times \frac{d\tau_I^*}{du}.$$

To ensure this derivative is non-zero, we must verify that $t^*(u) > \tau_I^*(u)$. In the run equilibrium, the crash occurs at ξ^* such that $AW(\xi^*) = \kappa$. If $\kappa < AW(t^*(u))$, then $\xi^* < t^*(u)$. Since $\tau_I^*(u) = \xi^* - \bar{\tau}_I^*(u) \leq \xi^*$, we have $\tau_I^*(u) < t^*(u)$. Therefore, $t^*(u) - \tau_I^*(u) > 0$. Since $G'(t^*(u) - \tau_I^*(u)) > 0$ and $d\tau_I^*/du < 0$ by Lemma 3, we conclude that:

$$\frac{dA\bar{W}}{du} < 0.$$

Thus, the peak withdrawal level $A\bar{W}$ is strictly decreasing in u for $u \in (\bar{h}(0), \bar{u})$.

□

A.4 Information diffusion speed β.

A.4.1 Change of Variables

To analyze the comparative statics with respect to the parameter β, we perform a change of variables to rescale time. Applying the change of variables $t \mapsto \tilde{t} = \beta t$, the scaled parameters become:

- Scaled communication speed: $\tilde{\beta} = 1$ (normalized).
- Scaled arrival rate of the initial event: $\tilde{\lambda} = \lambda/\beta$.
- Scaled utility flow from deposits: $\tilde{u} = u/\beta$.
- Scaled awareness window: $\tilde{\eta} = \beta\eta = \bar{\eta}$ (constant across β variations).

Parameters that do not involve time flows, such as the prior probability of fragility p and the bank's fragility threshold κ, remain unaffected. The equilibrium conditions in the scaled system are analogous to those in Proposition 1, but with scaled parameters $(\tilde{\beta} = 1, \tilde{\lambda}, \tilde{u}, \bar{\eta}, p, \kappa)$. It will be convenient to write $a := \frac{1}{\beta}$. There is a direct linear relationship between u and $1/\beta$: the scaling parameter a jointly varies $\tilde{\lambda} = a\lambda$ and $\tilde{u} = au$ while holding $\bar{\eta}, p, \kappa$ constant.

In that section (until the end of the appendix), we assume that the learning process admits such scaling, formally that if G is parametrized by β, writing G_β, then $G_\beta(t) = G_1(\beta t) = G(\tilde{t})$. It is immediate to check that standard processes (logistic, exponential, social learning from Section 7) all satisfy that property.

A.4.2 Comparative statics

Lemma 7. *Consider the scaled system with $\tilde{\beta} = 1$, and fix base parameters $\lambda_0 > 0$ and $u_0 > 0$. Vary the scaling parameter $a > 0$ such that $\tilde{\lambda}(a) = a\lambda_0$ and $\tilde{u}(a) = au_0$, holding $(\bar{\eta}, p, \kappa)$ constant. Suppose a run equilibrium exists in a neighborhood of the base parameters. If $a\lambda_0\bar{\eta} \leq 1$, then:*

$$\frac{d\bar{\tau}_I^*(a)}{da} \geq 0.$$

Remark 3. *Combining Lemmas 7 and 6, the effect on the scaled reentry time satisfies:*

$$\frac{d\tau_I^*}{da} = \frac{d\tau_I^*}{d\bar{\tau}_I^*} \cdot \frac{d\bar{\tau}_I^*}{da} = (\leq 0) \times (\geq 0) \leq 0.$$

That is, in the scaled system, higher a (equivalently, lower β) reduces reentry time.

To translate this to physical time, note that $\tau_{I,phys} = a \cdot \tau_I^*(a)$ (since physical time = scaled time $/\beta = a\times$ scaled time). Thus:

$$\frac{d\tau_{I,phys}}{da} = \tau_I^*(a) + a \cdot \frac{d\tau_I^*}{da} = \underbrace{\tau_I^*}_{>0} + \underbrace{a \cdot \frac{d\tau_I^*}{da}}_{\leq 0}.$$

The first term (direct scaling) is positive while the second (equilibrium effect) is non-positive. These effects work in opposite directions, so the net effect of β on physical reentry time is ambiguous and depends on parameter values.

Proof. The equilibrium condition requires either $\bar{\tau}_I^* = 0$ (corner) or $\bar{h}(\bar{\tau}_I^*; \tilde{\lambda}(a), \bar{\eta}, p) - \tilde{u}(a) = 0$ (interior). In the former case $\bar{\tau}_I^*(a)$ is constant in a, so the derivative is 0. In the later, we

apply the Implicit Function Theorem:

$$\begin{aligned}\frac{d\bar{\tau}_I^*}{da} &= -\frac{(\partial\bar{h}/\partial\tilde{\lambda})(\partial\tilde{\lambda}/\partial a) - \partial\tilde{u}/\partial a}{\partial\bar{h}/\partial\bar{\tau}_I^*} \\ &= -\lambda_0\frac{(\partial\bar{h}/\partial\tilde{\lambda}) - u_0}{\partial\bar{h}/\partial\bar{\tau}_I^*} \\ &= \frac{u_0 - \lambda_0(\partial\bar{h}/\partial\tilde{\lambda})}{(\partial\bar{h}/\partial\bar{\tau}_I^*)}\end{aligned}$$

The equilibrium $\bar{\tau}_I^*$ occurs on the increasing branch of $\bar{h}$, so $\partial\bar{h}/\partial\bar{\tau}_I^* > 0$. To prove the lemma's claim that $\frac{d\bar{\tau}_I^*}{da} \geq 0$, we need to show $u_0 - \lambda_0(\partial\bar{h}/\partial\tilde{\lambda}) \geq 0$.

We compute the derivative of $\bar{h}(\bar{\tau};\tilde{\lambda})$ with respect to $\tilde{\lambda}$. Applying the quotient rule to the closed form from Lemma 2 yields:

$$\frac{\partial\bar{h}}{\partial\tilde{\lambda}} = \bar{h}(\bar{\tau};\tilde{\lambda})\left(\bar{\tau} - E_{\tilde{\lambda}}[s|\bar{\tau}]\right),$$

where $E_{\tilde{\lambda}}[s|\bar{\tau}]$ denotes the posterior mean learning lag, given by:

$$E_{\tilde{\lambda}}[s|\bar{\tau}] = \frac{p\int_0^{\bar{\tau}} se^{\tilde{\lambda}s}g(s)ds + (1-p)\int_0^{\bar{\eta}} se^{\tilde{\lambda}s}g(s)ds}{p\int_0^{\bar{\tau}} e^{\tilde{\lambda}s}g(s)ds + (1-p)\int_0^{\bar{\eta}} e^{\tilde{\lambda}s}g(s)ds}.$$

Now substitute this expression for $\partial\bar{h}/\partial\tilde{\lambda}$ into the condition $u_0 - \lambda_0(\partial\bar{h}/\partial\tilde{\lambda}) \geq 0$, evaluated at the equilibrium $\bar{\tau}_I^*$:

$$u_0 - \lambda_0\left[\bar{h}(\bar{\tau}_I^*;\tilde{\lambda})\left(\bar{\tau}_I^* - E_{\tilde{\lambda}}[s|\bar{\tau}_I^*]\right)\right] \geq 0.$$

We can use the condition $\bar{h}(\bar{\tau}_I^*;\tilde{\lambda}) = \tilde{u}(a) = au_0$:

$$u_0 - \lambda_0\left[(au_0)\left(\bar{\tau}_I^* - E_{\tilde{\lambda}}[s|\bar{\tau}_I^*]\right)\right] \geq 0.$$

Since $u_0 > 0$, this reduces to showing:

$$a\lambda_0\left(\bar{\tau}_I^* - E_{\tilde{\lambda}}[s|\bar{\tau}_I^*]\right) \leq 1.$$

Since $E_{\tilde{\lambda}}[s|\bar{\tau}_I^*] \geq 0$ (from the definition) and $\bar{\tau}_I^* \in [0,\bar{\eta}]$ (equilibrium constraint), we have $\bar{\tau}_I^* - E_{\tilde{\lambda}}[s|\bar{\tau}_I^*] \leq \bar{\tau}_I^* \leq \bar{\eta}$. Applying the lemma's condition $a\lambda_0\bar{\eta} \leq 1$:

$$\tilde{\lambda}(a)\left(\bar{\tau}_I^* - E_{\tilde{\lambda}}[s|\bar{\tau}_I^*]\right) \leq a\lambda_0\bar{\eta} \leq 1.$$

Thus, $\frac{d\bar{\tau}_I^*}{da} \geq 0$ □

A.4.3 Proof of Corollary 3

Corollary 4. *Assume parameters $(u,\lambda,\kappa,p,\eta)$ satisfy $\eta \leq 1/\lambda$. There exists a threshold $\bar{\beta} \geq 0$ such that:*

- *No run equilibrium exists if $\beta < \bar{\beta}$.*

- *A unique run equilibrium exists if $\beta > \bar{\beta}$.*

Additionally:

- *If $\kappa + G(\eta) > 1$, then $\bar{\beta} > 0$.*
- *The peak withdrawal $A\bar{W} = \max_t AW(t)$ is increasing in β for $\beta > \bar{\beta}$.*

Proof. **Part 1: Existence Threshold $\bar{\beta}$.**

The proof is constructive and follows a similar structure as the proof of Proposition 3. I switch to scaled time coordinates. In the scaled system, a run equilibrium is characterized by a pair $(\tilde{\xi}^*, \bar{\tau}_I^*)$ satisfying three conditions analogous to Proposition 3: (i) crash condition $G(\tilde{\xi}^*) - G(\bar{\tau}_I^*) = \kappa$; (ii) reentry $\bar{\tau}_I^*(a) = \inf\{t \geq 0 : \bar{h}(t; a\lambda) \geq au\}$ is attained; and (iii) immediate exit $\bar{h}(\tilde{\xi}^*; a\lambda) > au$. I construct the set of a values for which such an equilibrium exists, then translate back to β.

Step 1: Existence and Properties of $\bar{\tau}_I^*(a)$.

Step 1a: Set of candidates a. From Lemma 2, $\bar{h}(t; a\lambda)$ is continuous and unimodal in t on $[0, \bar{\eta}]$, with $\bar{h}_0(a) := \bar{h}(0; a\lambda) > 0$ and peak value $\bar{h}_{\max}(a) = \max_{t\in[0,\bar{\eta}]} \bar{h}(t; a\lambda)$ achieved at some $t_{peak}(a) \in [0, \bar{\eta}]$.

Define $\bar{\tau}_I^*(a) = \inf\{s \in [0, \bar{\eta}] : \bar{h}(s; a\lambda) \geq au\}$ for all $a > 0$. For $au \leq \bar{h}_0(a)$, we have $\bar{\tau}_I^*(a) = 0$ (corner solution). For $au \in (\bar{h}_0(a), \bar{h}_{\max}(a)]$, the function $\bar{\tau}_I^*(a) \in (0, t_{peak}(a)]$ is the unique solution to $\bar{h}(t; a\lambda) = au$ on the increasing branch and is continuous and strictly increasing by the Implicit Function Theorem. For $au > \bar{h}_{\max}(a)$, no solution exists, defining the first cutoff. Let $A_1 = \{a > 0 : au \leq \bar{h}_{\max}(a)\}$.

Step 1b: Interval form.

We still need to establish that A_1 is an interval of the form $(0, a_1]$ for some $a_1 > 0$ (possibly $a_1 = \infty$). To show this, we analyze the monotonicity of $\bar{h}_{max}(a)/a$. From the derivative formula for $\bar{h}(\bar{\tau}; \tilde{\lambda})$ with respect to $\tilde{\lambda}$ (derived in Lemma 7), evaluated at $\bar{\tau} = t_{peak}(a)$:

$$\frac{d}{da}\left(\frac{\bar{h}_{max}(a)}{a}\right) = \frac{1}{a^2}\left(a\lambda\bar{h}_{max}(a)(t_{peak}(a) - E_{a\lambda}[s|t_{peak}(a)]) - \bar{h}_{max}(a)\right) \leq \frac{\bar{h}_{max}(a)}{a^2}(a\lambda t_{peak}(a) - 1),$$

where the second inequality follows from $E_{a\lambda}[s|t_{peak}(a)] \geq 0$. Under the maintained assumption $a\lambda\bar{\eta} \leq 1$ and since $t_{peak}(a) \leq \bar{\eta}$, we have $a\lambda t_{peak}(a) \leq 1$, implying $\frac{d}{da}(\bar{h}_{max}(a)/a) \leq 0$. Thus $\bar{h}_{max}(a)/a$ is non-increasing in a.

From this monotonicity, if $au \leq \bar{h}_{max}(a)$ for some a, then $a'u \leq \bar{h}_{max}(a')$ for all $a' < a$. This establishes that if $a \in A_1$, then $(0, a] \subset A_1$. Taking $a_1 = \sup A_1$, we obtain $A_1 = (0, a_1]$. Note that $\bar{\tau}_I^*(a)$ is either constant (corner case) or strictly increasing in a (Lemma 7)

Step 2: Existence of $\tilde{\xi}^*(a)$. Condition 2 defines $\tilde{\xi}^*(a) = G^{-1}(\kappa + G(\bar{\tau}_I^*(a)))$. This requires $\kappa + G(\bar{\tau}_I^*(a)) < 1$. Let $a_2 = \sup\{a \in (0, a_1) : \kappa + G(\bar{\tau}_I^*(a)) < 1\}$. Since $\bar{\tau}_I^*(a)$ is non-decreasing and G is strictly increasing, $G(\bar{\tau}_I^*(a))$ is non-decreasing. For $a \in (0, a_2)$, $\tilde{\xi}^*(a)$ is well-defined, continuous, and non-decreasing in a. Let $A_2 = (0, a_2)$.

Step 3: Verification of $\bar{h}(\tilde{\xi}^*(a); a\lambda) > au$. Suppose $a < a_2$. We analyze two cases based on whether $\bar{h}$ is globally increasing or not.

Case (i): $\bar{h}(t; a\lambda)$ is strictly increasing on $[0, \bar{\eta}]$. Since $\tilde{\xi}^*(a) > \bar{\tau}_I^*(a)$, we immediately have $\bar{h}(\tilde{\xi}^*(a); a\lambda) > \bar{h}(\bar{\tau}_I^*(a); a\lambda) \geq au$, for $a \leq a_2$. Set $\bar{a} = a_2$.

Case (ii): $\bar{h}(t; a\lambda)$ is unimodal or decreasing. For $a \in A_2$, a second solution $\bar{\tau}_O(a)$ to $\bar{h}(t; a\lambda) = au$ may exist on the decreasing branch; if no such solution exists, $\bar{\tau}_O(a) = \bar{\eta}$. The condition $\bar{h}(\tilde{\xi}^*(a); a\lambda) > au$ reduces to $\tilde{\xi}^*(a) < \bar{\tau}_O(a)$ in all cases. Define the gap function $\Delta(a) = \bar{\tau}_O(a) - \tilde{\xi}^*(a)$ for $a \in A_2$. We need to show that the set of a values where $\Delta(a) > 0$ has the form $(0, \bar{a})$ for some $\bar{a} \in [0, a_2]$.

We first handle the boundary cases. If $\Delta(a) > 0$ for all $a \in A_2$, then the immediate exit condition holds throughout, and we set $\bar{a} = a_2$. If $\Delta(a) < 0$ for all $a \in A_2$, then the immediate exit condition can never be satisfied in the candidate region, and we set $\bar{a} = 0$ (so the equilibrium set $(0, \bar{a})$ is empty).

For the remaining case where $\Delta(a)$ changes sign, we establish that $\Delta(a)$ is non-increasing, which ensures a unique crossing. The argument is similar as in the proof of Lemma 7.

Suppose $\bar{\tau}_O$ is interior. Applying the Implicit Function Theorem to $\bar{h}(t; a\lambda) - au = 0$ at $t = \bar{\tau}_O(a)$:

$$\frac{d\bar{\tau}_O}{da} = -\frac{\partial \bar{h}/\partial a}{\partial \bar{h}/\partial t} = -\frac{(\partial \bar{h}/\partial \tilde{\lambda})\lambda - u}{\partial \bar{h}/\partial t}.$$

The denominator $\partial \bar{h}/\partial t$ is negative at $\bar{\tau}_O(a)$ (since we are on the decreasing branch). The numerator is $u[\tilde{\lambda}(a)(\bar{\tau}_O(a) - E_{\tilde{\lambda}}[s|\bar{\tau}_O(a)]) - 1]$. Since $\bar{\tau}_O(a) \leq \bar{\eta}$ and $E_{\tilde{\lambda}}[s|\bar{\tau}_O(a)] \geq 0$, we have $\bar{\tau}_O(a) - E_{\tilde{\lambda}}[s|\bar{\tau}_O(a)] \leq \bar{\tau}_O(a) \leq \bar{\eta}$. Using the maintained condition $\tilde{\lambda}(a)\bar{\eta} \leq 1$, we obtain $\tilde{\lambda}(a)(\bar{\tau}_O(a) - E_{\tilde{\lambda}}[s|\bar{\tau}_O(a)]) \leq 1$, making the numerator ≤ 0. Thus, $\frac{d\bar{\tau}_O}{da} = -\frac{(\leq 0)}{(< 0)} \leq 0$, and $\bar{\tau}_O(a)$ is non-increasing in a. If $\bar{\tau}_O$ is an a corner, it is constant in a. Since $\tilde{\xi}^*(a)$ is non-decreasing in a (from Step 2), $\Delta(a)$ is non-increasing. Therefore, if $\Delta(a)$ changes sign, there exists a unique threshold $a_3 \in (0, a_2)$ where $\Delta(a_3) = 0$, with $\Delta(a) > 0$ for $a < a_3$ and $\Delta(a) < 0$ for $a > a_3$. We set $\bar{a} = a_3$ in this case.

Equilibrium exists if and only if $a \in (0, \bar{a})$.

Step 4: Uniqueness. For $au \leq \bar{h}_0(a)$, the reentry time is $\bar{\tau}_I^*(a) = 0$ (corner solution), then $G(\tilde{\xi}^*) = \kappa$; since G is strictly increasing, both $\bar{\tau}_I^*$ and $\tilde{\xi}^*$ are unique. For $au \in (\bar{h}_0(a), \bar{h}_{max}(a))$ and $a < \bar{a}$, the function $\bar{\tau}_I^*(a)$ is the unique solution to $\bar{h}(t; a\lambda) = au$ on the strictly increasing branch of the unimodal $\bar{h}$ (by construction in Step 1). Given $\bar{\tau}_I^*(a)$, the crash time $\tilde{\xi}^*(a) = G^{-1}(\kappa + G(\bar{\tau}_I^*(a)))$ is uniquely determined by the strict monotonicity of G. Thus, the equilibrium pair $(\tilde{\xi}^*(a), \bar{\tau}_I^*(a))$ is unique for all $a < \bar{a}$.

Step 5: Finiteness of $\bar{a}$. We show that $\bar{a} < \infty$ when $\kappa + G(\eta) > 1$. Specifically, we establish that $a_2 < \infty$ where $a_2 = \sup\{a \in (0, a_1) : \kappa + G(\bar{\tau}_I^*(a)) < 1\}$.

Rewrite the hazard rate as:

$$\bar{h}(\bar{\tau}; a\lambda) = \frac{pg(\bar{\tau})}{\int_0^{\bar{\tau}} e^{a\lambda(s-\bar{\tau})} g(s)ds + (1-p)\int_{\bar{\tau}}^{\eta} e^{a\lambda(s-\bar{\tau})} g(s)ds}.$$

For $\bar{\tau} < \eta$, as $a \to \infty$:

$$\frac{\bar{h}(\bar{\tau}; a\lambda)}{a} = \frac{pg(\bar{\tau})}{a\int_0^{\bar{\tau}} e^{a\lambda(s-\bar{\tau})} g(s)ds + a(1-p)\int_{\bar{\tau}}^{\eta} e^{a\lambda(s-\bar{\tau})} g(s)ds} \to 0,$$

since the first integral vanishes (as $s - \bar{\tau} < 0$) while the second grows unboundedly (as $s - \bar{\tau} > 0$). At $\bar{\tau} = \eta$:

$$\frac{\bar{h}(\eta; a\lambda)}{a} = \frac{pg(\eta)}{a\int_0^\eta e^{-a\lambda(\eta-s)}g(s)ds} \to \infty,$$

as the integral vanishes when $a \to \infty$. It follows from its definition that $\bar{\tau}_I^*(a) \to \eta$ as $a \to \infty$.

Equilibrium condition (ii) requires $G(\tilde{\xi}^*(a)) = \kappa + G(\bar{\tau}_I^*(a)) < 1$. But from the parameter assumption $\kappa + G(\bar{\tau}_I^*(a)) \to \kappa + G(\eta) > 1$, so condition (ii) cannot hold for sufficiently large a. Therefore $a_2 < \infty$, which implies $\bar{a} \leq a_2 < \infty$.

Step 6: Conclusion.

Translating back to the original parameter $\beta = 1/a$, the condition $a < \bar{a}$ becomes $\beta > 1/\bar{a}$. Defining $\bar{\beta} = 1/\bar{a}$ (with the convention that $\bar{\beta} = 0$ if $\bar{a} = \infty$), we obtain the desired result: a unique run equilibrium exists if and only if $\beta > \bar{\beta}$, and no equilibrium exists if $\beta \leq \bar{\beta}$. When $\kappa + G(\eta) > 1$, Step 5 ensures $\bar{a} < \infty$, hence $\bar{\beta} > 0$.

Part 2: Comparative Statics of $A\bar{W}$

We first establish the effect in the scaled system. By the Envelope Theorem applied to $AW(t; \tau_I) = G(t) - G(t - \tau_I)$:

$$\frac{dA\bar{W}}{d\tau_I^*} = G'(t^* - \tau_I^*) > 0,$$

where t^* is the time at which the peak is attained (strict positivity holds when $\kappa < AW(t^*)$). Combined with $\frac{d\tau_I^*}{da} \leq 0$ (from Remark 3), we have:

$$\frac{dA\bar{W}}{da} = \frac{dA\bar{W}}{d\tau_I^*} \cdot \frac{d\tau_I^*}{da} = (> 0) \times (\leq 0) \leq 0.$$

To translate to physical parameters, observe that $A\bar{W}$ is a dimensionless quantity (fraction of deposits). Under the scaling transformation, peak withdrawals in physical and scaled coordinates coincide: $A\bar{W}_{phys} = A\bar{W}_{scaled}$. Therefore, no "descaling" is required and:

$$\frac{dA\bar{W}}{d\beta} = \frac{dA\bar{W}}{da} \cdot \frac{da}{d\beta} = (\leq 0) \times \left(-\frac{1}{\beta^2}\right) \geq 0.$$

Thus, $A\bar{W}$ is non-decreasing in β for $\beta > \bar{\beta}$. The increase is strict if $\kappa < AW(t^*)$ and the inequality in Lemma 7 is strict (e.g., if $\eta < 1/\lambda$). □

B Data and Empirical Results

This appendix provides detailed documentation of the data sources, methodology, and robustness checks underlying the empirical analysis.

B.1 Data

My empirical analysis combines multiple datasets to construct measures of bank connectedness and vulnerability during the 2023 regional banking crisis.

Data sources.

- **Summary of Deposits (SOD) Data.** Branch-level deposit information for 2022 was obtained from the FDIC's Summary of Deposits (SOD) database. Data was accessed via the FDIC public API endpoint (`https://banks.data.fdic.gov/api/sod`). SOD data report branch conditions annually as of June 30.
- **Call Report Data.** Balance sheet quantities and deposit franchise estimates are obtained directly from Drechsler et al. (2025). Their dataset is constructed from quarterly regulatory filings (FFIEC Call Reports, forms 031/041) accessed via the Wharton Research Data Services (WRDS) platform, following standard procedures for variable definitions and time-series harmonization.
- **Stock Price Data.** Daily stock price and return data are obtained from the Center for Research in Security Prices (CRSP) database. Intraday trade data are obtained from the Trade and Quote (TAQ) database. Both CRSP and TAQ data are accessed via Wharton Research Data Services (WRDS).
- **Matching.** Data from the FDIC (SOD) and FFIEC (Call Reports) are matched at the Bank Holding Company (BHC) level using the holding company's RSSD ID. These regulatory data are then linked to CRSP daily stock data by mapping BHC RSSD IDs to CRSP PERMCOs using standard WRDS linking tables. For intraday TAQ data, historical stock identifiers (tickers) associated with the BHC's CRSP PERMCO are retrieved from CRSP's name history.

Sample. My analysis focuses on medium-to-large commercial banks with significant domestic deposit bases. The sample includes Bank Holding Companies (BHCs) with at least $3 billion in total assets (as of Q4 2021) and substantial domestic deposit operations (deposit-to-asset ratio above 65%, excluding broker-dealers, credit card banks, custodians, and foreign-owned banks).[39] The focus on medium-to-large institutions ensures the sample includes

[39]Sample criteria are inherited from Drechsler et al. (2025), whose deposit franchise estimates I employ, see below. Their estimates cover commercial banks (not BHCs) with at least $1 billion in total assets, though I further restrict the analysis to BHCs above $3 billion.

banks comparable in scale to those most affected during the 2023 crisis and maintains sufficient variability in depositor dispersion.[40] I exclude banks with deposits entirely concentrated in a single branch. All results are reported at the BHC level, with branch-level and bank-level data aggregated accordingly. The sample comprises 278 BHCs, of which 176 are publicly traded.[41]

Data Access Timing All data retrieved from FDIC API and WRDS were accessed on October 10, 2025.

B.2 Variable Construction and Descriptive Statistics

This section documents the construction of the key empirical measures used in Section 2: the solvency measure κ, depositor concentration (HHI), and cumulative stock returns during the crisis period. I then present descriptive statistics characterizing the distributions and properties of these measures across the sample of Bank Holding Companies.

B.2.1 Methodology

Deposit Franchise Value Construction. I obtain deposit franchise values directly from Drechsler et al. (2025). The total economic value of a bank is decomposed into its equity value and its deposit franchise value:

$$\underbrace{A - D}_{\text{MTM Equity Value}} + \underbrace{DF_I + DF_U}_{\text{Deposit Franchise Value}},$$

where A is the marked-to-market value of assets, D is the book value of total deposits, DF_I is the franchise value of insured deposits, and DF_U is the franchise value of uninsured deposits. I briefly review their construction here; see Drechsler et al. (2025) for complete details.

The marked-to-market equity value, $A-D$, is computed by adjusting reported equity (Q4 2022 Call Reports) for unrealized gains or losses on securities and loans through February 2023, using Bloomberg price indices following Drechsler et al. (2025).

The deposit franchise value for each deposit type (insured/uninsured) equals the net present value of expected future profits from these deposits. Drechsler et al. (2025) provides a methodology to estimate deposit betas for uninsured and insured deposits separately, combining these with estimated operating costs to determine deposit franchise value for each group. I use their deposit franchise values as of February 2023.

I obtain deposit franchise and equity values separately for each bank within a BHC from Drechsler et al. (2025), then aggregate to the holding company level using asset-weighted means. All components ($A - D$, DF_I, DF_U) are expressed as ratios to total book assets for comparability across institutions.

[40] Smaller banks are generally local and concentrated, making it hard to separate effects stemming from concentration and from size. The 3 billions threshold is chosen to match regulatory guidance: BHCs under $\$3B$ are not required to file the consolidated FR Y-9C (they file instead FR Y-9SP).

[41] A few publicly traded banks are not represented in the TAQ dataset, further reducing the sample for high-frequency analyses.

I introduce the solvency measure κ. It is defined as the critical fraction of total deposit franchise value ($DF_I + DF_U$) that must be lost for the bank's total value to fall to a distress threshold, $\underline{v}$, set at 3% of book assets in the implementation.[42] That is, κ solves:

$$A - D + (1 - \kappa)(DF_I + DF_U) = \underline{v},$$

where $A - D$, DF_I and DF_U are all expressed as ratios to total book assets. In principle $\kappa \in [0, 1]$, where $\kappa = 1$ implies robust solvency (economic equity remains above $\underline{v}$ even if the entire deposit franchise is lost). However, I do not cap κ at 1 in my empirical analysis. It allows me to better gauge the distance from this robust solvency point.[43]

HHI Calculation. I measure depositor concentration using the Herfindahl-Hirschman Index (HHI) of deposits for each BHC. The HHI is defined as:

$$\text{HHI} = \sum_{k \in \text{Branches}} \left(\frac{\text{Deposits in branch } k}{\text{Total Deposits in BHC}} \right)^2,$$

where the summation is over all branches k belonging to the BHC. This measure captures the probability that two randomly selected dollars of deposits within the BHC come from the same branch.

Cumulative Stock Returns. I compute cumulative stock returns for each BHC over the crisis period from March 6, 2023 (close of trading) to March 13, 2023 (close of trading), using daily total returns (including dividends, variable "ret") from the CRSP database. The cumulative return for BHC i over this period is calculated by compounding the daily returns:

$$\text{Cumulative Return}_{i,[06/Mar,13/Mar]} = \left(\prod_{t=\text{Mar 7}}^{\text{Mar 13}} (1 + \text{ret}_{i,t}) \right) - 1,$$

where $\text{ret}_{i,t}$ is the daily total return for BHC i on trading day t. The product is taken over the trading days from March 7, 2023, to March 13, 2023, inclusive.

B.2.2 Descriptive statistics.

Before turning to discussing robustness of the main findings of Section 2, I provide further descriptive analysis of my primary measures of risk: solvency κ and depositor HHI. This analysis doesn't require stock data and is performed on the full sample of BHCs, including those that are not publicly traded.

[42] 3% is chosen to match the Basel III capitalization ratios. Banks under 3% are considered severely undercapitalized.

[43] A κ of 2 for example would mean that we would need to destroy double the deposit franchise to make the bank insolvent.

Distribution of Solvency Measure κ Figure 12 presents the distribution of the solvency measure κ across BHCs in the sample. In blue are publicly traded BHCs used in regressions (176 entities), while the grey bars shows the full sample (278 BHCs). The distribution shows heterogenity: while many banks cluster around $\kappa = 1$, a significant fraction falls below this threshold, indicating vulnerability to deposit franchise losses. Banks with $\kappa > 1$ tend to stay near unity but do include a notable right tail of highly robust institutions.

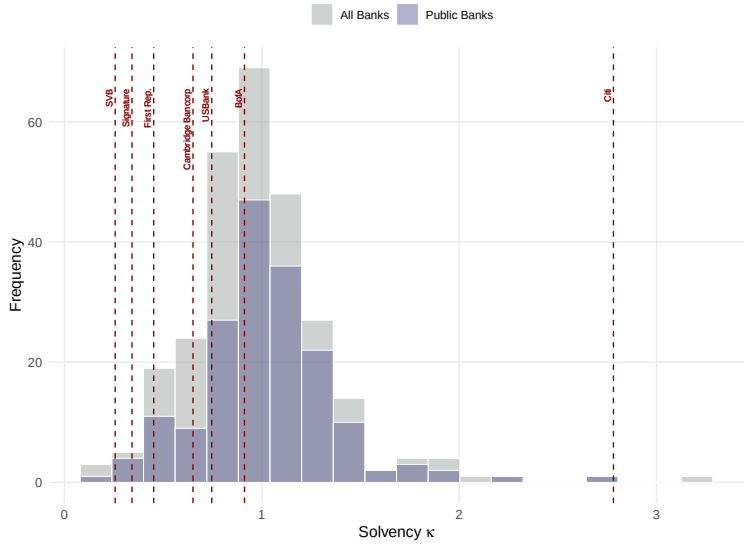

Figure 12: Distribution of κ across BHCs.

Reading note: Histogram showing solvency measure κ distribution across BHCs in sample. Most banks cluster near $\kappa = 1$ (solvent), with notable left tail of vulnerable banks ($\kappa < 1$) including crisis-affected institutions.

Distribution of HHI. Figure 13a shows the HHI distribution across BHCs, ranging from near-zero to close to one. Figure 13 respresents the same distribution but the x-axis is in log scale. Most banks exhibit relatively low HHI values (below 0.1), indicating diversified deposit bases, though a substantial minority shows high concentration. Traditional retail banks like Bank of America have low HHI, while SVB and Citigroup appear as high-concentration outliers. All banks experiencing difficulties during the 2023 crisis had high HHI values, with SVB representing the most extreme case.

Evolution of HHI. Figure 14 shows the evolution of average deposit HHI for BHCs from 1994 to 2022[44]. I also plot a selected sample of individual banks to illustrate their evolution. Note the y-axis is in log scale. The data reveal a secular increase in average HHI since 1994, somewhat slowed by the financial crisis and COVID-19, reaching historically high levels in the 2020s. Average HHI nearly doubled: from around 0.03 in 1994 to about 0.06 in 2022.

[44]The national average includes all commercial banks with over $3 billion in assets (in 2021-equivalent dollars, adjusted for inflation using CPI) and over 0.65 domestic deposits to asset ratio. The average is weighted by BHC asset size.

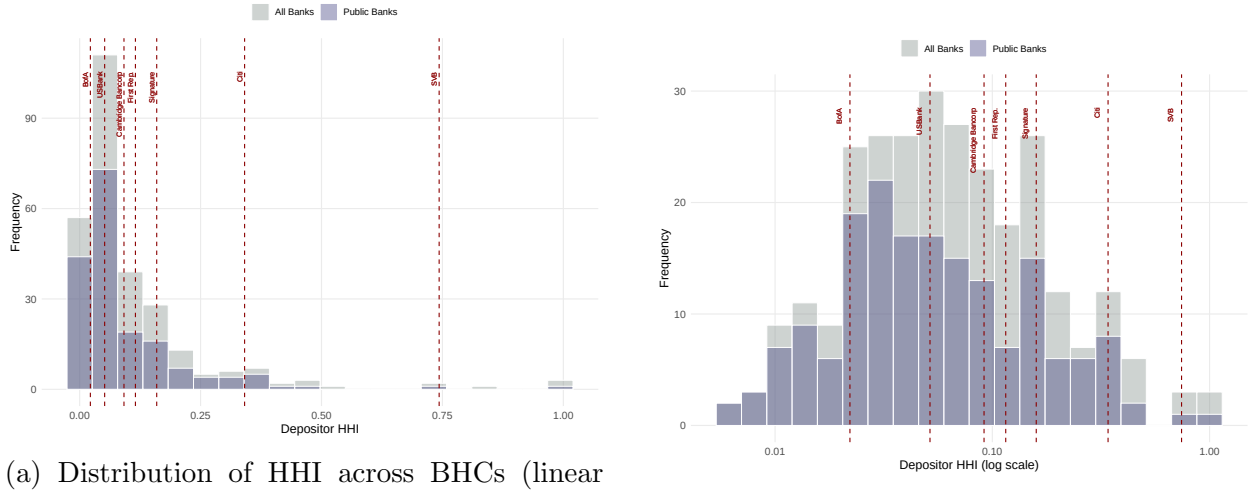

(a) Distribution of HHI across BHCs (linear scale).

(b) Distribution of HHI across BHCs (log scale).

Figure 13: Distribution of HHI across BHCs.

Reading note: Histogram of depositor HHI in linear (left) and log (right) scales. Most banks exhibit low HHI (diversified deposits), but substantial minority shows high concentration. Crisis-affected banks (SVB, First Republic, Citi) appear as high-HHI outliers.

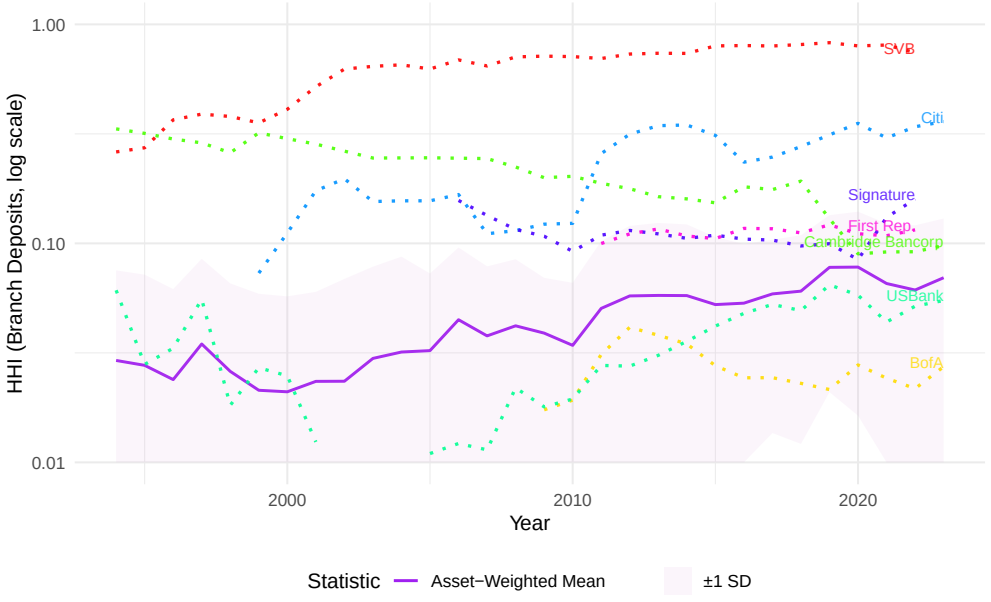

Figure 14: Evolution of Average Deposit HHI for medium to large BHCs (1994-2022)

Reading note: Time series of asset-weighted average HHI (purple line) with ±1 SD band (shaded) and selected individual banks (dotted). Log scale on y-axis. Secular increase from ∼0.03 (1994) to ∼0.06 (2022), with crisis-affected banks already exhibiting high HHI pre-2023.

While some larger banks such as Citi and US Bank substantially increased their HHI since 2005, the banks most impacted by the 2023 crisis displayed high HHI well before the event.

Correlation with Deposit Rates. Table 4 and Figure 15 explore the relationship between BHC-level HHI and the average deposit rates paid by these institutions[45]. I find a strong positive correlation, suggesting that banks with a more concentrated depositor base (higher HHI) tend to offer higher deposit rates. In the context of my model, this correlation could be explained by equilibrium effect: banks with a more concentrated deposit base compensate elevated risk by offering higher rates. More generally, such correlation might be explained by a "deposit clientele effect" as proposed by Benmelech et al. (2024)[46].

Dependent Variable:	**Deposit Rate**				
	(1)	(2)	(3)	(4)	(5)
Depositor HHI	0.022***	0.023***	0.022***	0.023***	0.022***
	(0.002)	(0.002)	(0.002)	(0.002)	(0.002)
Dom. Deposits (log)		0.000		0.000	0.001***
		(0.000)		(0.000)	(0.000)
Uninsured Share			0.001	-0.000	-0.003
			(0.002)	(0.002)	(0.002)
Wholesale sh. of dep.					0.037***
					(0.005)
Constant	0.006***	0.001	0.005***	0.000	-0.005
	(0.000)	(0.003)	(0.001)	(0.003)	(0.003)
Observations	278	278	278	278	278
R^2	0.399	0.404	0.400	0.404	0.493

*Note: *** p<0.01, ** p<0.05, * p<0.1.*

Table 4: Relationship between Depositor HHI and Deposit Rates (2022Q4).

Reading note: OLS regressions showing positive correlation between HHI and deposit rates. Column (4) with full controls shows HHI coefficient of 0.022, suggesting concentrated banks offer higher rates.

One may worry that the effect of HHI on run severity could be confounded by deposit rates. Indeed, higher deposit rates can reflect higher deposit betas (implying lower deposit franchise values) and may influence depositor behavior by making deposits more attractive to retain (as argued in my model). Notice however that such factors would imply *smaller* runs, not larger ones as I document.

Depositor concentration in the literature. I discuss here two related papers that also study depositor concentration, albeit they propose different measures. Already mentioned is the study by Benmelech et al. (2024). They study "bank density", defined as the number

[45]Deposit rate is computed at the BHC level as the ratio between total interest paid on deposits (net) and total deposits. Wholesale share of deposit is the share of time deposits above $\$250k$ on total domestic deposits.

[46]A short discussion of that paper bellow.

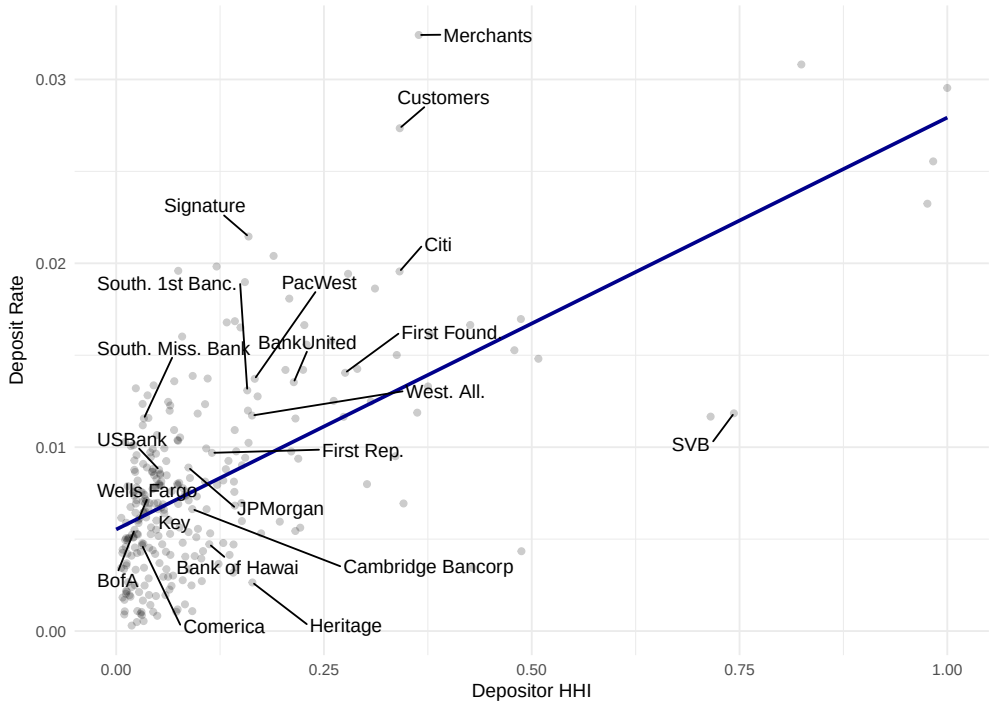

Figure 15: Scatter plot of HHI vs. Average Deposit Rate (2022)

Reading note: Scatter plot with fitted regression line showing positive relationship between depositor concentration (HHI) and deposit rates. Selected banks labeled, including crisis-affected institutions at high-HHI end.

of branches over the deposit volume per BHC. They find that banks with lower density (fewer branches per dollar of deposits) were more vulnerable to runs during the 2023 crisis, consistent with my HHI findings. While related, bank density does not capture the possibility that banks might have concentrated deposits in a few branches while having a large number of branches overall—a nuance better captured by HHI. Benmelech et al. (2024) interpret their results as evidence of a "deposit clientele effect", where concentrated banks cater to urban, educated, financially sophisticated depositors. My interpretation focuses more directly on HHI's role in facilitating depositor communication. Overall my view is that both frameworks are in agreement: they emphasize that information spreads faster within concentrated deposit bases.

Kundu et al. (2025) provide yet another alternative measure of depositor concentration: the share of deposits accumulated within the single largest branch (or county) of a BHC. They find that, on average, 30% of a bank's deposits are concentrated in a single county. Their measure is, in a sense, at the opposite end of the spectrum from Benmelech et al. (2024) bank density: the latter abstracts completely from the within-bank repartition of deposits, while this measure focuses on the largest single unit (branch or county) and ignores smaller ones. My HHI measure lies somewhere in the middle, capturing the overall distribution. The study by Kundu et al. (2025) is not focused on the 2023 runs but rather on the macroeconomic effects of the geographical concentration of deposits. Methodologically, Kundu et al. (2025) provides strong evidence supporting the validity of using SOD data for computing depositor concentration, particularly documenting that reporting errors should not be a major concern[47]

B.3 Robustness and Graphical Evidence

This section validates the main empirical findings from Section 2. I first present graphical evidence illustrating the interaction between depositor concentration and fundamental solvency documented in the regression analysis. I then assess robustness of the main results across alternative risk measures, control specifications, and sample restrictions.

Specification. As discussed in the main text, I focus on two baseline models:

$$\text{Stock Return}_i = \beta_1 \text{HHI}_i + \beta_2 \kappa_i + \text{Controls}_i + \epsilon_i, \tag{8}$$

$$\text{Stock Return}_i = \beta_1 \text{HHI}_i + \beta_2 \mathbb{1}_{\kappa_i<1} + \beta_3 \text{HHI}_i \times \mathbb{1}_{\kappa_i<1} + \text{Controls}_i + \epsilon_i, \tag{9}$$

where the dependent variable is the total stock return from March 6 to March 13, 2023. Specifications of controls vary across different robustness exercises, as discussed below.

B.3.1 Graphical Evidence

Figure 16 provides visual evidence for the interaction effect documented in the main text (Table 1). The figure plots the relationship between depositor concentration (HHI) and cumulative stock returns during the crisis period (March 6–13, 2023), separately for vulnerable banks ($\kappa < 1$, left panel) and robust banks ($\kappa \geq 1$, right panel).

[47]Indeed, a potential issue of the SOD data is that banks can choose where to report deposits. Interpreting SOD branch reporting requires careful consideration of potential biases in such choices.

Among vulnerable banks ($\kappa < 1$), the negative relationship between HHI and stock returns is pronounced. Banks with high depositor concentration experienced substantially larger price declines, with the linear fit capturing a steep downward slope. In contrast, among robust banks ($\kappa \geq 1$), the relationship is notably weaker. Most observations cluster in a region of moderate price drop regardless of HHI level, and the fitted line is much flatter. This visual evidence directly confirms the regression-based interaction effect: depositor concentration's impact on crisis outcomes appears clearly when fundamental vulnerabilities are present, but plays little role when banks have strong solvency buffers.

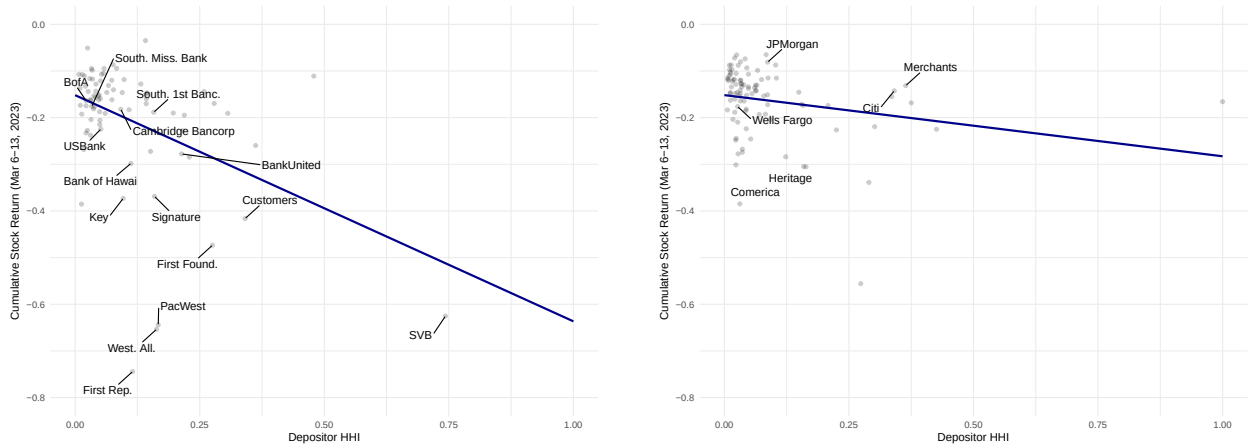

(a) $\kappa < 1$ (Vulnerable Banks)

(b) $\kappa \geq 1$ (Robust Banks)

Figure 16: Scatter plots of Cumulative Stock Returns vs. HHI by Solvency Subsample.

Reading note: Split sample analysis showing HHI effect varies by solvency. Left panel ($\kappa < 1$): steep negative relationship, vulnerable banks with high HHI experienced largest declines. Right panel ($\kappa \geq 1$): flat relationship, robust banks largely unaffected by HHI.

B.3.2 Robustness

Alternative risk measures and controls. To verify that the coordination risk captured by HHI is distinct from fundamental vulnerabilities, I assess the stability of the HHI coefficient across alternative specifications. I substitute κ with: (i) marked-to-market losses (as percentage of 2021 Q4 book value); (ii) uninsured deposit ratio relative to mark-to-market assets (as in Jiang et al. (2024)); and (iii) uninsured solvency κ_u, which is defined similarly to κ but only uninsured deposits face run risk. Control variables include log of domestic deposits, uninsured deposit share, and wholesale deposit share[48]. Figure 17 presents coefficient stability plots showing the point estimate of the HHI coefficient and confidence intervals across specifications, with results for both standard and winsorized HHI using conventional and robust standard errors.

The point estimate remains consistently negative, ranging between -0.2 and -0.5 across specifications. Controlling for the uninsured share of deposits seems to reduce the coefficient

[48]Defined as the share of time deposits above $250k on total domestic deposits.

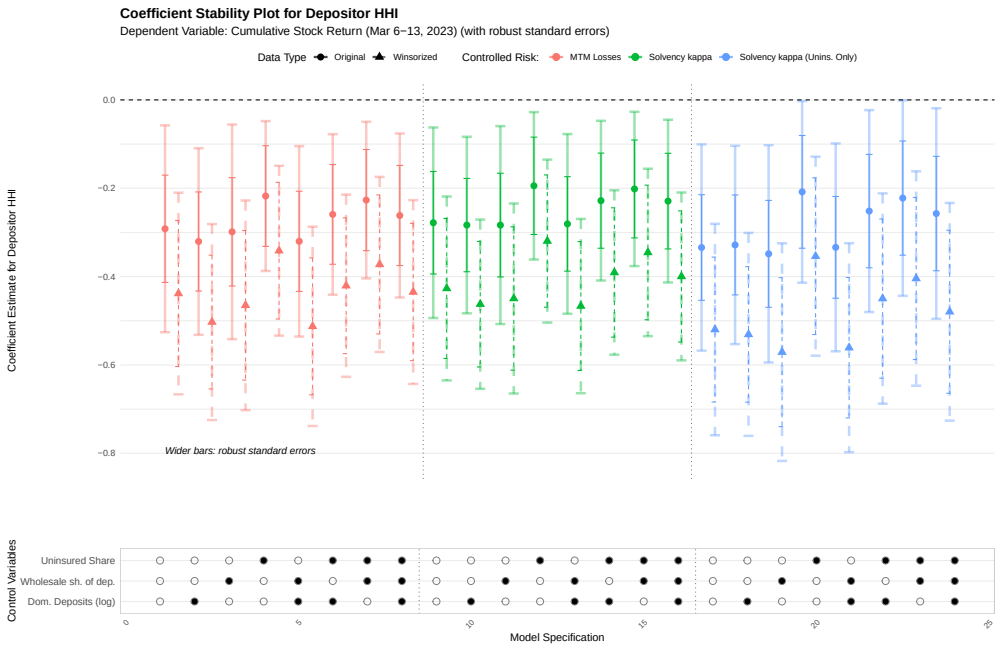

Figure 17: Coefficient stability plot for HHI.

Reading note: Estimated HHI coefficient ($\hat{\beta}_1$) across specifications varying fundamental risk measures (colors) and controls. Consistently negative (-0.2 to -0.5) across all specifications. Winsorized HHI yields larger magnitudes. Robust standard errors (wider intervals) suggest heteroskedasticity, but estimates remain significant.

magnitude. Winsorizing HHI strongly increases the coefficient magnitude across specifications (i.e. more negative), an effect likely due to the skewness of the HHI distribution. The main specification (non-winsorized) is therefore conservative. Finally, using robust standard errors increases confidence bounds noticeably, suggesting some heteroskedasticity in the data (again, likely due to the skewness of the HHI distribution). Estimates remain nonetheless significant.

To better visualize the role of controls, Table 5 presents the results of the main regression specifications using κ as the primary risk measure and with a full set of controls. Throughout bank size and the share of uninsured deposits are significant, with larger banks and those with a higher share of uninsured deposits experiencing more negative stock returns (consistent with findings throughout the literature). Coefficients on HHI are robust to introducing these controls, including when considering the interaction term.

Dependent Variable:	**Cumulative Stock Return (Mar 6-13, 2023)**			
	(1)	(2)	(3)	(4)
Solvency κ	0.087***		0.087***	
	(0.021)		(0.020)	
Depositor HHI		-0.232***	-0.229***	-0.123*
		(0.058)	(0.055)	(0.070)
Indicator ($\kappa < 1$)				-0.014
				(0.017)
$\kappa < 1\times$ Depositor HHI				-0.267**
				(0.111)
Uninsured Share	-0.257***	-0.213***	-0.190***	-0.177***
	(0.058)	(0.060)	(0.057)	(0.059)
Dom. Deposits (log)	-0.017***	-0.015**	-0.021***	-0.018***
	(0.006)	(0.006)	(0.006)	(0.006)
Wholesale sh. of dep.	-0.013	0.094	0.034	0.091
	(0.155)	(0.156)	(0.149)	(0.151)
Constant	0.120	0.177*	0.169*	0.215**
	(0.089)	(0.090)	(0.086)	(0.089)
Observations	176	176	176	176
R^2	0.285	0.279	0.350	0.335

*Note: *** p<0.01, ** p<0.05, * p<0.1.*

Table 5: Main Regression Results: Depositor HHI and Stock Returns.

Reading note: Full-control specification of main regressions. HHI coefficient robust to including log deposits, uninsured share, and wholesale share. Bank size and uninsured deposits remain significant predictors. Interaction term ($\kappa < 1\times$ HHI) are large and significant.

Excluding Failed Banks. To ensure that the main findings are not disproportionately influenced by institutions that failed during the March 2023 crisis period (namely, Silicon Valley Bank, Signature Bank, and First Republic Bank[49]), I re-estimate the set of regression specifications analyzed in the paragraph above, but this time excluding these failed banks from the sample. Figure 18 presents the results in the form of a coefficient stability plot.

[49]Silvergate Bank, having failed prior to the March 6–13, 2023 estimation window, is already excluded from the primary sample.

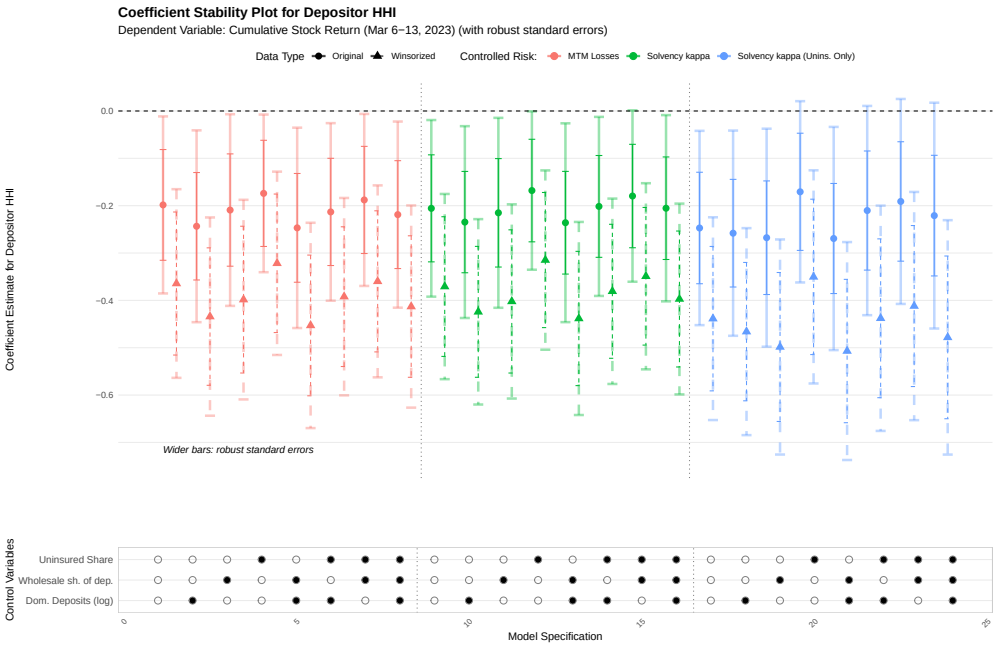

Figure 18: Coefficient stability plot for HHI (excluding failed banks).

Reading note: Robustness check excluding SVB, Signature, and First Republic. HHI coefficient remains negative and mostly significant, though slightly smaller magnitude. Some specifications with κ_u and uninsured controls cross zero with robust SE, but winsorized estimates remain robust.

The estimated HHI coefficient remains consistently negative and mostly statistically significant across the various specifications, albeit slightly smaller in magnitude. Confidence intervals cross zero (with robust standard errors) in some very specific cases: when using κ_u as the measure of fundamental risk and controlling for uninsured deposits simultaneously. If HHI are winsorized, the estimates are robust.

B.4 Model fitting

B.4.1 Methodology

This section details the methodology employed in Section 6 when fitting the model to high-frequency stock return data.

Data. I use high-frequency intraday stock price data sourced from the Trade and Quote (TAQ) database (available on WRDS). TAQ provides comprehensive trade and quote information for U.S. equities, identified by ticker. I map the RSSD IDs of banks in my sample to their CRSP PERMCOs, then to TAQ via tickers using CRSP name history. TAQ data is queried from March 6, 2023 (9:00 AM) to March 21, 2023 (4:50 PM)[50], covering trading days during and immediately following the acute crisis period. Individual trade prices are aggregated to 10-minute, then smoothed using a one-hour centered rolling window. Returns $R_{obs}(t)$ are derived as $R_{obs}(t) = (1 - P_s(t)/P_s(0))$, where $P_s(t)$ is the smoothed price at time t and $P_s(0)$ is the initial smoothed price (March 6, 2023, 9:00 AM). For failed banks, time series are truncated at the close of the last trading day before closure: March 9, 2023 for SVB and March 10, 2023 for Signature Bank.

B.4.2 Additional results.

Model Fit Examples. The Nonlinear Least Squares (NLS) estimation procedure yields a satisfactory fit to observed stock price dynamics for most banks in the sample. Figure 19 to 21 provides illustrative examples beyond those in the main text, comparing smoothed observed stock returns (cumulative percentage decline) against values predicted by the fitted model. Examples are organized into three categories based on severity: (1) large shocks, (2) medium shocks, and (3) small or no shocks. Each group uses its own scale for clarity.

For banks experiencing large shocks, the estimated curve $R_{model}(t)$ effectively captures the overall decline dynamics, including the initial rapid drop whose speed reflects the estimated $\hat{\beta}$ (particularly evident for SVB). Among banks that survived, the model captures the beginning of stabilization as peak withdrawals are reached (e.g., Customers Bancorp, Western Alliance), with correspondingly high estimated peaks. For medium-shock banks, estimated peaks are substantially lower, and the fitted curves exhibit the beginning of price recovery. Finally, for banks with small or no shocks, model fit is generally weaker, though the logistic curve still captures some price movements. These banks exhibit low estimated peaks and relatively flat fitted curves.

[50]While I computed cumulative returns only through March 13 for the results in Section 2, I continue through March 21 to include some of the recovery phase in model fitting. Each trading day extends from 9:00 AM to 4:50 PM to capture regular trading hours.

In all groups, instances of poorer fit or non-convergence can arise when a bank's stock price stabilizes for an extended period after the initial decline without a prompt reversal, or if the recovery is very slow. Since the specified $R_{model}(t)$ implies a symmetric profile around the peak withdrawal intensity (proxied as maximum price decline rate), it is less adept at capturing such slow, asymmetric recoveries. This limitation is visible for banks like PacWest Bancorp, where an initially rapid price decline is not followed by a correspondingly swift reversal within the estimation window. In such cases, the NLS procedure may estimate a lower $\hat{\beta}$ than warranted by the initial drop, effectively attempting to "postpone" the model-implied reversal beyond the observed data to achieve a better overall fit.

Richer models might better capture these asymmetric recovery patterns (see the extension section). However they often lack a simple closed-form expression for aggregate withdrawals or returns. Given the illustrative purpose of this model fitting exercise in the broader context of the paper, I retain the current specification.

Goodness of Fit. To complement the individual examples, I assess overall model fit across all banks using the R^2 from the NLS estimation, which quantifies the proportion of variance in observed stock returns explained by the fitted model $R_{model}(t)$. Figure 22 presents the distribution of values.

The median R^2 is approximately 0.81, indicating that the model explains a substantial portion of variance in stock returns for at least half of the banks. The distribution is somewhat right-skewed, with a tail of lower R^2 values corresponding to banks where model fit was less precise.

These R^2 values generally indicate strong explanatory power, though goodness-of-fit measures for logistic-based models warrant cautious interpretation. Logistic functions are inherently flexible and can adapt to various S-shaped patterns, potentially yielding high R^2 values even when the underlying data generating process deviates from a true logistic form. Nevertheless, combined with visual evidence from the fit examples, the overall high R^2 values support the model's utility for extracting dynamic parameters $(\hat{t}_{mid}, \hat{\beta}, \hat{\tau})$ that characterize observed stock price movements during the crisis.

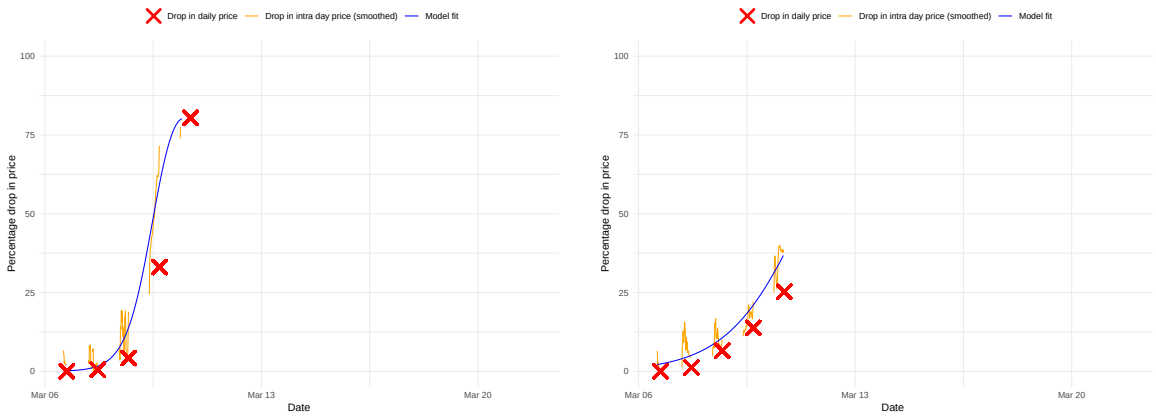

(a) SVB

(b) Signature

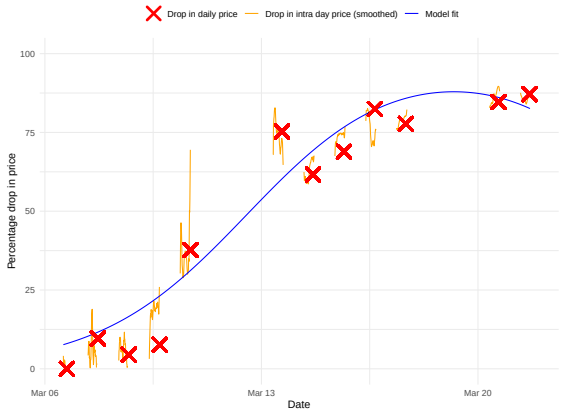

(c) First Rep.

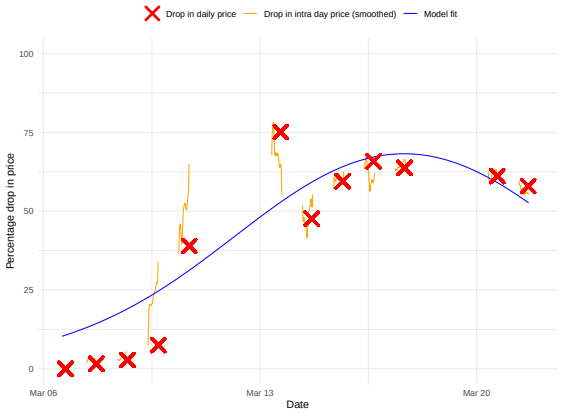

(d) PacWest

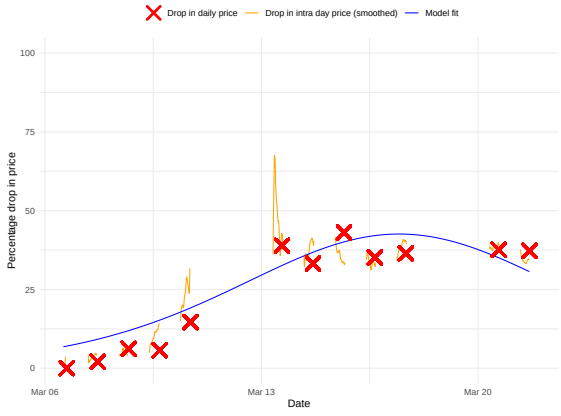

(e) Customers

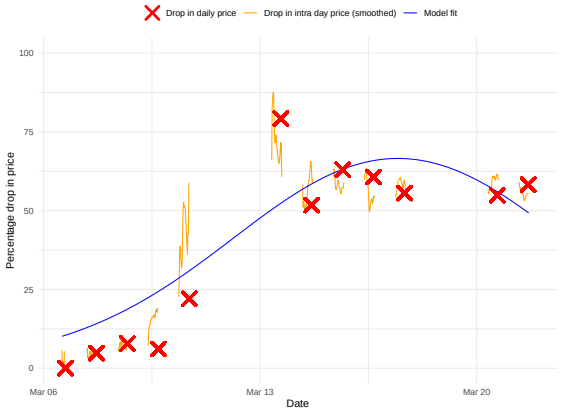

(f) West. All.

Figure 19: Stock prices and model fit for selected banks (Group: Large Shock).

Reading note: TAQ intraday prices (orange), CRSP daily returns (red), and fitted logistic curves (blue) for banks experiencing large shocks. Model captures rapid initial decline (high $\hat{\beta}$) and stabilization onset. Failed banks (SVB, Signature, First Rep.) show truncated series at closure.

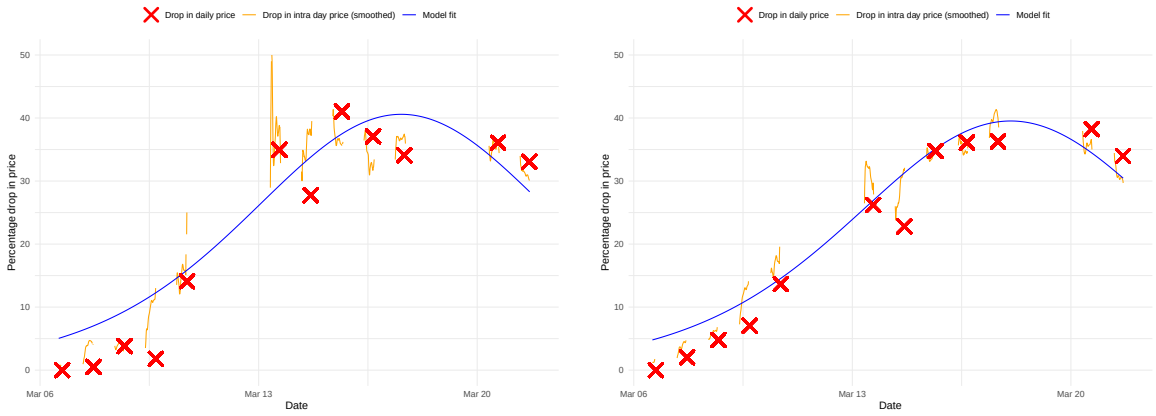

(a) Comerica

(b) BankUnited

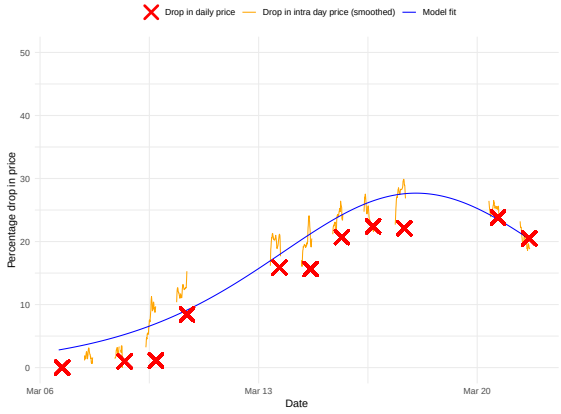

(c) USBank

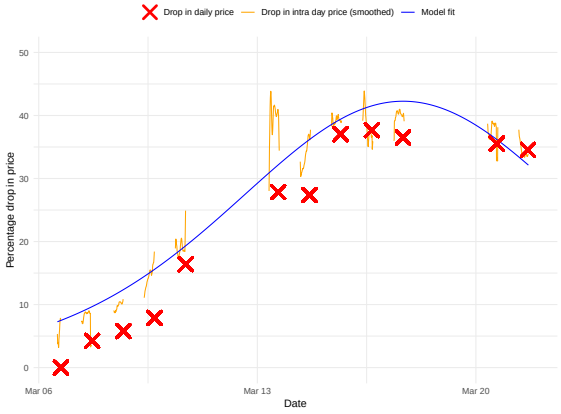

(d) Key

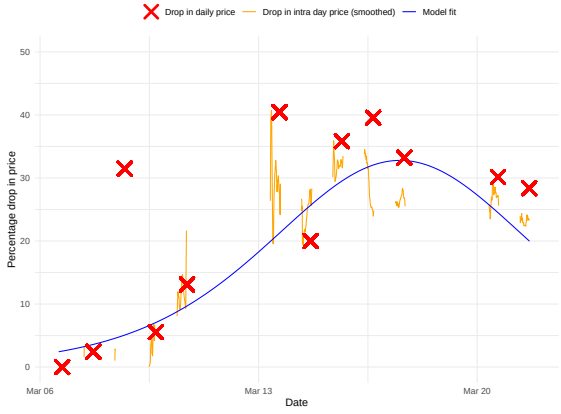

(e) Bank of Hawai

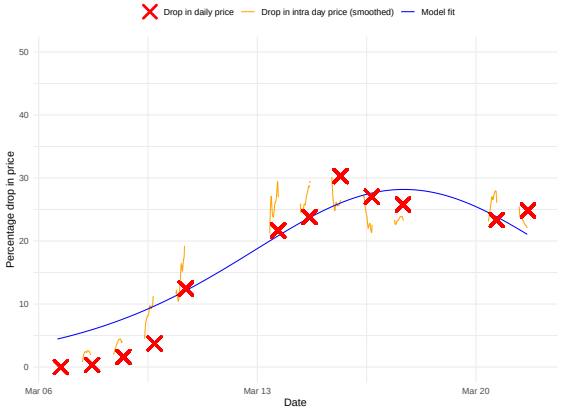

(f) Heritage

Figure 20: Stock prices and model fit for selected banks (Group: Medium Shock).

Reading note: Model fits for banks with moderate shocks. Lower estimated peaks ($\hat{\tau}_I$) compared to large-shock group. Fitted curves capture decline and beginning of recovery. Mid-range $\hat{\beta}$ values produce intermediate-speed dynamics.

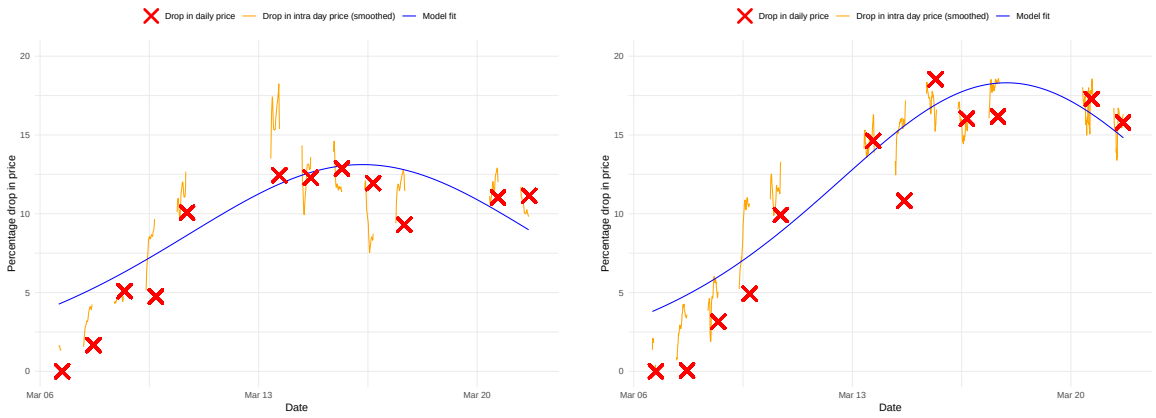

(a) Cambridge Bancorp

(b) BofA

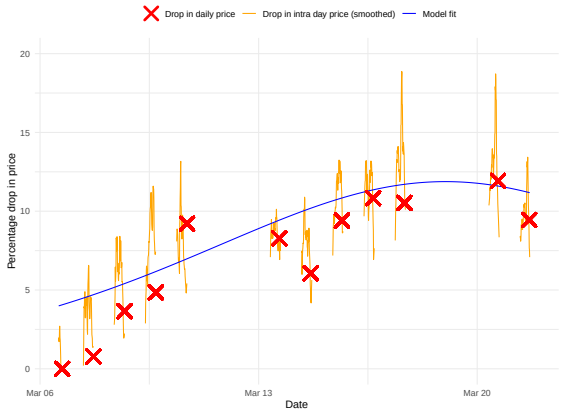

(c) JPMorgan

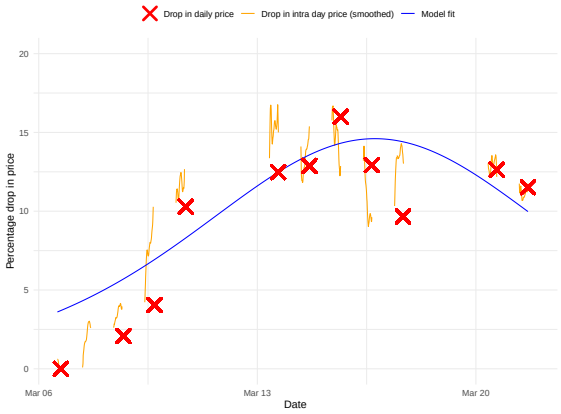

(d) South. Miss. Bank

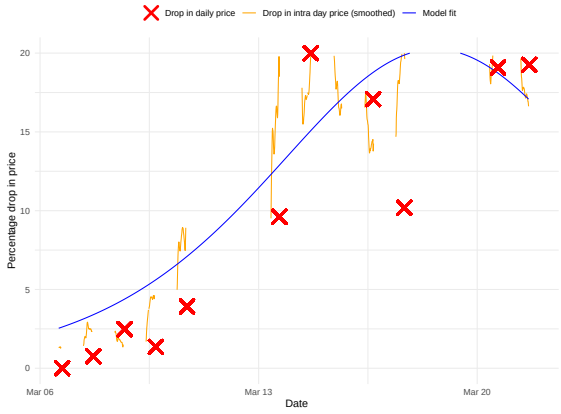

(e) South. 1st Banc.

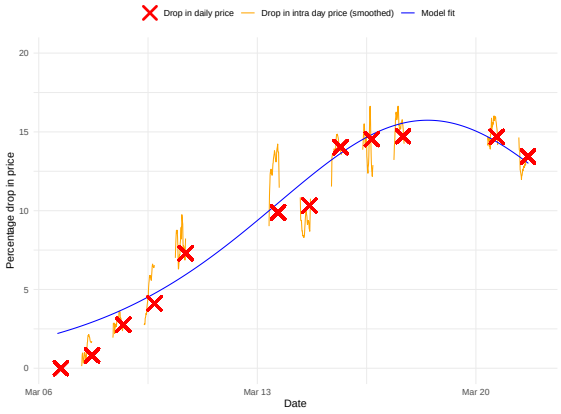

(f) Citi

Figure 21: Stock prices and model fit for selected banks (Group: Small Shock).

Reading note: Banks with minimal or no shocks. Model fit generally weaker but captures some price movements. Low estimated peaks and relatively flat fitted curves. Large banks (JPMorgan, Bank of America) show minimal price response despite high liquidity.

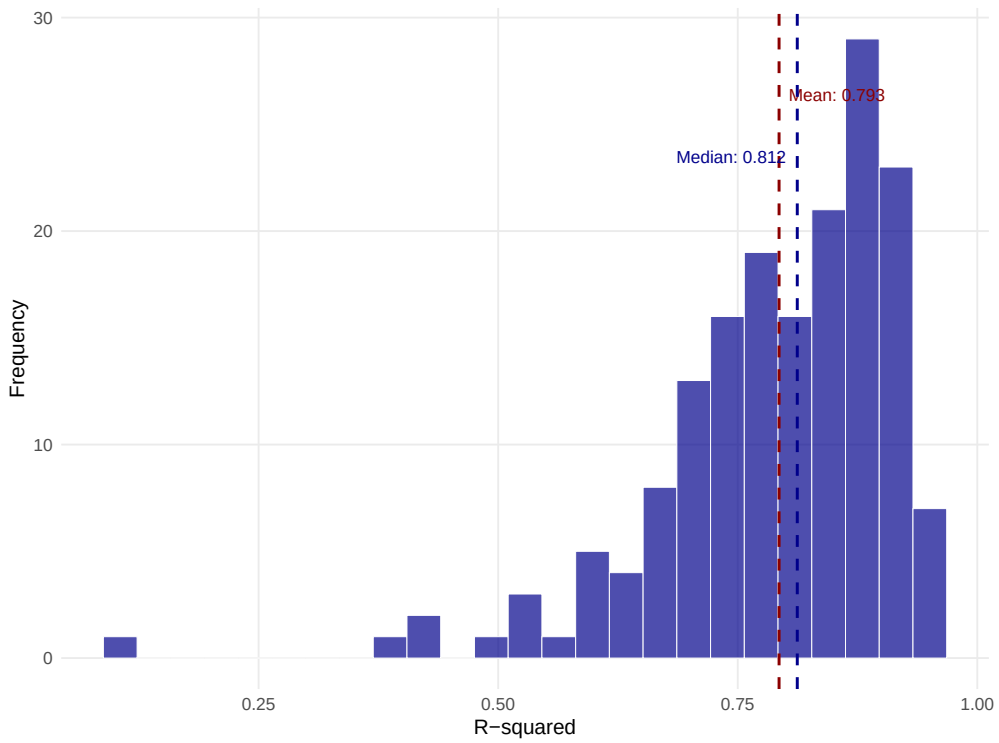

Figure 22: Histogram of r^2 of estimated NLS model on individual banks.

Reading note: Distribution of R^2 from NLS estimation across all banks. Median ≈ 0.81 indicates model explains substantial variance. Right-skewed distribution with tail of lower values for banks with poorer fit (asymmetric recoveries, stabilization periods).

C Computational Methods

This appendix provides detailed documentation of the numerical methods used to solve the model's equilibrium. While analytical characterization is possible for certain aspects, I solve equilibria numerically because (1) it provides more insight into how the model actually works (2) it extends naturally to alternative models from Section 7.

The complete Julia implementation of all computational methods described in this appendix is publicly available at `https://github.com/Robin-Lenoir/replication-social-bank-runs.git`.

C.1 Mathematical Framework

C.1.1 Problem Statement and Computational Challenge

The goal is to solve the equilibrium system formally defined in Proposition 1. The primary computational challenge arises from a fixed-point problem: the optimal withdrawal times for agents depend on the perceived hazard rate $h(\tau)$, which in turn depends on the equilibrium bank collapse time, ξ^*. Simultaneously, the collapse time ξ^* is determined by the aggregate withdrawals, which are a function of those same optimal withdrawal times. This interdependency makes a direct solver approach complex, as it would require iterating on the entire hazard rate function.

C.1.2 The Reversed Time Approach

My solution hinges on a change of variables to "reversed time", a concept formalized in Lemma A.1 of the proof appendix. Reversed time ($\bar{\tau} = \xi^* - \tau$) represents the time remaining until a potential collapse. The key observation from the lemma is that the hazard rate in reversed time, $\bar{h}(\bar{\tau})$, is completely independent of the crash time ξ^*. This allows one to solve for unconstrained optimal agent behavior *before* determining the equilibrium crash time, effectively decoupling the multi-variate fixed-point into a sequence of root-finding problems.

C.1.3 The Two Separable Equations

In reversed time coordinates, one can rewrite the equilibrium system in the following way:

Unconstrained Optimal Withdrawal Times The unconstrained optimal withdrawal policies solve:

$$\bar{\tau}_{OUT}^{UNC} = \sup\{\bar{\tau} : \bar{h}(\bar{\tau}) > u\} \tag{10}$$

$$\bar{\tau}_{IN}^{UNC} = \inf\{\bar{\tau} : \bar{h}(\bar{\tau}) > u\} \tag{11}$$

In equilibrium the domain of $\bar{\tau}_I$ is $[0, \xi^*]$ forcing potential corner solutions. It is useful however to first compute the unconstrained values, because they are independent of ξ^*.

Constraint Application and Equilibrium For the unconstrained withdrawal times, we can write the aggregate withdrawal function at the moment of collapse, ξ^*, as:

$$\mathcal{A}(\xi^*) =: AW(\xi^*; \xi^*) = G(\min(\xi^*, \bar{\tau}_{OUT}^{UNC})) - G(\min(\xi^*, \bar{\tau}_{IN}^{UNC})), \tag{12}$$

where the first entry in AW indicates that we evaluate aggregate withdrawal at $t = \xi^*$ and the second entry make explicit the crash time in the equilibrium under consideration. The equilibrium ξ^* must satisfy the condition $\mathcal{A}(\xi^*) = \kappa$: at crash-time, equilibrium withdrawals attain the bank capacity. As discussed below, one must also verify it is the first time the implied $AW(\cdot, \xi^*)$ crosses κ.

While the final equation for ξ^* is still non-linear, the system is now decoupled. One can first solve for the unconstrained $\bar{\tau}$ values and then take them as given when solving the final equation for ξ^*. Each step involves solving for one unknown in one equation, for which standard root-finding algorithms are well-suited.

C.1.4 Staged Computational Architecture

The solution method employs a three-tier staged approach that exploits this decoupled structure:

1. **Stage 1**: Solve learning dynamics $G(t)$.
2. **Stage 2**: Solve for unconstrained optimal withdrawal times $\bar{\tau}_{IN}^{UNC}$ and $\bar{\tau}_{OUT}^{UNC}$.
3. **Stage 3**: Solve the equilibrium condition for the crash time ξ^* using $\mathcal{A}(\xi)$.

C.2 Stage 1: Learning Dynamics Solver

C.2.1 Logistic Model Formulation

The learning process follows a logistic ODE describing information diffusion through the depositor population:

$$\frac{dG}{dt} = \beta G(t)(1 - G(t)) \tag{13}$$

where $G(t)$ represents the cumulative fraction of agents who have learned about potential bank fragility by time t, and $\beta > 0$ is the communication speed parameter.

C.2.2 Problem Setup

The ODE is solved over a time domain $[0, T]$ with initial condition $G(0) = G_0$, where G_0 is a small positive number (typically 10^{-4}) to initialize the process.

C.2.3 Technical Implementation

The implementation uses standard adaptive ODE solvers. I use a 5th-order Runge-Kutta with automatic step size control. The logistic equation's multi-scale nature—rapid initial growth followed by slower convergence—is handled efficiently by the solver's automatic step-size adjustments. I set tolerances to machine epsilon ($\approx 1 \times 10^{-16}$) to ensure maximum

precision for subsequent equilibrium calculations. The adaptive grid generated by the solver is inherited by all subsequent computational stages to maintain numerical consistency. The discrete solution points $(t_i, G(t_i))$ are converted to a continuous function $G(t)$ via linear interpolation.

C.2.4 PDF Computation

The learning probability density function is computed analytically from the ODE's right-hand side:

$$g(t) = \frac{dG}{dt} = \beta G(t)(1 - G(t)) \tag{14}$$

where $G(t)$ is the numerical solution from the ODE solver. I evaluate $g(t_i)$ at each grid point $\{t_i\}$ and create a corresponding interpolating function $g(t)$.

C.3 Stage 2: Computing Unconstrained Optimal Withdrawal Times

C.3.1 Problem Statement and Approach

The goal of this stage is to find the unconstrained optimal withdrawal times that solve:

$$\bar{h}(\bar{\tau}_{IN}^{UNC}) = u \quad \text{and} \quad \bar{h}(\bar{\tau}_{OUT}^{UNC}) = u \tag{15}$$

I solve this by first computing $\bar{h}(\bar{\tau})$ over its full domain and then extracting the roots from the list of values given by the precomputed function, leveraging its known unimodal structure.

C.3.2 Hazard Rate Function Computation

Grid Construction and Inheritance Strategy The computation operates on a reversed time grid derived from the forward time grid $\{t_i\}$ from Stage 1, preserving the adaptive density.

Efficient One-Shot Integration. The hazard rate uses Lemma 2's closed-form expression, which contains an integral term that is computationally expensive to evaluate repeatedly:

$$\bar{h}(\bar{\tau}) = \frac{pe^{\lambda\bar{\tau}}g(\bar{\tau})}{p\int_0^{\bar{\tau}} e^{\lambda s}g(s)ds + (1-p)\int_0^{\eta} e^{\lambda s}g(s)ds} \tag{16}$$

I resolve this bottleneck by computing the integral for all grid points in a single pass using cumulative summation with the trapezoidal rule. This operation avoids the high cost of repeated numerical integration calls inside an iterative root-finder. Once the integral term is computed for all grid points, $\bar{h}(\bar{\tau})$ can be evaluated efficiently on all grid points using vectorized operations.

C.3.3 Root Extraction via Grid Search and Interpolation

With $\bar{h}(\bar{\tau})$ evaluated at all grid points, root extraction is a two-step process:

1. **Grid Scan**: Create an indicator array $\mathbb{I}[\bar{h}(\bar{\tau}_j) > u]$ to identify the grid points that bracket the roots. $\bar{\tau}_{IN}^{UNC}$ is bracketed by the first transition from 0 to 1, and $\bar{\tau}_{OUT}^{UNC}$ by the last transition from 1 to 0.

2. **Interpolation**: Once the bracketing grid points are found, a precise root is obtained via linear interpolation. This is computationally inexpensive while being more accurate than simply snapping to the nearest grid point.

3. **Boundary Cases**: If no grid points satisfy $\bar{h}(\bar{\tau}_j) > u$, both withdrawal times are set to the domain boundary η.

C.4 Stage 3: Equilibrium Solver via Adaptive Bisection

C.4.1 Problem Statement and Mathematical Framework

The equilibrium crash time ξ^* satisfies $\xi^* = \inf\{t : AW(t;\xi^*) \geq \kappa\}$, where $AW(t;\xi)$ represents aggregate withdrawals at time t for a given reentry time $\tau_I = \xi - \bar{\tau}_{IN}^{UNC}$. I solve this by finding the root of $\mathcal{A}(\xi) = \kappa$, where:

$$\mathcal{A}(\xi) := AW(\xi;\xi) = G(\min(\xi, \bar{\tau}_{OUT}^{UNC})) - G(\min(\xi, \bar{\tau}_{IN}^{UNC})) \tag{17}$$

This formulation automatically handles constraint binding: as ξ varies, the effective exit and reentry times adjust via the min operators. By construction, $\bar{\tau}_{OUT}^{UNC} > \bar{\tau}_{IN}^{UNC}$ (agents re-enter after exiting). This implies $\mathcal{A}(\xi)$ is weakly increasing in ξ with three cases: (1) If $\xi < \bar{\tau}_{IN}^{UNC}$: $\mathcal{A}(\xi) = 0$ (no withdrawals yet). (2) If $\bar{\tau}_{IN}^{UNC} < \xi < \bar{\tau}_{OUT}^{UNC}$: $\mathcal{A}(\xi) = G(\xi) - G(\bar{\tau}_{IN}^{UNC})$ (strictly increasing, main case). (3) If $\xi > \bar{\tau}_{OUT}^{UNC}$: $\mathcal{A}(\xi) = G(\bar{\tau}_{OUT}^{UNC}) - G(\bar{\tau}_{IN}^{UNC})$ (constant; if this is less than κ, no run equilibrium exists).

Because $\mathcal{A}(\xi)$ is monotonic, the bisection will find at most one root ξ^* satisfying $\mathcal{A}(\xi^*) = \kappa$. However, this mathematical root is necessary but not sufficient for a valid equilibrium. The implied time-series $AW(t;\xi^*)$ may have crossed κ at some earlier time $t_0 < \xi^*$. In such cases, ξ^* is a "false equilibrium": the bank would have crashed at t_0, not ξ^*. When a false equilibrium is detected, there is no valid run equilibrium—monotonicity of $\mathcal{A}(\xi)$ ensures no other candidate exists.

Remark 4. *It is essential to distinguish between $AW(t;\xi^*)$, the time-series of withdrawals for a fixed collapse time parameter ξ^*, and the bisection object $\mathcal{A}(\xi) := AW(\xi;\xi)$. The latter conflates evaluation time with collapse time parameter, giving withdrawal volume at the candidate crash time.*

C.4.2 Bisection Algorithm

I solve $\mathcal{A}(\xi) = \kappa$ using a bisection algorithm complemented by a finite-difference check to ensure the correct (first) root is found. In particular, the algorithm validates equilibrium candidates using a finite-difference slope check. For each candidate ξ, I compute:

$$\Delta AW = AW(\xi + \epsilon;\xi) - AW(\xi;\xi) \tag{18}$$

where ϵ is the local grid spacing of the learning CDF interpolation. If $\Delta AW < 0$ at convergence, ξ lies on the decreasing branch of $AW(t;\xi)$, indicating a false equilibrium.

Algorithm Setup

- **Initialization**: I set search bounds, e.g., $\xi_{\min} = 0$ and $\xi_{\max} = T$.
- **Function evaluation**: $AW(\xi_{guess}) = G(\min(\xi_{guess}, \bar{\tau}_{OUT}^{UNC})) - G(\min(\xi_{guess}, \bar{\tau}_{IN}^{UNC}))$.
- **Error assessment**: $error = AW(\xi_{guess}) - \kappa$.

Iterations

1. **Case 1: Overshoot** ($\mathcal{A} > \kappa + \text{tol}$). The search has gone too far. Reduce upper bound: $\xi_{\max} \leftarrow \xi_{guess}$.
2. **Case 2: Undershoot, Valid Direction** ($\mathcal{A} < \kappa - \text{tol}$). The search is approaching the first root from below. Increase lower bound: $\xi_{\min} \leftarrow \xi_{guess}$.
3. **Case 3a: Converged, Valid Equilibrium** ($|AW - \kappa| \leq \text{tol}$ and $\Delta AW \geq 0$). Root found on increasing branch . Valid equilibrium: ξ^* is the first crossing of κ. Return ξ^*.
4. **Case 3b: Converged, False Equilibrium** ($|AW - \kappa| \leq \text{tol}$ and $\Delta AW < 0$). Root found on decreasing branch (indicating false equilibrium). The peak of $AW(t; \xi^*)$ occurred before ξ^* and exceeded κ, meaning the bank would have crashed earlier. No valid run equilibrium exists. Return failure.

If the search interval $|\xi_{\max} - \xi_{\min}|$ collapses to machine precision without convergence, no run equilibrium exists.

The No-Run Case If a run equilibrium does not exist for a given set of parameters, the algorithm identifies this through: (1) the search interval $|\xi_{\max} - \xi_{\min}|$ collapsing below tolerance without finding a root, (2) detection of a false equilibrium (Case 3b), indicating that while a mathematical root exists, the time-series dynamics would have caused an earlier crash.

C.5 Extensions to the Baseline Model

This section documents the computational methods for the three extensions: heterogeneous learning speeds, interest rates on deposits and endogenous social learning from observed withdrawals. Each extension preserves the staged approach but requires specific modifications to handle the increased complexity.

C.5.1 Heterogeneous Learning Speeds

Modified Learning Dynamics The key computational change is the coupled system of ODEs governing information diffusion:

$$\frac{dG_k}{dt} = \beta_k(1 - G_k(t)) \sum_{j=1}^{K} p_j G_j(t) \tag{19}$$

This represents agents in group k learning from the overall pool of informed agents $\omega(t) = \sum_j p_j G_j(t)$. Closed-form solution exists for certain distributions[51] but involves complex expressions and do not extend to the social learning setting below. I solve this system numerically using the same adaptive ODE solver as the baseline model.

Aggregate Withdrawal Computation The aggregate withdrawal function $\mathcal{A}(\xi) =: AW(\xi, \xi)$ to use in the bisection becomes a weighted sum across groups:

$$AW(\xi) = \sum_{k=1}^{K} p_k \left[G_k(\min(\xi, \bar{\tau}_{OUT,k}^{UNC})) - G_k(\min(\xi, \bar{\tau}_{IN,k}^{UNC})) \right] \tag{20}$$

Each group k has its own learning CDF $G_k(t)$ and hence, its own hazard rate. The unconstrained optimal withdrawal times $\bar{\tau}_{IN,k}^{UNC}$ and $\bar{\tau}_{OUT,k}^{UNC}$ are computed using the same root-finding approach as the baseline model, applied to each group. One key advantage of the approach described above is that one can remain agnostic on which group will have binding constraint and which will not (in particular it is possible for a group to have both $0 < \bar{\tau}_{IN}^{UNC}, \bar{\tau}_{OUT}^{UNC} < \xi$).

Computational Workflow

1. Solve the coupled ODE system for $\{G_k(t)\}_{k=1}^{K}$ on the adaptive grid.
2. Extract optimal withdrawal times for each group using the baseline algorithm.
3. Solve for equilibrium ξ^* using the weighted aggregate withdrawal function.

The equilibrium solver (Stage 3) remains unchanged except for the modified $AW(\xi)$ calculation.

Validation for Heterogeneous Groups Because the implied time-series $AW(t; \xi^*)$ may be multimodal (multiple humps from different group dynamics), the slope check I perform in the main case is insufficient. Rather, I validate that the root is a correct equilibrium by checking if $AW(t; \xi^*)$ crosses back below κ at any $t < \xi^*$, which would indicate ξ^* is a second crossing rather than the first. This requires computing $AW(t; \xi^*)$ over the grid for $t < \xi^*$, which is $O(n)$ but necessary only after convergence.

C.5.2 Interest Rates and Value Functions

Problem Formulation. With positive interest rate $r > 0$, agents maximize expected discounted utility. This introduces a value function $V(\bar{\tau})$ representing the continuation value of holding deposits in reversed time, where $\bar{\tau} = \xi^* - \tau$ is the time remaining until potential collapse (with τ being time since learning). The optimal holding decision becomes:

$$\text{Hold deposits if and only if } \bar{h}(\bar{\tau}) < u + rV(\bar{\tau}) \tag{21}$$

This modifies the threshold condition from $\bar{h}(\bar{\tau}) < u$ to $\bar{h}(\bar{\tau}) - rV(\bar{\tau}) < u$.

[51] The closed form solutions involves the moment-generating functions of the distribution, and are available whenever MGF admit closed forms.

Value Function Computation. The value function satisfies an ordinary differential equation derived from the Hamilton-Jacobi-Bellman equation. In reversed time, the HJB becomes:

$$V'(\bar{\tau}) = (\bar{h}(\bar{\tau}) + \delta)(1 - V(\bar{\tau})) + \max\{u + rV(\bar{\tau}) - \bar{h}(\bar{\tau}), 0\} \tag{22}$$

where $\delta > r$ is the deposit maturity rate. The boundary condition is $V(0) = (u+\delta)/(r+\delta)$, representing the present value of holding \$1 in a safe deposit: convenience yield u, interest r, and maturity payoff 1 at rate δ, evaluated at the crash time $\bar{\tau} = 0$ (which corresponds to $\tau = \xi^*$ in forward time).

I solve this ODE backward from $\bar{\tau} = \eta$ to $\bar{\tau} = 0$ using the adaptive grid inherited from the learning dynamics solver. This ensures consistency across all computational stages and avoids interpolation errors.

Modified Optimal Buffer Computation Although the value function implicitly contains the optimal holding strategy, I explicitly recompute the withdrawal times for clarity and numerical stability:

1. Define the modified threshold function: $\tilde{h}(\bar{\tau}) = \bar{h}(\bar{\tau}) - rV(\bar{\tau})$
2. Apply the baseline root-finding algorithm to find:

$$\bar{\tau}_{IN}^{UNC} = \inf\{\bar{\tau} : \tilde{h}(\bar{\tau}) > u\} \tag{23}$$

$$\bar{\tau}_{OUT}^{UNC} = \sup\{\bar{\tau} : \tilde{h}(\bar{\tau}) > u\} \tag{24}$$

This approach reuses the efficient grid-based root extraction from the baseline model while incorporating the value function effects. The subsequent equilibrium computation (Stage 3) proceeds unchanged with these modified withdrawal times.

C.5.3 Social Learning from Withdrawals

The Endogenous Learning Challenge Social learning fundamentally alters the model's structure by making learning dynamics depend on equilibrium behavior. Agents learn about bank fragility by observing others' withdrawals, creating a fixed-point problem: aggregate withdrawals determine learning, learning determines optimal behavior, and optimal behavior determines aggregate withdrawals.

Iterative Solution via Damped Fixed-Point Iteration I solve this fixed-point problem through a damped fixed-point iteration scheme on the aggregate withdrawal function in its entirety (rather than simply at collapse time - $AW(\xi, \xi)$):

1. **Initialization**: Obtain initial guess $AW^{(0)}(t)$ by solving the baseline model (word-of-mouth learning) without social learning effects.
2. **Iteration**: At each iteration $n \geq 1$:
   - Solve learning ODE with forcing term $AW^{(n-1)}(t)$: $\frac{dG}{dt} = \beta(1-G(t)) \times AW^{(n-1)}(t)$

- Given $G(t)$, compute hazard rates and optimal withdrawal times $\bar{\tau}_{IN}^{UNC}$, $\bar{\tau}_{OUT}^{UNC}$
- Compute implied equilibrium collapse time ξ^* and withdrawal function: $A\tilde{W}^{(n)}(t)$ (I reuse the bisection algorithm on ξ from the baseline but replace the withdrawe al times and learning functions by what is obtained in step 1 and step 2).
- Apply damping with fixed parameter $\alpha = 0.5$:

$$AW^{(n)}(t) = (1-\alpha)AW^{(n-1)}(t) + \alpha A\tilde{W}^{(n)}(t) \tag{25}$$

  Alternative damping schemes are possible but practice shows a uniform rule works well.
- Check convergence: $\|AW^{(n)} - AW^{(n-1)}\|_\infty < \epsilon$

3. **Convergence**: Stop when iteration error falls below tolerance, or maximum iterations is reached.

I assume the unimodal structure of AW persists under social learning dynamics, which is verified numerically in all computed equilibria. Throughout the iteration, η is fixed to its baseline value; it is not recomputed from the endogenous G curve.

Inner Loop Failure For a given $AW^{(n-1)}(t)$, the equilibrium solver (Stage 3 from the baseline model) may find that there is no "inner" equilibrium. That is, fixing the learning curve from $dG^{(n)} = \beta(1-G)AW^{(n-1)}$, we cannot find crash-time ξ^* satisfying the equilibrium condition. Without a crash time, the next outer iteration's aggregate withdrawal function cannot be constructed. I address this by setting $\xi^{(n)} = \xi^{(n-1)} + \eta/500$, and compute $AW(t) = G(t) - G(t - \xi^{(n)} + \bar{\tau}_I)$, allowing the iteration to continue. While this lacks theoretical foundation, it permits the algorithm to continue exploring for a potential solution.

Handling No-Run Cases The algorithm identifies no-run cases by failure to converge. In contrast to the baseline case, the identification is not fully grounded in theory and simply a pragmatic solution. The theoretical shortcoming is that there is a possibility that one may fail to capture a run equilibrium (and label it as non-run), in particular because the search path depends on the initial guess and the update rule in case of non-run in the inner loop. Empirically, non-convergence seems to reliably indicate that no social learning run equilibrium exists for the given parameters: varying initial guess, damping or update in case of inner failure do not "save" equilibria. Non-convergent sequences typically oscillate from the first few iterations or stay at $AW = 0$.

Computational Cost Convergence typically requires approximately 40 iterations for a convergence of order 10^{-5}. Each iteration involves solving a complex ODE with the time-varying forcing term $AW^{(n-1)}(t)$, which is computationally more demanding than the baseline logistic ODE. Total computation time is approximately 20 seconds, compared to 0.5 seconds for the baseline model.

C.6 Implementation Details and Figure Parameters

This section documents the exact parameter choices used to generate the figures in the main text.

C.6.1 Baseline Model Parameters

The baseline model parameters, used as the foundation for all figures unless otherwise specified, are in Table 6.

Parameter	Symbol	Value
Communication speed	β	1.0
Raw awareness window	$\bar{\eta}$	15.0
Awareness window	η	15.0 ($= \bar{\eta}/\beta$)
Utility flow from deposits	u	0.1
Prior fragility probability	p	0.5
Solvency threshold	κ	0.6
Exponential rate for t_0	λ	0.01
Initial learning condition	$G(0)$	0.0001
Time span	—	$(0, 2\eta) = (0, 30)$

Table 6: Baseline model parameters used throughout the paper.

C.6.2 Figure-Specific Parameters

Table 7 summarizes the parameter values used for each figure in the main text. When a cell shows a range (e.g., $[0.001, 0.2]$), this indicates comparative statics over that parameter range. All other parameters are held at baseline values unless otherwise specified.

C.6.3 Computational Settings

All computations use machine precision tolerances ($\approx 10^{-16}$) for ODE solving and 10^{-12} relative tolerance for equilibrium root-finding. The Julia implementation exploits the staged computational architecture to minimize redundant calculations, particularly by reusing learning dynamics across multiple equilibrium computations within parameter sweeps.

Figure	β	u	κ	r	Description
Fig. 1: Learning	$\{0.5, 1.0, 2.0\}$	0.1	0.6	—	Multiple β comparison
Fig. 2: Hazard Rate	1.0	0.1	0.6	—	Main scenario
Fig. 3a: Main Eq.	1.0	0.1	0.6	—	Main scenario
Fig. 3b: Fast Comm.	3.0	0.1	0.6	—	High β case
Fig. 3c: Low Utility	1.0	0.01	0.6	—	Low u case
Fig. 4: u Effects	1.0	$[0.001, 0.2]$	0.6	—	Comp. statics in u
Fig. 5: Cross-Effects	$[1, 10^4]$	$[0.001, 1]$	0.6	—	2D parameter sweep
Fig. 9: Heterogeneity	$\{0.125, 12.5\}$	0.1	0.3	—	Two-type model (90%/10%)
Fig. 10: Interest-rate	1.0	0.0	0.6	0.06	Interest-bearing deposits
Fig. 11: Social Learning	0.9	0.5	0.25	—	Social learning dynamics

Table 7: Parameter values for main text figures. All use $p = 0.5$, $\lambda = 0.01$, $\eta = 15/\beta$, time span $(0, 2\eta)$ unless noted. Ranges indicate comparative statics. Figure 4 uses 5000 grid points, Figure 5 uses 500×500 grid with $\beta = 1/\text{meeting time}$ where meeting time $\in [0.0001, 1]$. Figure 9 uses heterogeneous β values with population shares $(0.9, 0.1)$, $p = 0.9$, $\lambda = 0.1$, $\bar{\eta} = 30.0$. Figure 11 uses $p = 0.99$, $\lambda = 0.25$, $\bar{\eta} = 30.0$ with social learning dynamics.